The fission of heated nuclei in reactions involving heavy ions: static and dynamical aspects

A review dedicated to the memory of Georgi Nikolaevich Smirenkin

M. G. Itkis
Joint Institute for Nuclear Research, Dubna

A. Ya. Rusanov
Institute of Nuclear Physics, Kazakhstan National Nuclear Center, Alma-Ata

Fiz. Élem. Chastits At. Yadra **29**, 389–488 (March–April 1998)

The various aspects of the formation of the fragment mass–energy distributions from the fission of excited nuclei in the range $Z^2/A = 20-43$ in heavy-ion reactions are reviewed. These are: the actual temperature of the fissioning nucleus after the emission of prefission particles, the effect of the angular momentum transferred to the nucleus by the incident ion, the static features of the formation of the fragment distributions of very light nuclei, the role and nature of dynamical effects in the descent of the nucleus from the saddle point to the scission point in the case of heavy nuclei, and the properties of quasi-fission. A fairly complete summary is given of both the experimental data on all these aspects and the theoretical understanding based on current ideas about the fission process. © *1998 American Institute of Physics.*
[S1063-7796(98)00302-7]

INTRODUCTION

For many years now the diverse aspects of nuclear fission have been studied in numerous laboratories around the world. Nuclear fission is a phenomenon so complicated that even now there is no clear, comprehensive picture of it. At high nuclear excitation energies $E^* \geqslant 40-50$ MeV, when shell effects become unimportant and the nucleus loses its structural individuality, fission becomes simpler. Theoretical descriptions[1] show that in this case the fissioning nucleus can be treated as a drop of charged, incompressible nuclear liquid. The liquid-drop model (LDM) predicts a symmetric, single-humped distribution of fragments in mass and energy which is Gaussian in a first approximation. Numerous experimental studies have unconditionally confirmed this property of heated nuclei: the fission is predominantly symmetric, in contrast to the spontaneous and low-energy fission of actinide nuclei, which in the majority of cases split into unequal parts, and the individual shell properties of the fissioning nucleus and the fragments are clearly manifested. The observed universality of symmetric fission at higher excitations can serve as the experimental foundation for viewing the liquid-drop model as the basis for the theory of nuclear fission. In turn, the study of symmetric fission, in particular, such characteristics as the average fragment kinetic energy $\bar{E}_k$ and its variance σ_E^2, the nuclear "stiffness" (rigidity) $d^2V/d\eta^2$ to mass-asymmetric deformations η (this parameter is directly related to the experimentally observed variance of the mass distribution σ_M^2), the fission barriers $\bar{E}_f$, and the effective moments of inertia J_{eff}, provide a direct method of verifying the predictions of this model.

In our earlier review[2] we touched briefly on some problems in the fission of heated nuclei such as the formation of the fragment mass–energy distributions and the role played by the saddle point in this process. However, most of our attention in that study[2] was focused on nuclei in the neighborhood of lead, in connection with the discovery of the multimode fission of preactinide nuclei. In the present review we shall study the fission of heated nuclei in a wider range of compound-nucleus mass numbers $A_{\text{CN}} \sim 100-270$ and, accordingly, Z_{CN} in the range from 47 to 108.

All the nuclei in this range can be classified according to a simple feature: the presence or absence of the stage of descent from the top of the barrier to the scission point.

Nuclei with fissility parameter $Z^2/A \geqslant 32$ are characterized by the presence of this stage, the duration of which increases with increasing nuclear mass and which is associated with increased manifestation of dynamical effects in the fission process.[3] Alternative ideas about the role of the saddle point or the scission point in the formation of the fragment mass distributions in the fission of heavy nuclei have been around for a long time, but even the first heavy-ion experiments, in which the fragment mass and charge distributions were studied for nuclei with $Z^2/A > 33$ (Refs. 4 and 5), revealed a sharp increase in σ_M^2 (decreased stiffness) with increasing Z^2/A. This could not be described quantitatively or even qualitatively by the statistical model[6] or the dynamical model with zero viscosity.[7] It was then concluded that to make the calculations agree with experiment, it was necessary to use effective stiffnesses averaged over the entire path from the saddle point to the scission point in accordance with the time behavior of the process.[5]

Great progress in the theoretical description of the mass–energy distributions was made by Adeev *et al.* (see their review[3] and references therein), who used the dynamical diffusion model including two-body viscosity to explain the observed experimental trends in the behavior of σ_M^2 and

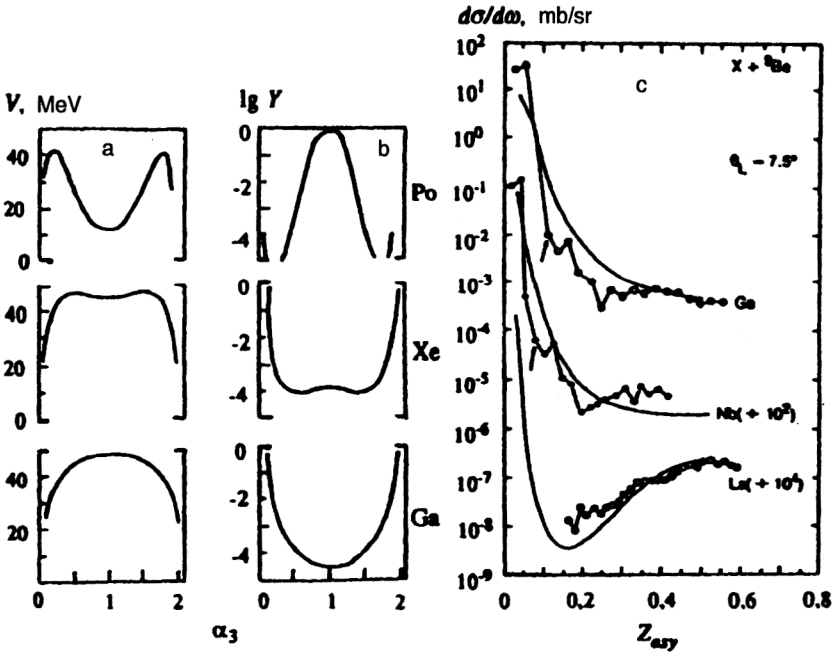

FIG. 1. (a) Theoretical calculations[18] of the potential energy V for Ga, Xe, and Po nuclei as a function of the mass-asymmetry coefficient α_3. (b) Fragment mass distributions calculated using the statistical approach[18] from the dependences $V(\alpha_3)$ for the same nuclei. (c) Experimental data[19] on the charge distribution of fragments from the reactions ^{74}Ge, ^{93}Nb, ^{139}La+^{9}Be.

σ_E^2 as a function of the nucleon content of the nucleus.

Other authors of theoretical[8] and experimental[9,10] studies have adopted different approaches to the study of fission dynamics. These authors studied the higher moments (3rd and 4th) of the fragment energy distributions, which turned out to be sensitive to the definition of the scission point. They solved one of the important, long-standing problems of fission physics: that of the neck thickness, zero or finite, at which scission occurs.

Section 4 of the present review is devoted to the experimental study of the dynamical aspects of the formation of the mass–energy distributions.

A completely different situation arises for light nuclei with $Z^2/A \leqslant 31$. For them the saddle point and the scission point are close together in both the deformation and the potential energy, and so the dynamics of the descent of the nucleus to the scission point hardly plays any role. The fission of these nuclei can be treated in the static approach, and it can be expected that the experimental data may serve as a test of the various classical (nondynamical) versions of the liquid-drop model,[11–16] which predict the existence (for zero angular momentum) of the Businaro–Gallone[17] (BG) point at which the nucleus becomes completely unstable to mass-asymmetric deformations η. This model predicts that the fragment mass distributions in the fission of nuclei above this point in Z^2/A should be nearly Gaussian, and that in approaching this point they should greatly broaden and become flat in a large neighborhood of $A/2$ at the BG point. For even lighter nuclei they should become U-shaped.[18–20] This is illustrated in Fig. 1 (Refs. 18 and 20), which shows (a) the theoretical calculations of the nuclear potential energy V as a function of the mass asymmetry for these nuclei;[18] (b) the corresponding fragment mass distributions calculated from $V(\alpha_3)$ in the statistical approach;[18] and (c) the experimental data of Ref. 19 on the fragment charge distributions in the fission of the compound nuclei ^{83}Kr, ^{102}Rb, and ^{148}Pm.

The locations of the BG point on the mass-number axis differ strongly in different versions of the LDM. For example, in the simple Myers–Swiatecki model[13] with sharp nuclear boundary this point lies at $Z^2/A \sim 19$ for the β-stability valley, while in the Krappe–Nix–Sierk[15] or Sierk[16] models, which include short-range nuclear forces and diffuse nuclear boundary, it lies at $Z^2/A \sim 22–23$ (depending on the parameters).[3,21,22] Therefore, the actual location of this point on the mass-number axis is of fundamental importance for choosing a model which describes experiment.

Light nuclei near the BG point have a low fission probability which falls off exponentially with decreasing Z^2/A. This makes the study of the fragment mass–energy distributions in reactions involving light charged particles with energy $<80–100$ MeV (low ℓ) difficult.[23–26] It is therefore most reasonable to use ions which are not very heavy ($A \leqslant 30$) in reactions in which the fission probability grows significantly with increasing ℓ (Refs. 27–34). Section 3 of this review is devoted to the experimental studies of the fragment mass–energy distributions near the BG point which we determined earlier.[22,35]

In heavy-ion reactions it is easy to reach excitation energies at which the nucleus is so heated that its shell properties can be neglected. However, then the nucleus acquires a significant angular momentum ℓ, which begins to strongly affect the features of the fission process, as it greatly changes the shape of the fissioning nucleus and lowers the fission barrier.[16,36] This in the end leads to a difference between the experimentally observed characteristics of the fragment mass–energy distributions and the characteristics for a nonrotating nucleus. Comparison with the theoretical predictions of the LDM[11–16] therefore requires accurate knowledge of the experimental ℓ dependence of the mass–energy distributions. This is the subject of Sec. 2 of this review.

The multiplicities of prefission neutrons $\bar{\nu}_{pre}$ have been

studied intensively in recent years. For highly excited nuclei, these turned out to be significantly larger than the values predicted by the standard statistical model. These results suggest that fission is a rather slow, high-friction process, owing to the manifestation of the viscosity of nuclear matter.[37] The emission of these neutrons ν_{pre} greatly reduces the excitation energy (or temperature) of the fissioning nucleus.

The statistical analysis of the experimental data requires knowledge of only the temperature at which the nucleus actually undergoes fission, and, accordingly, this requires knowledge of the exact number of prefission neutrons. There is a great deal of experimental data on $\bar{\nu}_{\text{pre}}$ in the literature, but naturally they do not encompass all the nuclei and energies needed for analyzing the mass–energy distributions. The authors of Refs. 22 and 38 constructed an empirical systematics of the number $\bar{\nu}_{\text{pre}}$ allowing the determination of the effective temperature of the fissioning nucleus after the emission of prefission neutrons $\bar{\nu}_{pre}$. Section 1 of this review is devoted to this problem.

The first two sections of this review are thus a sort of prelude to the last two, dealing with the analysis of the mass–energy distributions. At the same time, the first two sections are of independent interest. This work is based on experiments in which the authors have been involved at the Alma-Ata isochronous cyclotron to study reactions involving light charged particles, and at the Nuclear Reaction Laboratory of the JINR, Dubna, using heavy-ion beams. The present study is a continuation of our series of studies of the characteristics of nuclear fission; see our earlier reviews.[2,39]

1. THE EMISSION OF PRE- AND POST-FISSION NEUTRONS AND THE EFFECTIVE TEMPERATURE OF HEATED FISSIONING NUCLEI

1.1. General ideas

The experimental study of the yields of neutrons accompanying fission has developed rapidly in recent decades, especially for heavy-ion reactions.[40–56] (See also the reviews on this subject.[37,57,58]) These studies have focused on the regularities in multiple neutron emission $\bar{\nu}$ at excitation energies E^* at which the fission process becomes an emission process. In this case, the observed yields $\bar{\nu}$ contain a significant contribution of prefission neutrons $\bar{\nu}_{\text{pre}}$ emitted not from fragments ($\bar{\nu}_{\text{post}}$), but from the fissioning nucleus before it splits.

Analysis of the experimental results has shown that the magnitude and energy dependence of the two components of the total neutron multiplicity,

$$\bar{\nu}_t(E^*)=\bar{\nu}_{\text{pre}}(E^*)+\bar{\nu}_{\text{post}}(E^*), \tag{1}$$

are unexplained within the traditional statistical ideas, because at average excitation energies $E^*\sim 50-100$ MeV the number $\bar{\nu}_{\text{pre}}$ turned out to be much larger (by almost an order of magnitude in the case of actinide nuclei) than predicted by statistical models. The theoretical description of the dependence $\bar{\nu}_{\text{pre}}(E^*)$ required consideration of the dynamics of the fission process, including such characteristics as the viscosity of nuclear matter (see, for example, the reviews[37,59]).

According to the present ideas, which have a broad experimental foundation, up to the threshold of emission fission, neutrons are emitted predominantly from excited fragments accelerated in the field of their mutual Coulomb repulsion, i.e., $\bar{\nu}_t\cong\bar{\nu}_{\text{post}}$. The emission of post-fission neutrons itself is described by the evaporation model. It is isotropic in the fragment rest frame, but strongly anisotropic in the lab frame, where the angular distribution takes the form of fairly narrow rosettes in the fragment motion. This feature is used to separate post-fission neutrons from pre-fission ones. The primary emission mechanism for the latter is, as for post-fission neutrons, evaporation (equilibrium, isotropic in the c.m. frame). A fraction of the pre-fission neutrons associated with the start of the emission chain is emitted directly as a result of the nonequilibrium interaction of the bombarding particle with the nucleus. Such neutrons can be distinguished from the shape of their angular and energy distributions (see, for example, Refs. 40–43 and 55.

The emission of post-fission neutrons only slightly affects the observed characteristics of the fission process, for example, the fragment mass–energy distributions, and the magnitude of the effect and of the corresponding corrections depends on the measurement method.[60–62] The emission of pre-fission neutrons has very serious consequences, as it globally affects the entire fission process. It leads to new possibilities, "chances," for the fission process, bringing into play reactions in which nuclei with smaller mass and excitation energy undergo fission. This creates serious difficulties in the study of the energy dependence of the fission characteristics. It is said that fission acquires an emission nature. The distortions arising for a given characteristic are determined by $\bar{\nu}_{\text{pre}}$. As a rule, they are considerably larger than the effects associated with neutron emission from fragments, and they cannot be diminished or eliminated by changing the measurement technique, as in the case of $\bar{\nu}_{\text{post}}$. For this reason, we shall mainly focus on the component $\bar{\nu}_{\text{pre}}$. In emission fission, a nucleus with initial excitation energy E^* can undergo fission in one of (A_t,xnf) reactions, where A_t refers to the bombarding particle, and $x=0,1,\ldots,x_{\max}(E^*)$ is the number of neutrons which can be emitted before fission. Each such reaction gives a contribution $\sigma_{fx}(E^*)$ to the total fission cross section:

$$\sigma_f(E^*)=\sum_{x=0}^{x_{\max}(E^*)}\sigma_{fx}(E^*) \tag{2}$$

and the average yield of pre-fission neutrons is

$$\bar{\nu}_{\text{pre}}(E^*)=\sum_{x=0}^{x_{\max}(E^*)} x\,\frac{\sigma_{fx}(E^*)}{\sigma_f(E^*)}. \tag{3}$$

Any characteristic of emission fission is a superposition (average)

$$\begin{aligned}\bar{F}(E^*,A)&=\sum_{x=0}^{x_{\max}(E^*)}F_{A-x}(E^*-\bar{E}_\nu x)\,\frac{\sigma_{fx}(E^*)}{\sigma_f(E^*)}\\ &\cong F_{A-\hat{x}}(E^*)-\bar{E}_\nu\bar{\nu}_{\text{pre}}(E^*)\,\frac{dF_{A-\hat{x}}(E^*)}{dE^*}+\cdots\\ &\cong F_{A-\hat{x}}(E^*-\bar{E}_\nu\bar{\nu}_{\text{pre}}),\end{aligned} \tag{4}$$

where $F_{A-\hat{x}}(U_x)$ is the same characteristic for the residual nucleus $A-\hat{x}$ with excitation energy $U_x=E^*-\bar{E}_\nu x$, $\bar{E}_\nu$ is the average neutron separation energy for the neutron cascade, including the binding energy and the kinetic energy ε, i.e.,

$$\bar{E}_\nu=\bar{B}_n+\bar{\varepsilon}, \tag{5}$$

and $\hat{x}$ is the integer closest to $\bar{\nu}_{\text{pre}}$. The approximate equality in (4) indicates that the observables depend on the number of neutrons emitted before fission and the method of introducing corrections for this effect. The assumption that a change of the mass number $A\to A-\hat{x}$ has much less effect than a change of the excitation energy $E^*\to E^*-\bar{E}_\nu\bar{\nu}_{\text{pre}}$ now becomes obvious for most characteristics, and we shall neglect it.

1.2. The empirical systematics of $\bar{\nu}_{\text{pre}}$ and $\bar{\nu}_{\text{post}}$

Although there is quite a large amount of experimental data on $\bar{\nu}_{\text{pre}}$ and $\bar{\nu}_{\text{post}}$, it naturally does not encompass all the nuclei and energies needed for analyzing characteristics such as the fragment mass–energy distributions. The theory in this area has not progressed to the point of being able to predict all the observed regularities of the pre- and post-neutron yields. Therefore, the authors of Refs. 38 and 22 developed and then improved an empirical systematics, based on the above-cited experimental studies, of the multiplicities $\bar{\nu}_{\text{pre}}$ and $\bar{\nu}_{\text{post}}$ as functions of A and E^* of fissioning nuclei.

As an example, in Fig. 2 we show a selection of the original experimental data on the energy dependence for the nuclei which have been studied in greatest detail.[46,47,49,51] It shows that in both cases the total neutron yield is satisfactorily described as a linear function of E^*, the excitation energy of the initial compound nucleus. We also see that these functions and their derivatives with respect to E^* are monotonic and vary rather slowly with the mass number A. This allows the creation of a fairly simple approximation for the dependence of the two components of the neutron yield on these two parameters of the fissioning nucleus.

In Fig. 3 we show the A and E^* dependences of $\bar{\nu}_{\text{pre}}$ and $\bar{\nu}_{\text{post}}$. The "experimental" points were obtained by linear interpolation or extrapolation of the energy dependences, examples of which are given in Fig. 2 (solid lines). As a rule, they pertain to specific initial compound nuclei. The exception is the group U–Cm, and in Fig. 3 we indicate the range of their mass numbers. The linear dependence on A holds well for $\bar{\nu}_{\text{pre}}$. The family $\bar{\nu}_{\text{pre}}(A,E^*)$ as a whole has the form of a set of lines $E^*=\text{const}$ diverging with increasing A and described by the expression

$$\bar{\nu}_{\text{pre}}(A,E^*)=1.98-0.0133A-0.0376E^*+0.00042AE^*. \tag{6}$$

In contrast, the analogous family $\bar{\nu}_{\text{post}}(A,E^*)$ is a set of diverging lines which curve:

$$\bar{\nu}_{\text{post}}(A,E^*)=-4.52-0.0017A+0.0705E^* +0.000155A^2-0.000216AE^*. \tag{7}$$

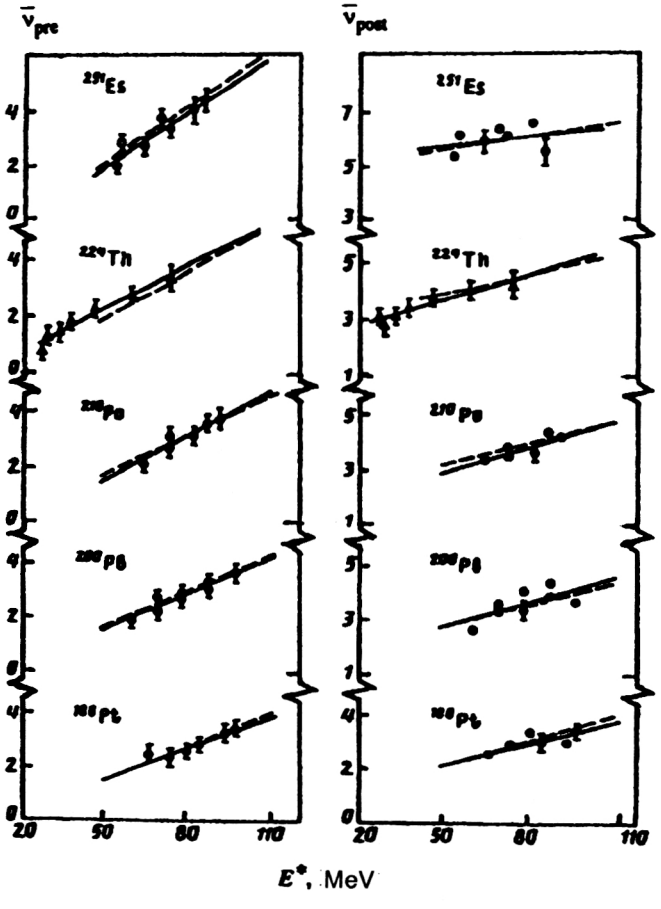

FIG. 2. Examples of the energy dependences of the neutron yields[38] $\bar{\nu}_{\text{pre}}$ and $\bar{\nu}_{\text{post}}$ for various nuclei and their linear description. The solid lines are for the least-squares method, and the dashed lines are for the systematics (6) and (7). The experimental data are from Refs. 46, 47, 49, 51.

The straight line in Fig. 3 approximately reproduces the observed dependence $\bar{\nu}_{\text{post}}(A,0)$ for spontaneous fission. We stress the fact that the quadratic term $\sim A^2$ in (7) "bends" the family of lines in Fig. 3, in qualitative agreement with the behavior of $\bar{\nu}_{\text{post}}(A,0)$.

The accuracy of the description of $\bar{\nu}_{\text{pre}}$ and $\bar{\nu}_{\text{post}}$ is estimated from (6) and (7) to be[38] 6–7% for excitation energies $E^*\leqslant 110$ MeV.

At higher excitation energies ($\geqslant 120$–250 MeV) the nuclear deexcitation process is more complicated: a significant number of preequilibrium neutrons ν_{pe} and protons appear (this probably depends on the type of incident ion[40,43]). These carry off a significant fraction of the excitation energy ΔE_{pe}, which, in general, is difficult to take into account exactly. Measurements of the spectra of fission neutrons have been used[40–43,55] to extract the values of $\bar{\nu}_{\text{pe}}$ and $\Delta\bar{E}_{\text{pe}}$ for various reactions and to estimate the nuclear excitation energies E^{**} after emission of $\bar{\nu}_{\text{pe}}$. Figure 4 shows the systematized[22] data, for various ranges of nuclei, on the experimentally measured values of $\bar{\nu}_{\text{pe}}$ and $\Delta\bar{E}_{\text{pe}}$, which can be used to estimate E^{**}.

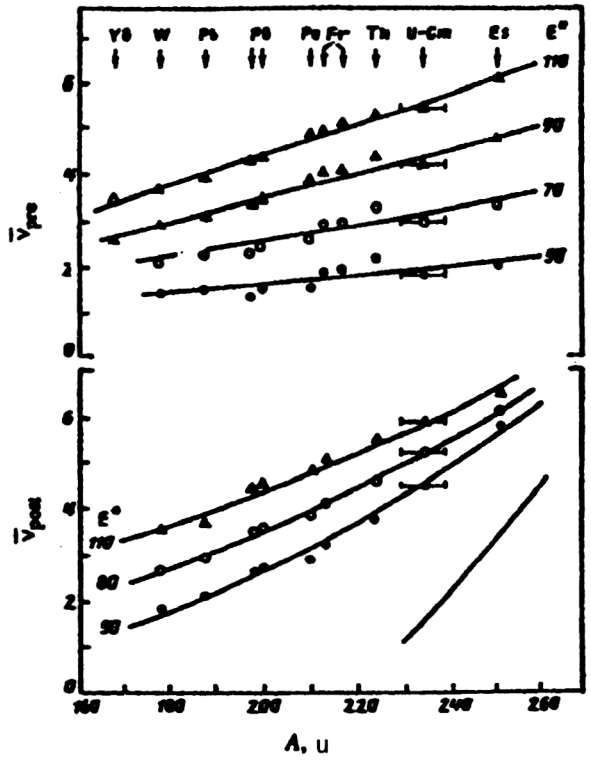

FIG. 3. Dependence of $\bar{\nu}_{pre}$ and $\bar{\nu}_{post}$ on the mass number A and the excitation energy E^* of the fissioning nucleus. The lines reproduce the description of the points according to (6) and (7), obtained by interpolation and extrapolation of the linear dependences $\bar{\nu}_{pre}(E^*)$ and $\bar{\nu}_{post}(E^*)$, examples of which are shown by the solid lines in Fig. 2. The line at the bottom describes the dependence $\bar{\nu}_{post}(A,0)$ for spontaneous fission.

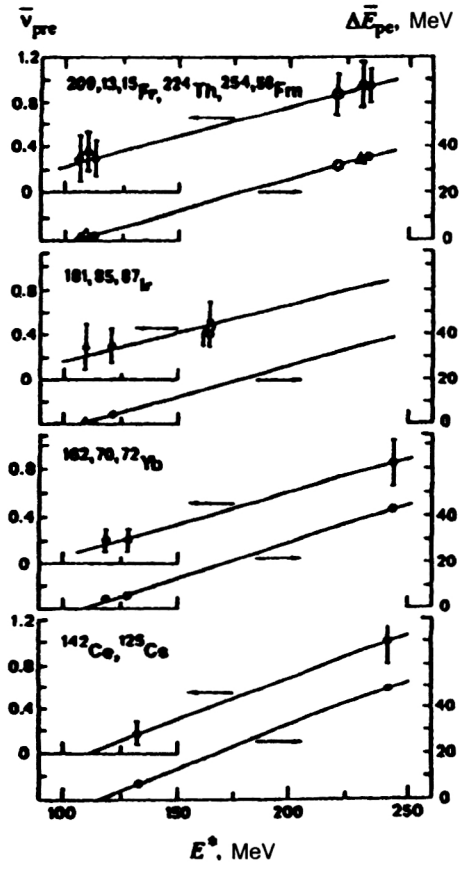

FIG. 4. Systematics[22] of the average number of preequilibrium neutrons $\bar{\nu}_{pe}$ and the energy transfer $\Delta\bar{E}_{pe}$ for the indicated ranges of nuclei as functions of the excitation energy E^* in various reactions. The data are from Refs. 43 and 55.

Analysis[22] shows that the empirical expression (6) can give a fairly good description of $\bar{\nu}_{pre}$ for given Z and E^* only in the range $A=(A_\beta-5)\pm3$, where A_β is the mass number of the fissioning nucleus with a given Z for the β-stability valley:

$$A_\beta-2Z=0.4A_\beta^2/(A_\beta+200), \tag{8}$$

where $(A_\beta-5)$ is the average value of the mass number of the fissioning neutron-deficient nucleus, usually obtained in heavy-ion reactions. Most of the experimental data on the multiplicity $\bar{\nu}_{pre}$ analyzed in Ref. 38 were obtained close to this value for various Z. The systematics (6) does not reproduce the isotopic dependence in a wider range of A than that indicated. Since in the data used below for analyzing the mass–energy distributions the length of the isotopic chains can reach $\Delta N\sim12$, this systematics was improved in Ref. 22 by introducing the corresponding parameter.

It should be noted immediately that in the literature there is little experimental information on the isotopic dependence of $\bar{\nu}_{pre}$ for various nuclei, and the authors of Ref. 22 used a variety of data obtained in reactions involving heavy ions from ^{12}C to ^{40}Ar. In Fig. 5a we show the energy dependence of $\bar{\nu}_{pre}$ for three isotope chains of the nuclei Fr, Pb, and Yb (here the results of Refs. 40, 43, 47–50, 55, 57, and 58 have been used). For the data with $E^*>115$ MeV from Refs. 40, 49, and 55 the excitation energy has been corrected by $\bar{\nu}_{pe}$ and $\Delta\bar{E}_{pe}$ in accordance with Fig. 4. In comparing the yields $\bar{\nu}_{pre}$ at $E^*=$const (dot–dash lines), the lack of experimental data forced us to extrapolate it in small ranges for some isotopes using the linearity of the dependence of $\bar{\nu}_{pre}$ on E^* (solid lines). The data shown in this form in Fig. 5a suggest the presence of a rather strong isotopic dependence of $\bar{\nu}_{pre}$, and Fig. 5b demonstrates it for the same nuclear chains at fixed Z and E^*. The dashed lines correspond to the calculations using Eq. (6) with fixed excitation energy. It is clearly seen that the values of $\bar{\nu}_{pre}$ are described satisfactorily in a rather narrow range of A. The solid lines show the results of the calculations using the improved[22] systematics:

$$\bar{\nu}_{pre}^{A}=\nu_{pre}^{A_\beta}-0.0055\delta^2+0.071\delta+0.30, \tag{9}$$

where $\delta=(A-A_\beta)$, A_β is as before the value of A for the β-stability valley (8) at fixed Z, and $\bar{\nu}_{pre}^{A_\beta}$ is the value of $\bar{\nu}_{pre}$ calculated from (6) for $A=A_\beta$. The coefficients in (9) were fitted to obtain the best description of $\bar{\nu}_{pre}(A)$ in Fig. 5b. Therefore, the calculations using Eqs. (6) and (9) must give values of $\bar{\nu}_{pre}^{A}$ very close to experiment. The good agreement between the improved systematics and the earlier, unstudied data of Refs. 55, 63, and 64 was demonstrated in Ref. 22.

Now the known number $\bar{\nu}_{pre}$ for a specific reaction can be used to calculate the effective temperature of the rotating

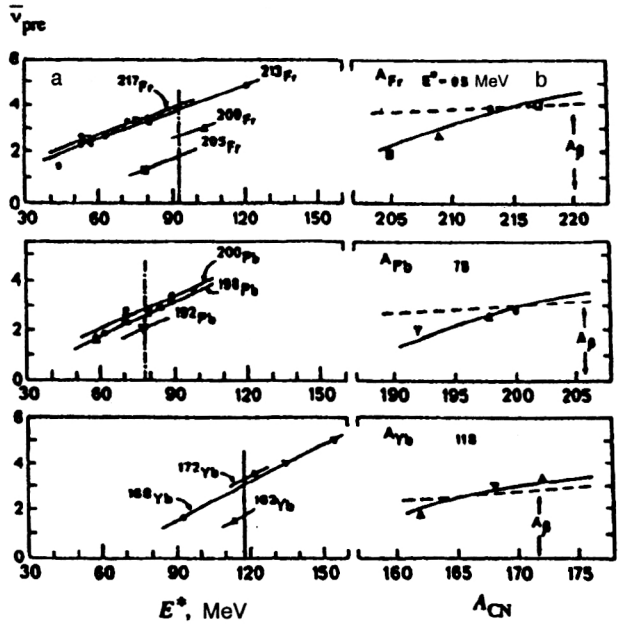

FIG. 5. (a) Energy dependence of the multiplicity $\bar{\nu}_{pre}$ for chains of Yb, Pb, and Fr isotopes.[22] The data are from Refs. 43, 49, 50, 55, 57, and 58. (b) Dependence of $\bar{\nu}_{pre}$ on A_{CN} at the fixed E^* shown by the dot–dash lines in Fig. 5a. A_β is the value of A_{CN} for the β-stability valley (8). The dashed lines were calculated using the systematics (6), and the solid lines using the systematics (6) and (9).

nucleus at the saddle point after the emission of $\bar{\nu}_{pre}$ when, of course, the initial excitation E^*, $\tilde{E}^*$, $E^*(\ell)$, and the temperature θ^0_{sp} are known:

$$E^*=E_{CM}+(\Delta M_i+\Delta M_t-\Delta M_{CN}), \quad (10)$$

$$\tilde{E}^*=E_{CN}+(\Delta M_i+\Delta M_t-\Delta \tilde{M}_{CN}), \quad (11)$$

$$E^*(\ell)=\tilde{E}^*-E^{gs}_{rot}(\ell), \quad (12)$$

$$\theta^0_{sp}=\{[E^*(\ell)]/a\}^{1/2}, \quad (13)$$

$$\theta^{ef}_{sp}=\{[E^*(\ell)-\bar{\nu}_{pre}\bar{E}_\nu-\tilde{E}_f(\ell)]/a\}^{1/2}. \quad (14)$$

In these expressions (10)–(14), E^* is calculated using the experimental values of the ion ΔM_i, target ΔM_t, and compound-nucleus ΔM_{CN} mass defects from Ref. 65, $\tilde{E}^*$ is calculated using the liquid-drop values of the mass defect for $\Delta \tilde{M}_{CN}$ from Ref. 66, $E^*(\ell)$ is calculated with inclusion of the rotational energy of the nucleus in the ground state $E^{gs}_{rot}(\ell)$ using the Sierk LDM[16] or the Cohen–Plasil–Swiatecki LDM for rotating nuclei,[36] $E_f(\ell)$ is the fission barrier, and a is the level-density parameter, usually taken to be $a=A/8$ or $a=0.093A$. In addition, in Refs. 22, 35, and 67 it was assumed that each emitted neutron decreases the nuclear angular momentum by $2\hbar$.

1.3. Theoretical aspects of the neutron emission dynamics ν_{pre}

In Refs. 21, 22, 35, 67, and 68 in finding the temperature θ^{ef}_{sp} (14) it was implicitly assumed that all neutrons $\bar{\nu}_{pre}$ are emitted before reaching the saddle point. For light nuclei with $Z^2/A\leqslant 30-32$, where there is practically no stage of descent from the saddle point, this assumption is well justified. However, for heavy actinide nuclei it is most probably not valid, because for these nuclei the saddle and scission configurations are separated by a fairly long descent stage, and if fission is a slow process, as now generally assumed,[37] some fraction of the total $\bar{\nu}_{pre}$ can be emitted during this descent.

When studying the fragment mass distributions, it is desirable to know what part of $\bar{\nu}_{pre}$ is emitted before the fragment formation region and what part is emitted after it, as the second part of $\bar{\nu}_{pre}$ is not very important for determining the actual temperature. Even ten years ago there were alternative ideas about the role of the saddle point or the scission point in fragment mass formation. At present, the following can be stated on the basis of the experimental (Refs. 2, 4, 5, 21, 22, 26, 35, and 67–70) and theoretical[3] (using the diffusion model) studies: for nuclei with $Z^2/A\leqslant 33$ the fission barrier dominates, while for heavier nuclei the descent stage dominates, and the heavier the nucleus, the more the saddle point is "forgotten." We shall discuss this in more detail later, and for now we return to $\bar{\nu}_{pre}$. Unfortunately, there is no direct experimental information on the amount of $\bar{\nu}_{pre}$ emitted in the early stages of the fission process.

Recent theoretical approaches to describing $\bar{\nu}_{pre}$ have been developed in Refs. 59, and 71–80 on the basis of Langevin dynamics[59,71–75,78] of the diffusion model[76,77] and the statistical model with delayed fission.[79,80] One of the important features of the models of Refs. 59 and 71–78 is the dimensionless parameter describing the damping of the collective motion for the fission mode[81,82] $\gamma=\beta/2\omega_0$, where β is the damping coefficient characterizing the viscosity of nuclear matter and $\omega_0\sim 1\times 10^{21}$ sec^{-1} is the frequency of the oscillator describing the potential energy V at the top of the barrier.

In Refs. 59 and 72–75 the coefficient β is not a given constant, but depends on the basic fission deformation: from the ground state until the neck appears $\beta=\text{const}=2\times 10^{21}$ sec^{-1}, and then up to the scission point β grows linearly to 30×10^{21} sec^{-1}. This behavior of β is not rigorously justified, but in Ref. 72 is motivated by the fact that for $\beta=\text{const}$ it is impossible to describe simultaneously the fission probability, which requires small viscosity $\beta=2-3\times 10^{21}$ sec^{-1}, and $\bar{\nu}_{pre}$, which requires on the average $\beta=20\times 10^{21}$ sec^{-1}. The behavior of β in Refs. 59 and 72–75 can be understood qualitatively if it is assumed that in the fissioning nucleus it is as if the two-body dissipation mechanism dominates (in magnitude) until the neck is formed, and so small values of β characterize the situation, while after the neck is formed and as it becomes thinner it is as though a mechanism like surface friction with large β dominates, as required to describe the fusion process, which in some respects is the reverse of fission.[83] With this behavior of β, universal for all nuclei, it proved possible[59,72–75] to reproduce satisfactorily reproduce both the fission probability and $\bar{\nu}_{pre}$ for a wide range of nuclei from ^{178}W to ^{251}Es.

However, it should be noted that such an "exotic" dependence of β on the deformation may not be required for

the simultaneous description of the fission characteristics.[59,72–75] For example, the authors of Ref. 78 used the standard wall-and-window one-body dissipation mechanism, including the temperature dependence of the surface energy, which tends to lower the fission barrier, and were able to reproduce simultaneously the fusion cross section, the fission cross section, the fragment evaporation cross section, $\bar{\nu}_{pre}$, and $\bar{E}_k$, the average total fragment kinetic energy, though only for the single nucleus ^{200}Pb at two excitation energies. It is interesting that those authors[78] also attempted to describe all these characteristics by using the two-body dissipation mechanism, and succeeded in reproducing everything but $\bar{E}_k$. It turned out to be much smaller than the experimental values.

Back[76] also satisfactorily described the energy dependence of $\bar{\nu}_{pre}$ for the nuclei ^{213}Fr, ^{224}Th, and ^{251}Es without using a deformation-dependent β. He used $\gamma=5$ ($\beta=$const $\sim 10\times 10^{21}$ sec^{-1}), but did not consider or describe the fission probability.

Returning to the models of Refs. 72–75, the results for which are summarized in Ref. 59, it should be stressed that they are best developed for the theoretical analysis of $\bar{\nu}_{pre}$ and, moreover, in describing the dependence $\bar{\nu}_{pre}(\tilde{E}^*)$ they include the splitting of the total $\bar{\nu}_{pre}$ into two components needed for analyzing the mass–energy distributions: $\bar{\nu}^{gs}_{pre}$, the number of neutrons from the ground state (before the barrier), and $\bar{\nu}^{ss}_{pre}$, the number from the descent from the saddle point to the scission point:

$$\bar{\nu}_{pre}=\bar{\nu}^{gs}_{pre}+\bar{\nu}^{ss}_{pre}. \qquad (15)$$

Unfortunately, this model was not used to describe the fragment mass–energy distributions, and it is not known whether or not the fragment kinetic energy and the mass and energy variances can in general be reproduced by using the variable β, especially since the amount $\bar{\nu}_{pre}$ emitted before the mass formation is unknown. However, the model can be viewed as a first approximation and used to calculate the temperature θ^{ef}_{sp} with the number $\bar{\nu}^{gs}_{pre}$, which for heavy nuclei with a long descent corresponds better to reality than use of the total number $\bar{\nu}_{pre}$.

Another important aspect of this problem is the effect of the angular momentum ℓ on $\bar{\nu}_{pre}$. In the experimental studies of Refs. 21, 22, 35, 38, 67, and 70 it was assumed that there is no ℓ dependence up to excitation energies $\tilde{E}^*$ $\sim$100–110 MeV, as is confirmed by direct experimental data for ^{160}Yb (Ref. 64) and ^{200}Pb (Refs. 45 and 47). However, at higher energies $\sim$160 MeV it is present in the experiment of Ref. 43 and in the theoretical studies of Ref. 71, 72, 84, and 85. This is seen in Fig. 6a, where we show the experimental and theoretical dependence of $\bar{\nu}_{pre}$ on $\tilde{E}^*$ for ^{198,200}Pb. The open symbols show the data obtained in the reaction ^{19}F+^{181}Ta, and the closed circles and triangles show the data for the reactions ^{30}Si+^{170}Er and ^{28}Si+^{170}Er, respectively.[45,47] The solid lines are the theoretical calculations of $\bar{\nu}_{pre}$ from Refs. 59, 72, and 75 for the reactions involving ^{19}F and ^{30}Si, and the dashed lines give the components $\bar{\nu}^{ss}_{pre}$ for these reactions. It is clearly seen that the experimental points for all three reactions coincide with each other within the errors, and that the theoretical curves disagree: for the reaction involving ^{30}Si the calculated result is clearly too low. In Fig. 6b we show the theoretical dependences of the components $\bar{\nu}^{gs}_{pre}$ in percent of the total $\bar{\nu}_{pre}$ obtained from the calculations in Fig. 6a for the same reactions. The curves strongly disagree at high excitations. Accordingly, in analyzing the mass–energy distributions in Ref. 70 the theoretical dependence of $\bar{\nu}^{gs}_{pre}$ and $\bar{\nu}^{ss}_{pre}$ on ℓ was neglected, and the values of $\bar{\nu}^{gs}_{pre}$ calculated for reactions of the type ^{16}O+X and ^{19}F+X were used, because reactions close to these play an important role in the analysis of the experimental data on the mass distributions in Ref. 70.

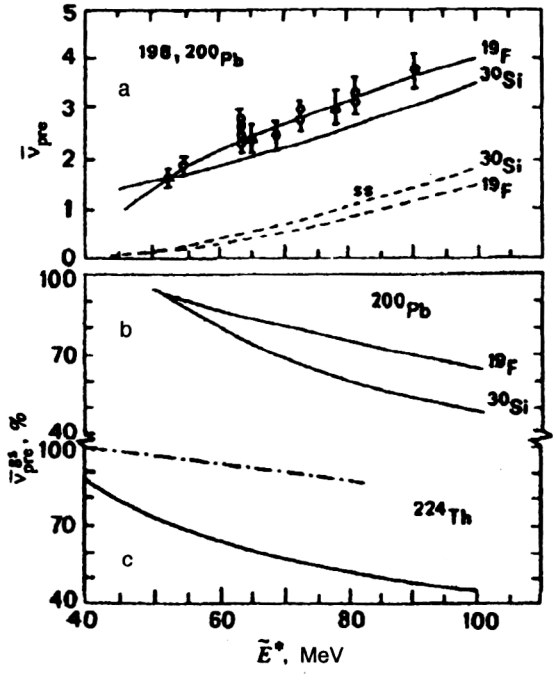

FIG. 6. (a) Dependence of the experimental[45,47] (points) and theoretical[59,72,75] (solid lines) numbers $\bar{\nu}_{pre}$ for compound nuclei ^{198,200}Pb on the excitation energy $\tilde{E}^*$ in the reactions ^{19}F+^{181}Ta, ^{30}Si+^{170}Er, and ^{28}Si +^{170}Er. Theoretical calculations[59,72,75] were made for the first two reactions. The dashed lines are the calculation of the part of the total $\bar{\nu}_{pre}$ emitted during the descent, $\bar{\nu}^{ss}_{pre}$, for these reactions. (b) Calculated dependence[59,72,75] of the number of neutrons (in % of the total $\bar{\nu}_{pre}$) emitted before the fission barrier, $\bar{\nu}^{gs}_{pre}$, on $\tilde{E}^*$ for ^{200}Pb in the same reactions as in Fig. 6a. (c) Theoretical $\tilde{E}^*$ dependences of $\bar{\nu}^{gs}_{pre}$ for the compound nucleus ^{224}Th formed in the reaction ^{16}O+^{208}Pb, calculated in Refs. 59, 72, and 75 (solid line) and in Ref. 76 (dot–dash line) in % of the total number $\bar{\nu}_{pre}$.

Figure 6c shows how the values of $\bar{\nu}^{gs}_{pre}$ can differ in different theoretical approaches: the solid line shows the values calculated in Refs. 59 and 72–75, and the dot–dash line shows the results of the Back study[76] for the same nucleus ^{224}Th. This difference is a consequence of the behavior of β near the ground state. In Refs. 59 and 72–75 the values of β are small (2×10^{21} sec^{-1}) and the neutron fraction $\bar{\nu}^{gs}_{pre}$ is small, while in Ref. 76 the coefficient β is independent of the deformation and large (10×10^{21} sec^{-1}) and the fraction $\bar{\nu}^{gs}_{pre}$ is significant.

Recently, $\bar{\nu}_{pre}$ and its components were calculated for ^{250}Cf (Ref. 86) using the model of Ref. 59. It was found that as ℓ increases from 0 to 30$\hbar$, $\bar{\nu}_{pre}$ actually remains the same, but $\bar{\nu}^{gs}_{pre}$ is decreased by a factor of $\sim$1.5. There are direct experimental data on $\bar{\nu}_{pre}$ for the fission of ^{248}Cf produced in two reactions: ^{11}B+^{237}Np and ^{16}O+^{232}Th (Ref. 56), which show that $\bar{\nu}_{pre}$ is higher, though slightly, for the second reaction at the same excitation energy $E^*\sim$60 MeV. This fundamentally contradicts the model of Refs. 59 and 72–75, and in Ref. 56 was attributed to the large dynamical delay time for the heavier ion in the process of ion–target fusion and formation of the compound nucleus.

We shall see that the model of Refs. 59 and 72–75 is not free of defects and incompletely justified assumptions. However, at present it is the model which is best developed and tested for describing $\bar{\nu}_{pre}$ in a fairly wide range of nuclei. Another fact in its favor is that the splitting of the total $\bar{\nu}_{pre}$ into $\bar{\nu}^{gs}_{pre}$ and $\bar{\nu}^{ss}_{pre}$ is apparently confirmed in Ref. 87 in describing the energy dependence of the anisotropy of the fission fragments from ^{224}Th in the reaction ^{16}O+^{208}Pb, where the flattening of the anisotropy at high excitation energies can be satisfactorily described by using $\bar{\nu}^{gs}_{pre}$ from Refs. 72–75
and not with β=const=20×10^{21} sec^{-1}. However, this feature of the anisotropy can again be explained without resorting to the idea of $\bar{\nu}^{gs}_{pre}$, as demonstrated earlier[88] for lighter nuclei.

The strong and weak points of the model of Ref. 59 and 72–75 were evaluated in Ref. 70 on the basis of its results for $\bar{\nu}^{gs}_{pre}$, and a simple systematics was constructed for $\bar{\nu}^{gs}_{pre}$ as a function of the excitation energy $\tilde{E}^*$ and the fissility parameter x:[13]

$$x=\frac{Z^2/A}{50.883(1-1.7826[(N-Z)/A^2])}. \tag{16}$$

This is shown in Fig. 7 for $\tilde{E}^*$=50, 75, and 100 MeV in percent of the total number $\bar{\nu}_{pre}$. Here we clearly see that on the logarithmic scale $\bar{\nu}^{gs}_{pre}$ is linear in x in two ranges, and has a kink at x=0.745. The solid lines are the empirical description

$$\log\bar{\nu}^{gs}_{pre}(\%)=0.0056\tilde{E}^*-0.1115x-0.0116\tilde{E}^*x+2.16 \quad \text{for } x\leqslant0.745,$$

$$\log\bar{\nu}^{gs}_{pre}(\%)=0.0188\tilde{E}^*-6.734x+0.0198\tilde{E}^*x+7.17 \quad \text{for } x>0.745. \tag{17}$$

We see that for $\tilde{E}^*\leqslant$100 MeV, $\bar{\nu}^{gs}_{pre}$ differs from the total $\bar{\nu}_{pre}$ (100%) beginning at $x\sim$0.6: up to this value of x practically all the neutrons are emitted before reaching the saddle point. The picture is reversed in the case of very heavy nuclei. For example, for $x\sim$0.9 only 10–12% of the neutrons are emitted before reaching the barrier and $\sim$90% are emitted during the descent. On the whole, this makes sense, because nuclei in this range of x have fission barriers $\tilde{E}^*_f\leqslant$1 MeV (for ℓ=0), and are close in deformation to the ground state, so that the entire nuclear deexcitation process occurs during the descent stage.

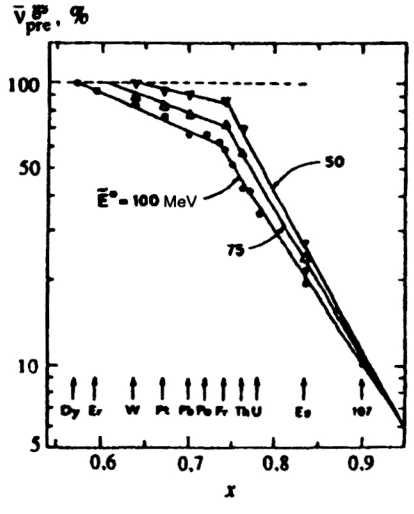

FIG. 7. Theoretical calculations[59,72,75] (all points) of the dependence of $\bar{\nu}^{gs}_{pre}$ (in % of the total $\bar{\nu}_{pre}$) on the fissility parameter x at three values of the excitation energy: $\tilde{E}^*$=50, 75, and 100 MeV. The solid lines are the description of $\bar{\nu}^{gs}_{pre}(x,\tilde{E}^*)$ according to Eq. (17) (Ref. 70).

Let us consider variants of the possible neutron emission stages and the effect of this factor on determining the temperature of the fissioning nucleus:

1. Neutrons are not emitted before reaching the saddle point, and the temperature at the barrier is calculated by (13), i.e., as the initial value θ^0_{sp}.

2. All the neutrons $\bar{\nu}_{pre}$ for any nucleus are emitted before reaching the barrier. Then we find the temperature at the saddle point from (14) and denote it by θ^{ef1}_{sp}.

3. A number of neutrons $\bar{\nu}^{gs}_{pre}$ given by (17) is emitted before reaching the barrier. The temperature is determined as in the preceding case, but instead of the total $\bar{\nu}_{pre}$ we use $\bar{\nu}^{gs}_{pre}$ and denote the temperature by θ^{ef2}_{sp}.

When applied to analysis of the mass–energy distributions, these three methods of determining the temperature implicitly contain the assumption that the mass distribution is formed at the saddle point. Let us consider an alternative assumption: that the mass distribution is formed at the scission point, as assumed for actinide nuclei in Refs. 89–92.

Here we denote the thermal excitation energy of the nucleus at the scission point and the corresponding temperature by E^{ef3}_{sc} and θ^{ef3}_{sc}, and obtain them from the expressions[90–92]

$$\tilde{E}^{ef3}_{sc}=\tilde{E}^*+Q_{ff}-\bar{E}_k-\bar{\nu}_{pre}\bar{E}_\nu-E^{sc}_{rot}-E_{def},$$

$$\theta^{ef3}_{sc}=(E^{ef3}_{sc}/a)^{1/2}, \tag{18}$$

where Q_{ff} is the reaction energy for symmetric fission, $\bar{E}_k$ is the average total kinetic energy of the fragments, $\bar{\nu}_{pre}\bar{E}_\nu$ is the average energy carried off by all the neutrons, E^{sc}_{rot} is the rotational energy of the nucleus at the scission point, and E_{def} is the energy going into fragment deformation.

Some of the components in (18) require explanation of how they are actually determined. It would seem that there is no problem with $\bar{E}_k$, as the existing systematics[93,94] indicate a strong linear dependence of $\bar{E}_k$ on the Coulomb parameter $Z^2/A^{1/3}$. However, the systematics of Refs. 93 and 94 include *all* the data on $\bar{E}_k$: the data for both spontaneous and low-energy fission, in which shell effects dominate, and the data for the fission of highly excited nuclei in heavy-ion reactions. In earlier studies[2,21,95] we showed that when data on $\bar{E}_k$ are chosen only for sufficiently heated nuclei, the nature of the dependence $\bar{E}_k(Z^2/A^{1/3})$ changes: beginning at $Z^2/A^{1/3}=900-1000$ the data tend to lie lower than the linear dependence[2,21,95] (see Fig. 24 below):

$$\bar{E}_k=0.131Z^2/A^{1/3}, \tag{19}$$

which in the range $Z^2/A^{1/3}=0-900$ gives a good description of experiment. The deviation increases roughly linearly with increasing $Z^2/A^{1/3}$. In Ref. 70 we approximated $\bar{E}_k$ by the function

$$\bar{E}_k=0.104Z^2/A^{1/3}+24.3 \tag{20}$$

for the range $Z^2/A^{1/3}=900-1800$. Here we did not include the data on $\bar{E}_k$ in quasifission reactions involving ions $A_i>30$ from Refs. 89 and 96. Equations (19) and (20) were used to find the values of $\bar{E}_k$ for determining E_{sc}^{ef3} (18).

Let us now consider E_{rot}^{sc}, the rotational energy at the scission point. It is defined as[2,22,70,97]

$$E_{rot}^{sc}=\ell^2\hbar^2/2J_{\perp}^{sc}+\theta_{sc}^{ef3}/2, \tag{21}$$

where $J_{\perp}^{sc}$ is the nuclear moment of inertia about the axis perpendicular to the fission axis. In the end the question reduces to finding $J_{\perp}^{sc}$. In the LDM of Strutinskiĭ *et al.*[11] the scission point is defined as the critical point corresponding to loss of stability of the nucleus to breakup into two fragments and is given in units of J_0, the moment of inertia of a solid spherical nucleus. For the nuclei considered here $J_{\perp}^{sc}\sim 4.2J_0$, from which we find that

$$E_{rot}^{sc}\sim E_{rot}^{0}/4.2+\theta_{sc}^{ef3}/2. \tag{22}$$

It is known from the classical model of a rotating liquid drop[36] that

$$E_{rot}^{0}=34.540(\ell^2/A^{5/3})\ \text{MeV}. \tag{23}$$

In calculating E_{rot}^{0} we used the exact value of $J_{\perp}^{sc}$ from Ref. 11, which itself varies weakly from 4.1 at $x=0.6$ to 4.3 at $x=0.95$.

It must be made clear that in the LDM[11] the scission point is not characterized by zero neck thickness. Breaking occurs for finite thickness without a change of the overall elongation of the nucleus, not by gradual thinning of the neck with increasing deformation of the fissioning nucleus, as is often assumed.

The question of the location of and conditions for scission of a nucleus into fragments is of fundamental importance for understanding fission and will be dealt with separately below in Sec. 4.

We still need to discuss the deformation energy E_{def} in (18). Unfortunately, little can be said about it without serious theoretical analysis. This parameter depends strongly on the particular model defining it, on the parametrization of the shape of the fissioning nucleus, on the viscosity coefficient β, and on the conditions under which the nucleus undergoes scission. We also do not know its behavior as a function of the nucleon content of the nucleus. Therefore, following Ref. 37, we shall assume that $E_{def}=0$ and that the values of E_{sc}^{ef3} and θ_{sc}^{ef3} calculated from (18) are the maximum values of these quantities.

Now let us make some remarks about the points raised in this section.

As mentioned above, in Refs. 21, 22, 35, 38, 67, 68, and 70 the decrease of the nuclear temperature only due to the neutron emission $\bar{\nu}_{pre}$ and $\bar{\nu}_{pe}$ has been taken into account. But now there are sufficient experimental data on pre-fission charged particles—protons $\bar{p}_{pre}$ and α particles $\bar{\alpha}_{pre}$, which also decrease the nuclear excitation energy.[98,99] However, at the energies studied ($E^*\leqslant 100-120$ MeV) on the average only very few of them, depending on the nucleon content, are emitted (altogether less than 0.1 per fission event). The total energy carried off by $\bar{p}_{pre}$ and $\bar{\alpha}_{pre}$ was estimated in Ref. 70. It turned out to be 1–2 MeV and, in principle, must be taken into account. However, there is something which allows it to be neglected, at least in determining θ_{sp}^{ef} at the barrier.

First, in theoretical calculations at $E^*\sim 60$ MeV (Ref. 86) it has been shown that in the deexcitation of a nucleus, a pre-fission charged particle (if one is emitted at all in the fission process) is usually emitted first, and then this is followed by neutron emission. The charged-particle emission therefore practically always occurs before the barrier is reached.

Second, in recent years there have been quite a few theoretical studies (for example, Refs. 100–105) where the Thomas–Fermi or Hartree–Fock approximations were used to study the effect of the temperature on the surface and Coulomb energies of the nucleus. In the end, they showed that an increase of the temperature tends to lower the fission barrier (this is somehow similar to the effect of the angular momentum ℓ), and at some fairly high temperature the barrier can completely disappear even for $\ell=0$. Strictly speaking, this lowering of the fission barrier must be taken into account in the analysis, and the first direct attempts to do so have already been made in describing the fission cross sections[78,102,106] and also $\bar{\nu}_{pre}$ (Ref. 78).

In the final analysis, it is important that for the temperature range considered here, $\theta_{sp}^{ef1,2}=1-2$ MeV, the effective barrier is decreased on the average by about 1–2 MeV according to various theoretical estimates. Since an increase of E^* leads, on the one hand, to an increase of the numbers $\bar{p}_{pre}$ and $\bar{\alpha}_{pre}$, and, on the other, to a decrease of the effective barrier height, the net result is a cancellation of the two effects (of course, within certain limits and not for all nuclei), i.e., the temperature actually does not change at the saddle point.

It is therefore desirable to take into account $\bar{p}_{pre}$ and $\bar{\alpha}_{pre}$

only when determining θ_{sc}^{ef3}, the temperature at the scission point. However, unfortunately, there are too few data to do this correctly for any nucleus or reaction, and so we shall neglect this effect.

Let us summarize the discussion in this section. The systematized information on pre- and post-fission neutrons is, on the one hand, of independent interest for understanding the dynamics of the fission process (see Refs. 37 and 59) and, on the other, of pragmatic interest (as in our case): without knowledge of $\bar{\nu}_{pre}$ and its component $\bar{\nu}_{pre}^{gs}$ it is impossible to understand and quantitatively analyze many of the experimental results on the characteristics of the fragment mass–energy distributions in nuclear fission according to the current ideas about the temperature of the fissioning nucleus.

2. ANGULAR MOMENTUM AND THE FRAGMENT MASS–ENERGY DISTRIBUTIONS

There is now a great deal of data on the fragment mass and energy distributions in the fission of heated nuclei, but these data are quite heterogeneous and often contradictory. They have been obtained for various excitations and a wide variety of reactions, involving electrons, light charged particles, etc., up to uranium ions in inverse kinematics. It has been shown in several experimental studies (for example, Refs. 22, 35, 67, 70, 97, 107, and 108) that the characteristics of the mass–energy distributions, in particular, the variance of the mass distribution (MD) σ_M^2, depend strongly on the angular momentum ℓ transferred to the nucleus by the incident ion. In addition, it has been learned that the sensitivity coefficient $d\sigma_M^2/d\ell^2$ is a function of temperature. To somehow systemize all the data on the fragment mass–energy distributions it is necessary to have accurate knowledge of the nature and magnitude of the effect of ℓ on the fissioning nucleus and the fragment characteristics.

2.1. Theoretical ideas

There are quite a few studies devoted to the various aspects of the theoretical understanding of the effect of ℓ on the fragment mass–energy distributions for various nuclei.[3,107–131] The earliest studies were those of Moretto *et al.* (see, for example, Ref. 109), where the fairly simple ridge-line model (conditional saddle points in the space of mass-asymmetric deformations;[18] see also Ref. 114), similar to the LDM, was used to calculate the potential energies of light nuclei with $A=120-150$ as a function of the mass asymmetry for various ℓ. For nuclei above the BG point in Z^2/A these calculations predict narrowing of the parabolic potential curve (increased stiffness) as ℓ increases for fragment masses near $A/2$. For the fission of very light nuclei lying beyond the BG point it predicts a changeover, via a flat distribution, from a curve close to an inverted parabola to the standard parabolic dependence. If it is agreed that the shape of the potential-energy curve in the statistical limit is responsible for the shape of the fragment mass distribution, then, in general, an increase of ℓ will lead, according to Refs. 18 and 109, to a decrease of the variance σ_M^2 of the mass distribution.

This is illustrated in Fig. 8a, where we show a typical example of calculations of the potential energy of the ^{105}Ag nucleus as a function of the fragment Z (conditional barriers) and the angular momentum ℓ, performed in Ref. 112 using the model of Refs. 18 and 109.

Similar calculations based on the ridge-line potential have been carried out for various nuclei in many studies.[109–113] As noted in Refs. 18 and 109, this model will give results consistent with experiment only if the saddle configuration of the fissioning nucleus coincides with the scission-point configuration or is at least close to it (the deformations α_{sp} and α_{sc} and the potentials $V_{sp}(M)$ and $V_{sc}(M)$, respectively), i.e., when the stage of descent from the top of the barrier is absent. This possibility is realized in the fission of light nuclei with $Z^2/A<32$ ($x<0.6–0.7$) (Refs. 2 and 3), and the lighter the nucleus, the closer α_{sp} is to α_{sc}.

Sierk[115] and Carjan and Kaplan[116] have also calculated, for ^{110}Sn and ^{149}Tb, respectively, the potential energies as functions of the charge (mass) asymmetry and ℓ in various models of a rotating liquid drop taking into account the finite range of the nuclear forces.[16] The results of these calculations are shown in Figs. 8b and 8c and are similar to those of Ref. 109.

As mentioned above, for nuclei with $Z^2/A>32$ the descent stage already begins to play an important role, and the picture of the formation of the mass distributions becomes more complicated.[3] Moretto and Schmitt[118] tried to apply the statistical formalism of the model in Refs. 18 and 109 to the calculation of the fragment mass yields for the fission of the heavy nucleus ^{237}Bk, obtained in the reaction ^{197}Au(^{40}Ar,f), however, not for the saddle configuration, which has a cylindrical shape for this nucleus, but for the scission configuration of two touching liquid-drop spheres (the fragments). The result was as before: the width of the mass distribution decreases with increasing ℓ, as is seen in Fig. 8d, taken from Ref. 118. This contradicted the experiment of Ref. 108, where the fission of the somewhat lighter nucleus ^{205}At in the two reactions ^{nat}Re(^{20}Ne,f) and ^{165}Ho(^{40}Ar,f) was studied. The inverse dependence was found: the width of the mass distribution increases sharply with increasing ℓ. The authors[108] tried to attribute this to a new mechanism of "fast fission," when the critical angular momentum is $\ell_c>\ell_{E_f=0}$, i.e., when the fission barrier $\tilde{E}_f$ at large ℓ becomes zero and classical compound-nucleus formation does not occur.[125] However, further studies of the fission of Pt, Po, and Ku nuclei[67,97,107] showed that the same effect occurs at much lower ℓ and that therefore the interpretation on the basis of the fast-fission mechanism is unconvincing. This will be shown below.

In Ref. 119, Gregoire and Scheuter were among the first to use the diffusion model to describe the mass distributions of the same nucleus ^{205}At. They studied the mass yields, taking the scission-point configuration to correspond to the condition that the thickness of the neck between the two fragments is $r_n\sim 0$. As ℓ increases from 0 to 70$\hbar$ the width

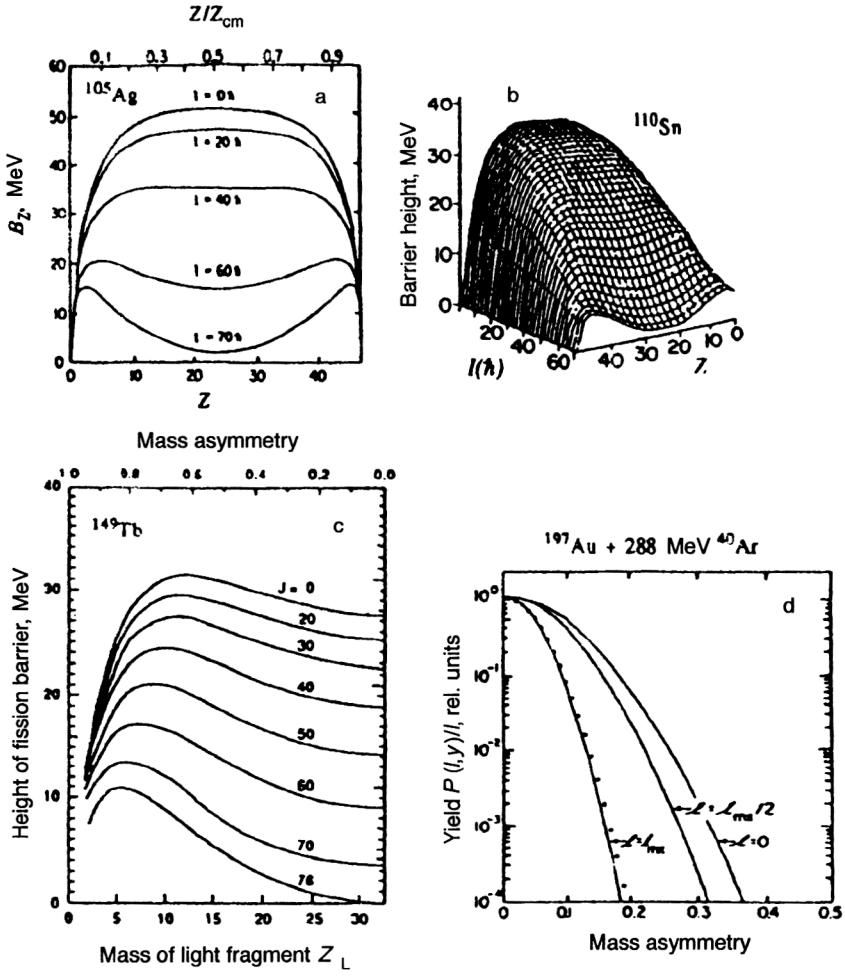

FIG. 8. (a) Calculations[112] of the potential energy B_Z of the ^{105}Ag nucleus (conditional barriers) as a function of the fragment charge Z and angular momentum ℓ; (b) and (c) are the same as (a), but the calculation is made using the Sierk model[16] in Refs. 115 and 116 for ^{110}Sn and ^{149}Tb, respectively. (d) Calculations of the fragment mass yields from Ref. 118 as a function of ℓ.

of the mass distribution in Ref. 119 hardly changed as the friction coefficient changed by a factor of 20. This result is also inconsistent with experiment.[108]

This discrepancy was to some degree corrected by Faber in Refs. 120 and 121. In Ref. 121 he presents maps of the potential (free) energy of the same nucleus ^{205}At as a function of the mass asymmetry, the angular momentum ℓ, and the neck parameter r_n at the nucleus temperature $\theta = 1.6$ MeV. These maps—two-dimensional landscapes of the free energy—are shown in Fig. 9a. It follows[121] from them that the dependence of the mass asymmetry on ℓ is opposite to that on variation of the neck thickness: for defor-

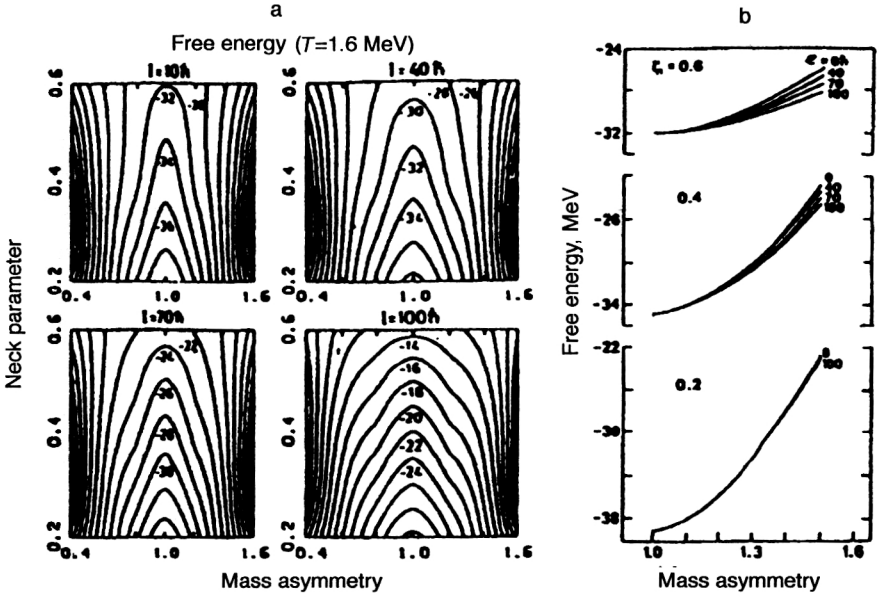

FIG. 9. (a) Maps of the free energy of ^{205}At calculated in Ref. 121 as a function of the mass asymmetry, the neck parameter r_n, and the angular momentum. (b) Dependence of the free energy of ^{205}At on the mass asymmetry and angular momentum at fixed r_n (see the text), obtained from (a).

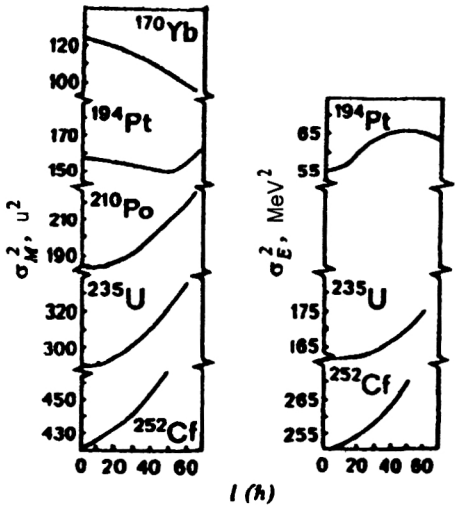

FIG. 10. Theoretical dependence of the variances σ_M^2 and σ_E^2 of the mass and energy distributions on the angular momentum ℓ for the indicated nuclei.[3,117]

mations near the saddle (thick neck) an increase of ℓ leads to broadening of the parabolic potential-energy curve $V(M)$ (decreased stiffness). In approaching the scission point (thin neck) the ℓ dependence of $V(M)$ completely disappears, and for $r_n=0$ (touching fragments) the parabola $V(M)$ narrows (increased stiffness) with increasing ℓ, as in Ref. 118. This is seen more clearly in Fig. 9b, obtained from Fig. 9a. There we give the dependences of the free energy on the mass asymmetry (only the branch for heavy fragments is shown) and on ℓ for fixed neck parameter r_n. For clarity, the curves for different $\ell \neq 0$ are shifted by $A/2$ (the mass asymmetry here is 1) relative to the curve for $\ell=0$. Therefore, to understand the experimental facts in the fission of heavy nuclei[67,97,107,108] on the basis of Ref. 121 it is necessary to assume that deformations near the saddle, possibly during the descent, and certainly not at the scission point for $r_n=0$ are responsible for the formation of the fragment mass distributions. Adeev *et al.*[3,117] used the dynamical diffusion model including two-body viscosity to calculate the fragment mass distributions for a wide range of nuclei from ^{172}Yb to ^{248}Fm as functions of E^* and ℓ. They showed that the "memory" of the prehistory of the fissioning system in its descent to the scission point plays an important role in forming the mass–energy distributions, and that this in turn depends on the extent and time of the descent: for a short descent (light nucleus) the mass distribution is formed right at the barrier, and for a long descent (heavy nucleus) it is formed at some intermediate deformation between the saddle and the scission point. From this point of view, in Refs. 3 and 117 it was found that for light nuclei roughly up to $x \sim 0.65$, $d\sigma_M^2/d\ell < 0$, while for heavy nuclei $d\sigma_M^2/d\ell > 0$. This agrees qualitatively with experiment, as will be shown below. The ℓ dependences of the variances of the mass distribution σ_M^2 and of the energy distribution σ_E^2 calculated in Refs. 3 and 117 for various nuclei are shown in Fig. 10. They confirm this picture: for heavy nuclei (Po, U, Cf) both variances grow with increasing ℓ, for the lighter nucleus ^{172}Yb σ_M^2 decreases, and for ^{194}Pt we have an intermediate situation.

This discussion would seem to pertain mainly to the fragment mass distributions. There is considerably less theoretical information about the energy characteristics: the average total kinetic energy $\bar{E}_k$ and its variance σ_E^2. The authors of many studies[2,3,97,116,126–130] have assumed that the coupling between the rotational degrees of freedom and the internal ones is small. In this case $\bar{E}_k$ should be observed to increase by an amount equal to the rotational energy of the nucleus (21), where in (21) the nuclear moment of inertia $J_\perp$ and temperature θ can be defined either at the saddle point (θ_{sp}) or at the scission point (θ_{sc}), depending on how the problem is actually treated by different groups of authors.

In Refs. 115 and 107 it was assumed that not all the energy E_{rot} (21) goes into increasing $\bar{E}_k$, but that part goes into rotational motion of the fragments, and another part[115] can go into internal excitations of the fissioning nucleus or the fragments. Accordingly, the final energy $\bar{E}_k$ will also depend on how the energy E_{rot} is redistributed among the various degrees of freedom. Unfortunately, at the present time the theory has only begun to tackle this problem (see, for example, Refs. 3, 116, and 131). Moreover, there is little direct experimental information, and it is often contradictory.[129,130] Therefore, more data must be obtained for various regions of fissioning nuclei, energies, and incident ions.

In the case of the variance σ_E^2, its ℓ dependence has been studied theoretically in only two publications: in Ref. 107 using the well known Wilkins statistical model[132] of the scission point including rotation, and in Ref. 3 using the diffusion model. In the first case the values of σ_E^2 calculated for Pt isotopes turned out to be considerably smaller than the experimental values with a weak positive dependence on ℓ. In the second, the ℓ dependence of σ_E^2 is also rather weak, and the coefficient $d\sigma_E^2/d\ell^2$ depends on the nucleon content, increasing from 0.003 to 0.01 MeV$^2/\hbar^2$ for nuclei in the range from Pt to Cf, as is shown in Fig. 10.

Mention should also be made of Ref. 131, where the diffusion model[3] with two-body viscosity was used to calculate $\bar{E}_k$, σ_E^2, and σ_M^2 for the very heavy ^{272}108 nucleus at $\theta_{sp} \sim 2$ MeV, which has fission barrier ≈ 0. It turned out that as ℓ increases from 0 to $30\hbar$ the calculated value of $\bar{E}_k$ does not grow; instead, it decreases by 2 MeV. This result was not commented on in Ref. 131, and it can probably be interpreted as follows. For a nucleus this heavy, as ℓ increases near the scission point the nucleus becomes more elongated, owing to centrifugal forces. As a consequence, the energy of the Coulomb repulsion decreases more quickly than $\bar{E}_k$ increases owing to E_{rot}. The experimental data for heavy systems indicate that $\bar{E}_k$ is not independent of either ℓ or E^* (Refs. 67 and 89). In the calculations of Ref. 131, σ_E^2 is practically independent of ℓ, while σ_M^2 grows by ~12%.

2.2. Experimental results

The experimental study of the effect of ℓ on the mass–energy distributions began over 30 years ago,[1)] with the now

classical study of Plasil *et al.*[62] This subject was later touched upon to some extent in Refs. 2, 21, 22, 35, 67, 89, 97, 107–109, 111, 113–115, 127, 129, 130, and 133–135. Unik *et al.*[129] studied the fission of ^{210}Po in reactions involving p, α, and ^{12}C by the E_1-E_2 technique using a semiconductor spectrometer. They found that $\bar{E}_k$ depends strongly on both E^* ($d\bar{E}_k/dE^*\sim 0.06$ MeV/MeV) and ℓ ($d\bar{E}_k/d\ell^2 \sim 3$ keV/$\hbar^2$), which more than twice exceeds the prediction of (21). No statistically significant effects were obtained for the ℓ dependence of the variances σ_M^2 and σ_E^2. The results of Ref. 129 were not confirmed by Cuninghame *et al.*:[130] the values of $\bar{E}_k$ for fragments of ^{208}Po produced in reactions involving α particles and ^{12}C and ^{16}O ions turned out to be similar and independent of ℓ. As in Ref. 129, the variances σ_M^2 and σ_E^2 did not manifest any explicit ℓ dependence. The authors of Ref. 97 also used an E_1-E_2 spectrometer in reactions involving ^{3}He, ^{4}He, ^{12}C, and ^{16}O ions to measure the fragment mass–energy distributions for the same nuclei $^{208-210}$Po as in Refs. 129 and 130. The results were analyzed using the simple hypothesis of linear dependence of $\bar{E}_k$, σ_E^2, and σ_M^2 on θ_{sp} and $\bar{\ell}^2$:

$$X(\theta_{sp},\ell^2)=X_0+\frac{\partial X}{\partial\theta_{sp}}\theta_{sp}+\frac{\partial X}{\partial\ell^2}\bar{\ell}^2, \qquad (24)$$

where $X(\theta,\bar{\ell}^2)$ are the average moments of the mass–energy distributions and $X_0=X(0,0)$. Equation (24) satisfactorily describes the experimental data, and the authors of Ref. 97 obtained the values $d\bar{E}_k/d\bar{\ell}^2=2.9\pm0.7$ keV/$\hbar^2$, which is close to the estimate (21), and $d\sigma_M^2/d\bar{\ell}^2 \sim 0.02$ u^2/$\hbar^2$. As before, no effect of $\bar{\ell}^2$ on σ_E^2 was found.

In Ref. 133, Ngo *et al.*, studying fission for the same Po–At nuclei by the time-of-flight method, found that, in disagreement with Refs. 97 and 129 but in agreement with Ref. 130, $\bar{E}_k$ depends very weakly on ℓ: $d\bar{E}_k/d\bar{\ell}^2 < 1$ keV/$\hbar^2$. This result was later confirmed in Ref. 134. Meanwhile, in Refs. 108 and 133, and also in Ref. 134, for the ^{205}At nucleus produced in reactions involving ^{20}Ne and ^{40}Ar it was found that σ_M^2 depends strongly on ℓ, while in Ref. 134 it was also found that σ_E^2 depends on ℓ. Both variances grow with increasing ℓ.

The fragment mass–energy distributions in the fission of lighter nuclei $^{176-186}$Pt were studied experimentally in reactions involving ^{32}S and ^{16}O ions in Ref. 107. The results[107] agree with those of Refs. 108 and 134 for the variances σ_M^2 and σ_E^2. The growth of $\bar{E}_k$ observed in Ref. 107 turned out to be related not to the variation of ℓ, but to the increase of the excitation energy E^*. The estimated values of the derivatives were, as in Ref. 129, $d\bar{E}_k/dE^*\sim 0.06$, but for $d\bar{E}_k/d\bar{\ell}^2\sim 0$. It was later shown in Ref. 67, by analyzing the data of Ref. 107, that $d\bar{E}_k/dE^*$ is decreased by a factor of two if the correction to $\bar{E}_k$ for the emission of a realistic number of neutrons ν_{post} from Ref. 38 is introduced, which is more correct. This effect was also mentioned in Refs. 37 and 136.

Now let us consider in more detail the results of experimental studies and analyses performed directly in order to estimate quantitatively the effect of ℓ on the mass–energy distributions.

For convenience and to adhere to our classification described in the Introduction, we first consider the traditional region of heavy nuclei.

2.2.1. The region $Z^2/A \geq 31$

In Ref. 67 the fission of ^{206,204}Po and ^{260,256}104 was studied and analyzed for the reactions

^{3}He+^{204}Pb→ ^{207}Po→f (Ref. 69)
^{12}C+^{194}Pt↘
^{16}O+^{190}Os↘
^{20}Ne+^{186}W→ ^{206,204}Po→f
^{24}Mg+^{180}Hf↗
^{28}Si+^{176}Yb↗
^{40}Ar+^{164}Dy↗
^{16}O+^{244}Cm↘
^{20}Ne+^{240}Pu↘
^{24}Mg+^{236}U→ ^{260}104→f
^{28}Si+^{232}Th↗
^{48}Ti+^{208}Pb→ ^{256}104→f

at two energies for each ion. The data of Ref. 107 on the fission of the compound nucleus ^{186}Pt produced in the reactions

^{16}O+^{170}Yb↘
^{186}Pt→f
^{32}S+^{154}Sm↗

were also analyzed.

In Ref. 22 the fragment mass–energy distributions from the fission of ^{186}Os (Ref. 62) were analyzed as in Ref. 67:

^{4}He+^{182}W↘
^{12}C+^{174}Yb→ ^{186}Os→f.
^{16}O+^{170}Er↗

Finally, in Ref. 70 all these data were reanalyzed by taking into account the isotopic dependence of $\bar{\nu}_{pre}$ from Refs. 38 and 22 and $\bar{\nu}_{pre}^{gs}$, which is naturally reflected in the temperature dependence of the mass–energy distributions. The data of Ref. 108 for the reactions

^{20}Ne+^{nat}Re↘
^{205,206}At→f
^{40}Ar+^{165}Ho↗

were also analyzed in Ref. 70.

In Fig. 11 we show the fragment mass distributions $Y(M)$, and in Fig. 12 we show the energy distributions $E_k(M)$ and the variance $\sigma_E^2(M)$ for the heated fissioning nuclei ^{206,204}Po and ^{256,260}104, produced in reactions involving ^{20}Ne, ^{28}Si, ^{40}Ar, and ^{48}Ti. The Gaussian form of $Y(M)$, the parabolic dependence $E_k(M)$, and the weakly M-dependent variance $\sigma_E^2(M)$ are characteristic signs of a liquid-drop nature of the fragment mass–energy distributions.[2,3,6,12,18,137] For ^{28}Si and heavier ions the regions

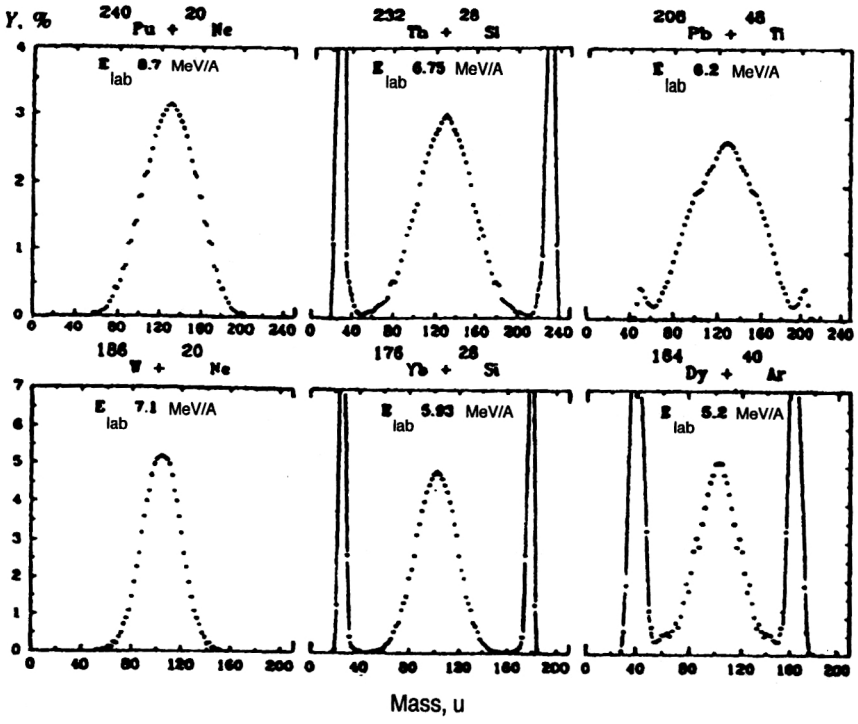

FIG. 11. Mass distributions of fragments of ^{204,206}Po and ^{256,260}104 in several reactions.[67]

of elastic, quasielastic, and deep-inelastic processes are distinguished at the edges of $Y(M)$. For reactions involving ^{48}Ti ions the shape of $Y(M)$ is clearly non-Gaussian, which for similar ions and heavy nuclei indicates, according to Refs. 68, 70, 89, 91, 96, and 138, that quasi-fission[139] contributes to the observed mass distribution. This will be discussed in detail in Secs. 3 and 4 below.

In Fig. 13 we show the dependences of the fragment $\bar{E}_k$ on the initial excitation energy $E^*(\ell)$ (12) and on the average squared angular momentum $\overline{\ell^2}$ for four nuclei: ^{260,256}104, ^{204,206,207}Po, ^{186}Pt, and ^{186}Os, produced in the reactions listed above.

Figure 13 shows that $\bar{E}_k$ is practically independent of ℓ and E^*. The complete set of results gives the upper limit $d\bar{E}_k/d\overline{\ell^2} \leqslant 0.3$ keV/$\hbar^2$. Since $(d\bar{E}_k/d\overline{\ell^2})_{\text{exp}} \ll d\bar{E}_{\text{rot}}/d\overline{\ell^2}$, it can be stated that a large part of the rotational energy goes not into the kinetic energy of the fragments, but into other degrees of freedom.

The absence of any effect of ℓ on $\bar{E}_k$ can be explained using the measured average multiplicity of γ rays $\bar{M}_\gamma$ from fragments in reactions involving light charged particles[140,143] (p and α) and heavy ions,[134,138,141,142,144–147] which showed that $\bar{M}_\gamma$ grows with increasing E^* and ℓ. In Ref. 67 it was found that the ℓ dependence of $\bar{M}_\gamma$ and of the energy carried off from the fragments by γ rays $\bar{E}_\gamma$ almost exactly corresponds to the variation of $\bar{E}_{\text{rot}}$ at the saddle point (for light nuclei) or at the scission point (for heavy nuclei). Therefore, the rotational energy of the fissioning nucleus apparently is to a large degree transformed into angular momentum (spin) of the fragments and is liberated at later stages by γ emission from the fragments.

Let us now turn to the second moments of the fragment mass–energy distributions, σ_M^2 and σ_E^2. In analyzing the experimental data on the variances it is convenient to study the temperature dependence of these quantities following from the fairly general results of statistical mechanics.[148] In particular, it follows that if $V(\alpha,S)$ is the dependence of the deformation potential energy on the variable S, then its distribution about the average value $\bar{S}$ in accordance with the deformation α_0 can be written as

$$P_{\alpha_0}(S) \approx \exp\left[-\frac{(S-\bar{S})^2}{2\sigma^2_{S,\alpha_0}}\right], \quad \sigma^2_{S,\alpha_0} = \frac{\theta_{\alpha_0}}{K_{S,\alpha_0}},$$

$$K_{S,\alpha_0} = \left(\frac{d^2Y}{dS^2}\right)\Bigg|_{\substack{S=\bar{S} \\ \alpha=\alpha_0}}, \tag{25}$$

where θ_{α_0} is the temperature and K_{S,α_0} is the stiffness to variations of S (both at the point $\alpha=\alpha_0$). A more general expression for the temperature dependence of the variance σ_S^2 can be obtained by taking into account the zero-point energy. Dropping the index α_0, we obtain

$$\sigma_S^2 = \frac{\hbar\omega_S}{2K_S}\coth\frac{\hbar\omega_S}{2\theta} = \begin{cases} \theta/K_S & \text{for } \theta \gg \hbar\omega_S \\ \hbar\omega_S/2K_S & \text{for } \theta < \hbar\omega_S, \end{cases} \tag{26}$$

where $\omega_S = (K_S/\mu_S)^{1/2}$ is the oscillation frequency and μ_S is the reduced mass for oscillations of the mode S.

The experiment is consistent with this prediction; in particular,

(a) the mass and energy distributions obey the Gaussian law (25);

(b) as follows from studies of the fission of preactinide nuclei at low temperatures carried out using light charged particles,[2] the dependences of σ_M^2 and σ_E^2 on θ_{sp} follow (26), where $\sigma_E^2(\theta_{\text{sp}})$ corresponds better to the case $\theta_{\text{sp}} < \hbar\omega_E$,

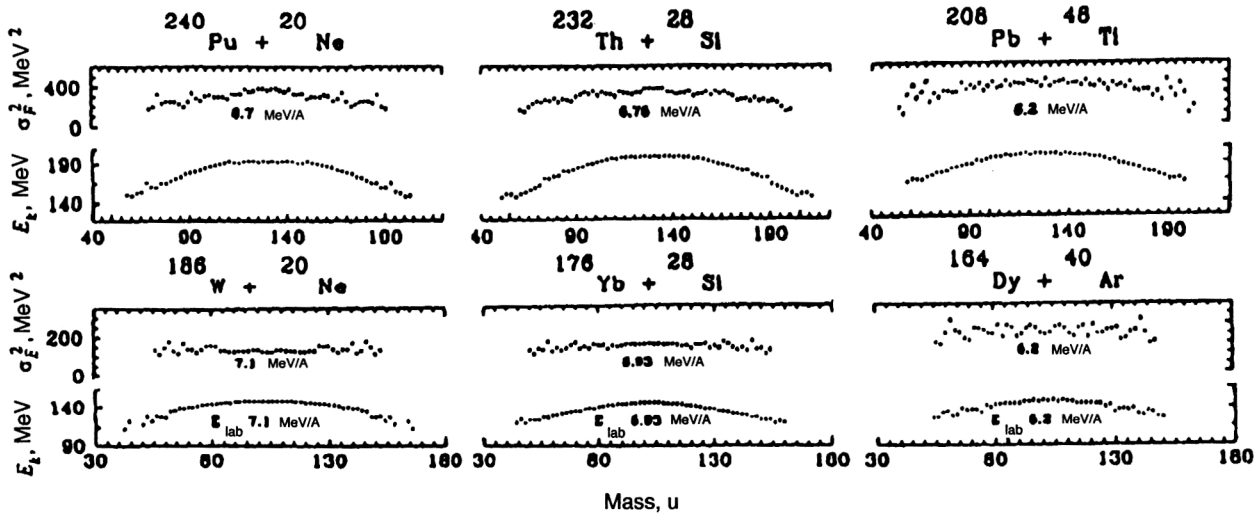

FIG. 12. Energy distributions E_k and σ_E^2 as functions of the fragment mass M for the same nuclei and reactions as in Fig. 11 (Ref. 67).

while $\sigma_M^2(\theta_{sp})$ corresponds to the linear approximation $\theta_{sp} \gg \hbar\omega_M$, in view of the fact that $\hbar\omega_E/\hbar\omega_M \sim 5-10$ MeV and $\hbar\omega_M \sim 0.5$ MeV (Ref. 2).

The last result is also consistent with the analyzed data of Refs. 67 and 107: σ_M^2 depends linearly on θ_{sp}^0, while the dependence $\sigma_E^2(\theta_{sp}^0)$ is concave, in agreement with (26), and poorly approximated by a quadratic parabola. These facts formed the basis of the data analysis in Ref. 67. In Fig. 14 we show $\overline{\ell^2}$, σ_M^2, and σ_E as functions of the initial temperature θ_{sp}^0. The experimental values of the last two characteristics, the mass variance and the square root of the energy variance, are satisfactorily described by straight lines.

There is a clear correlation between the temperature dependences of these characteristics for various bombarding ions (Fig. 14): they all are fan-shaped with intersection point at $\theta_{sp}^0 \sim 1.2-1.4$ MeV, when the angular momenta for all reactions become roughly the same. The experimental data[69] obtained for the ^{204}Pb(^{3}He,f) reaction can be included in these families of curves for Po nuclei. The angular momenta transferred in this reaction are much smaller than in heavy-ion reactions, and so the open squares in Fig. 14 lie close to the family boundary at $\overline{\ell^2} \sim 0$. Figure 14 corresponds to case 1 of the preceding section, i.e., it was constructed by assuming that no neutrons are emitted before reaching the saddle point. It is mainly illustrative, because in a realistic situation the prefission neutrons carry off a significant amount of the excitation energy.

Let us now separately consider the fission of ^{205,206}At nuclei[108] in the reactions ^{20}Ne+^{nat}Re with Ne ion energies of 124 and 204 MeV and ^{40}Ar+^{165}Ho with Ar ion energies from 180 to 390 MeV. For the second reaction involving ^{40}Ar ions the analysis of Ref. 70 used the lowest six energies in the range $E_{Ar}=180-280$ MeV. These were chosen because as the Ar ion energy increases after the steep, roughly linear growth of the FWHM of the mass distribution, the FWHM dependence on E^* becomes nearly flat beginning at $E_{Ar}=300$ MeV. In Ref. 108 and later in the theoretical studies of Ref. 125 this strong growth and subsequent flattening of the width of the mass distribution was attributed to a new mechanism of "fast fission," which begins to operate when, as the ion energy increases, the critical angular momentum ℓ_c becomes larger than the value $\ell_{E_f=0}$ at which the fission barrier vanishes. The authors of Ref. 125 think that in this case a classical compound nucleus is not formed; instead, the system directly enters the fission channel. However, recent theoretical[149] and experimental[37,43,136] studies have shown that even for $E_f=0$ fission is a slow process, and the role of the barrier in this case is effectively played by the viscosity.[149] The term "fast fission" is therefore not really correct.[136] On the basis of this conclusion, the authors of Ref. 70 associated the growth of the width (variance) of the At mass distribution with the usual effect of ℓ. As seen in Fig. 14, in the production of ^{204,206}Po nuclei close to ^{205,206}At by ions up to ^{40}Ar, all the results, including those for ^{40}Ar ions, fit into a single picture, in which rapid growth of σ_M^2 is observed also at values of ℓ considerably smaller than $\ell_{E_f=0}$. Moreover, the flattening of the width of the mass distribution at high excitations can apparently be qualitatively attributed to the fact that the nuclear temperature is strongly lowered in the fission process owing to the emission of a large number of prefission particles. This process begins to have a strong effect at $E^* \geqslant 180-200$ MeV, and no matter how high the initial excitation was, by the time the nucleus reaches the scission point it has an excitation of no more than 50–70 MeV (Refs. 37 and 150). However, it is not impossible that the flatness of the width of the mass distribution just indicates that the quasi-fission mechanism is operating, as in Ref. 89.

As an example, in Fig. 15 we show the σ_M^2 dependences, but now on the effective temperatures at the saddle point and the scission point for ^{205,206}At nuclei and the same ^{260}104 nucleus as in Fig. 14. We clearly see how the temperature range is narrowed, depending on the number of neutrons $\bar{\nu}_{pre}$ or $\bar{\nu}_{pre}^{gs}$ used in the analysis. Naturally, the temperature dependence of σ_M^2 also changes. For a heavy nucleus, the energy dependence of $\bar{\nu}_{pre}$ is such that there is almost complete

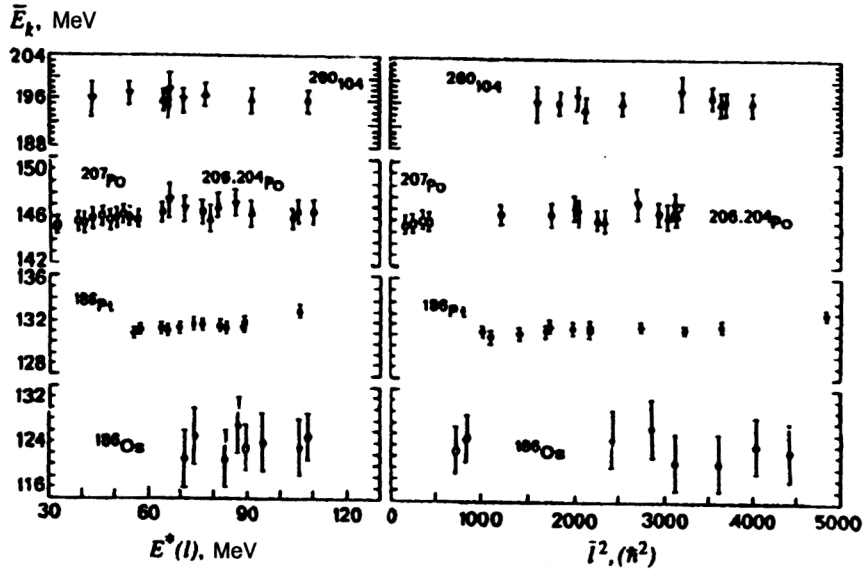

FIG. 13. Dependence of the average total fragment kinetic energy $\bar{E}_k$ for the indicated nuclei in various reactions (see the text) on the excitation energy $E^*(\bar{\ell})$ (12) (left-hand side) and on the average squared angular momentum $\bar{\ell}^2$ (Refs. 22, 62, 67, 69, and 107).

equalizing of the temperatures, with weak dependence on the initial E^*.

The analysis of characteristics like those in Figs. 14 and 15 performed in Ref. 67 showed that, in general, the dependences of σ_E^2 and σ_M^2 on θ_{sp} and $\bar{\ell}^2$ are nonlinear and that (24) represents the Taylor-series expansion of $X(\theta_{sp},\bar{\ell}^2)$ with only linear terms. To it should be added the quadratic and cross terms:

$$X(\theta_{sp},\bar{\ell}^2)=X_0+\frac{\partial X}{\partial\theta_{sp}}\theta_{sp}+\frac{1}{2}\frac{\partial^2 X}{\partial\theta_{sp}^2}\theta_{sp}^2+\frac{\partial X}{\partial\bar{\ell}^2}+\frac{\partial^2 X}{2\partial\bar{\ell}^2}\Bigg)^2(\bar{\ell}^2)^2+\frac{\partial^2 X}{\partial\theta_{sp}\partial\bar{\ell}^2}\theta_{sp}\bar{\ell}^2. \quad (27)$$

We recall that X is either σ_M^2 or σ_E^2. In Ref. 67 it was shown that the quadratic terms in (27) can be neglected without seriously affecting the description in terms of the linear and cross terms. It was also shown that it is possible to take $(\sigma_M^2)_0=\sigma_M^2(0,0)=0$. In our case this always implies the assumption that the fragment mass–energy distributions are formed at the point $\theta_i^j=0$, i.e., at the barrier or the scission point (i=sp or sc, and j=ef1, ef2, or ef3). In Fig. 15 the

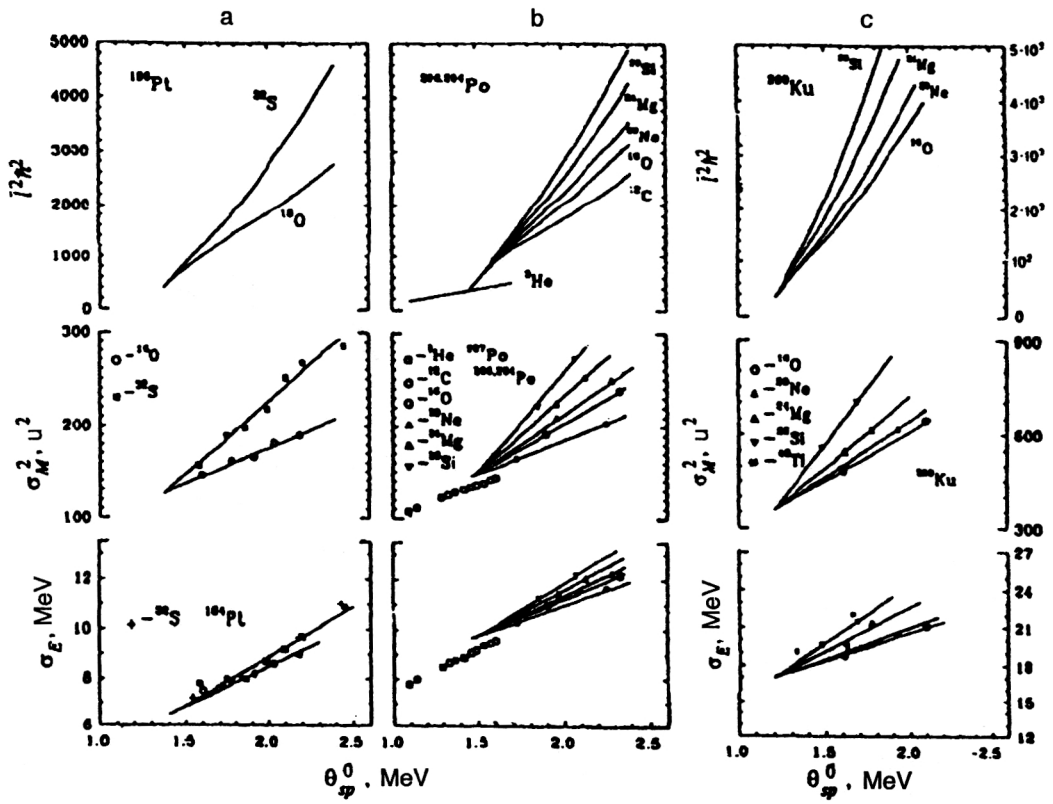

FIG. 14. Dependence of σ_M^2, σ_E, and $\bar{\ell}^2$ on θ_{sp}^0 (13) for the nuclei ^{184,186}Pt, ^{204,206,207}Po, and ^{260}104 produced in reactions involving various ions.

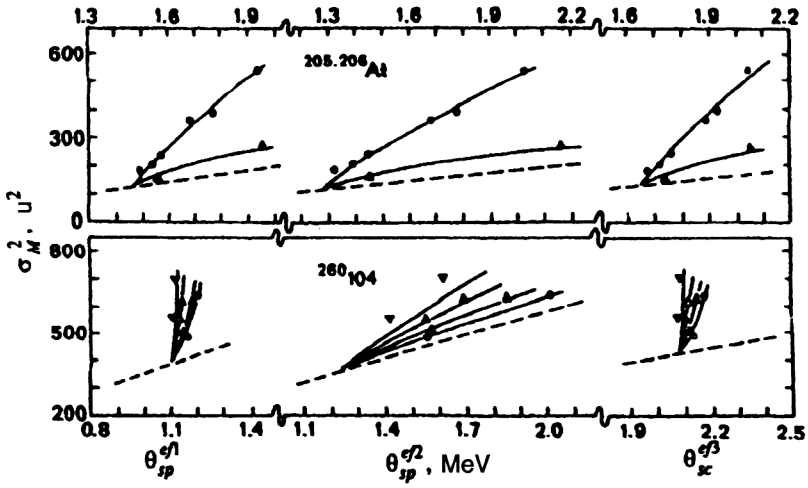

FIG. 15. Dependence of σ_M^2 for ^{205,206}At and ^{260}104 on the effective temperature at the saddle point θ_{sp}^{ef1}, θ_{sp}^{ef2} and at the scission point θ_{sc}^{ef3}. The solid lines are the empirical description[70] according to (27) (see the text), and the dashed lines are the dependence of σ_M^2 on θ_i^j for $\ell=0$.

solid lines show the least-squares description of the experimental data on $\sigma_M^2(\theta_i^j, \overline{\ell}^2)$ according to (27) without the quadratic terms and with the condition $(\sigma_M^2)_0=0$. The data are described satisfactorily in all six cases, except for the reaction ^{28}Si+^{232}Th, for which a quasi-fission process analogous to that studied in Refs. 89 and 96 for the reaction ^{238}U+^{27}Al occurs. In those studies[89,96] asymmetry of the forward–backward emission and broadening of the mass distributions was observed in the angular distributions for various fragment mass ranges. In Fig. 15 the dashed lines show the dependences $\sigma_M^2(\theta_i^j)$ for $\ell=0$. Looking as the cases with θ_{sp}^{ef1} and θ_{sc}^{ef3} for the ^{260}104 nucleus, we see that practically the entire increase of σ_M^2 comes from increase of ℓ, because the temperature varies weakly in these cases. The presence of the cross term in (27) causes the total derivative $d\sigma_M^2/d\overline{\ell}^2$, which can be referred to as the coefficient describing the sensitivity of σ_M^2 to $\overline{\ell}^2$, to begin to depend on θ_i^j: it is larger at lower temperature.

In Ref. 70 an analysis exactly like that in Fig. 15 was performed for the data on ^{186}Os (Refs. 62 and 22), ^{186}Pt (Refs. 107 and 67), and ^{204,206,207}Po (Ref. 67). The results for the last two nuclei are shown in Fig. 14.

All the information on the total derivative $d\sigma_M^2/d\overline{\ell}^2$ is shown in Fig. 16 as a function of Z^2/A for several values of the temperature θ_i^j: for θ_{sp}^{ef1} in Fig. 16a, for θ_{sp}^{ef2} in Fig. 16b, and for θ_{sc}^{ef3} in Fig. 16c. The data for ^{205,206}At fit in well with the dependence on the nucleon content found for other nuclei, and so the fast-fission mechanism is not needed in this case to explain the growth of σ_M^2 with ℓ even for $\ell_c > \ell_{E_f=0}$.

The results given in Fig. 16 show that the dependence of $d\sigma_M^2/d\overline{\ell}^2$ on Z^2/A is different for different definitions of the temperature θ_i^j.

The solid lines in Fig. 16 show the empirical description of Ref. 70. The strong growth of $d\sigma_M^2/d\overline{\ell}^2$ for heavy nuclei seen in Figs. 16a and 16c is mainly due to the effect of ℓ rather than θ_i^j. When the temperature at the saddle point is a function of the number of neutrons ν_{pre}^{gs}, the growth of this coefficient with Z^2/A is much more moderate.

Almost all our discussion so far has pertained to the fragment mass distributions. The situation is practically the same for the variance of the energy distributions σ_E^2, and so we shall not dwell on it, but just present the final results later on.

We thus see that for nuclei with $Z^2/A \geq 31$ an increase of ℓ always leads to an increase of σ_M^2 and σ_E^2, and the heavier and less excited the nucleus, the stronger the effect of ℓ. For the fairly light ^{186}Os nucleus the coefficient $d\sigma_M^2/d\overline{\ell}^2$ is close to zero.

In summary, the longer the descent from the top of the barrier and the more important the role played by dynamical effects, the stronger the effect of the angular momentum transferred by the incident ion to the fissioning nucleus.

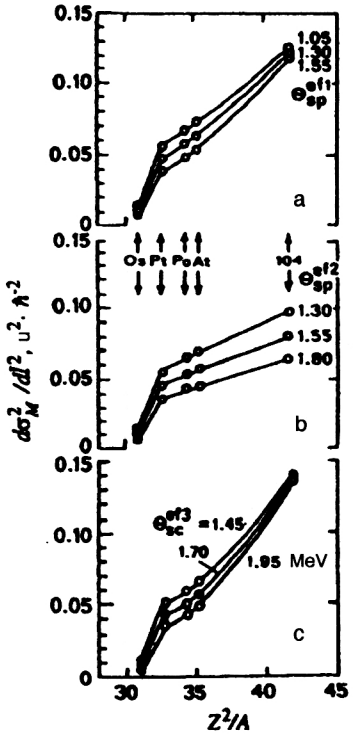

FIG. 16. Dependence of the sensitivity coefficient $d\sigma_M^2/d\overline{\ell}^2$ on Z^2/A at the indicated temperatures: (a) θ_{sp}^{ef1}, (b) θ_{sp}^{ef2}, (c) θ_{sc}^{ef3} for ^{186}Os–^{260}104 nuclei (points). The solid lines are the analytical description of these dependences from Ref. 70.

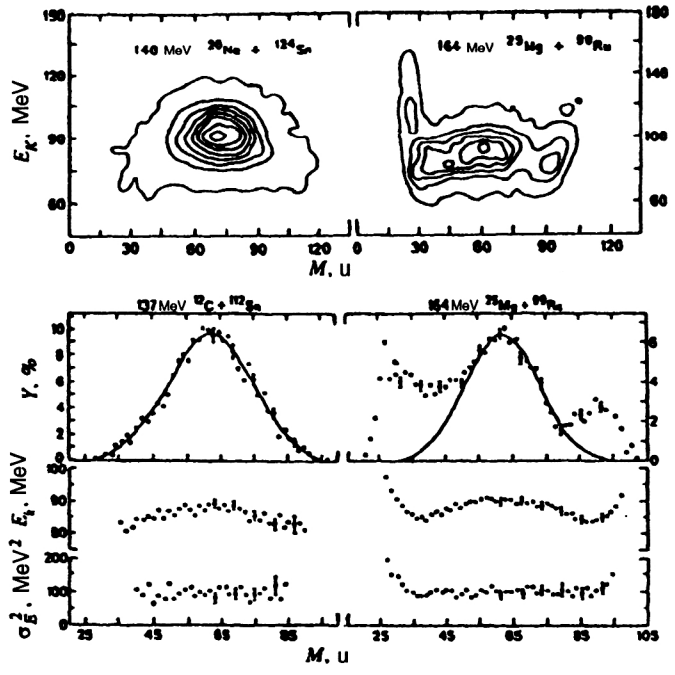

FIG. 17. Upper figure: The two-dimensional matrices $N(M,E_k)$ for the indicated reactions. Lower figure: The mass yields Y, E_k, and σ_E^2 as functions of the fragment mass M for the indicated reactions.

2.2.2. Nuclei with $Z^2/A=20-30$

For light nuclei there is much less experimental information on the ℓ dependence of the fragment mass–energy distributions than in the case considered above. It is essentially all contained in Refs. 22, 35, 111, 115, and 127. These studies, using ions like Mg, Al, Cl, and so on, have shown that, in contrast to the fission of heavy nuclei, there is not only the angular-momentum effect, but also the problem of separating "true" (classical) fission from deep-inelastic transfer and quasifission,[151] which strongly change the shape of the mass distributions, depending on the ion energy and on the emission angle of fragment-like reaction products.[22,111–113,126,127,152] There are practically no such problems for lighter ions at energies below 10 MeV/nucleon.[19,22–25,109–111,113,128,153–156] This is illustrated in Fig. 17 (Ref. 22). In the upper part of this figure we show the two-dimensional matrices $N(M,E_k)$ for two of the reactions studied, ^{20}Ne(140 MeV)+^{124}Sn and ^{25}Mg(164 MeV)+^{99}Ru. The results for the reaction involving ^{20}Ne represent a standard, nearly triangular, distribution, which means that the mass distribution has a Gaussian form. However, the picture for the reaction involving ^{25}Mg is considerably more complicated. The region of the symmetric peak is clearly seen for masses near $A/2$, and along the edges of the distributions we see, first, events from the elastic–quasielastic peak and, second, the range of masses and energies where the contribution from deep-inelastic transfer reactions is clearly manifested. In the lower part of Fig. 17 we give the mass–energy distributions of fission fragments from ^{124}Ba formed in reactions using ^{12}C and ^{25}Mg. The data for reactions with ^{12}C are similar to those with ^{20}Ne, but those for reactions with ^{25}Mg merit separate discussion. The mass distribution has a complicated structure reminiscent of the distribution for ^{111}In from Ref. 151 in the ^{84}Kr+^{27}Al reaction and shown below in Fig. 20. In Ref. 151 this structure was delimited to three regions and soundly interpreted. The symmetric peak near $M=A/2$ is true fission via a compound nucleus, and this was described by a Gaussian in Ref. 22. The edges of the distribution near $M=A_i$ and A_t are the result of quasielastic and deep-inelastic transfer reactions, and are shown by the dashed lines in Fig. 20 for ^{111}In. This is also expressed as an increase of E_k and σ_E^2 for these masses. The intervening "shoulders" between these two mass ranges were interpreted[151] as the result of the decay of a long-lived nuclear system without passing through the compound-nucleus stage, i.e., the quasi-fission process (open circles in Fig. 20). Here we are interested only in true fission, and in the opinion of the authors of Ref. 22 it can be distinguished fairly well from other processes.

Agarwal *et al.*[111] studied the reactions ^{16}O+^{92}Mo and ^{52}Cr+^{56}Fe leading to the compound system ^{108}Sn. For the first reaction they observed broad, Gaussian-like behavior, practically independent of angle, of the charge (mass) distribution of the reaction products near $\frac{1}{2}Z_{CN}\pm 10$, which can be identified as true fission. For the second reaction they observed angle-dependent, narrow charge distributions. They showed that, even for the angle $\theta_{CM}\sim 90°$, these are formed by the decay products of a long-lived system which had not completely reached statistical equilibrium, i.e., using modern terminology, a quasi-fission process. For this reason it is senseless to compare the characteristics of the mass distributions of fragments or fragment-like products of these reactions, because they characterize different processes.

A similar situation was observed in Ref. 127 for a large number of reactions and also in Ref. 113, where the reactions ^{16}O+^{89}Y and ^{37}Cl+^{68}Zn leading to the production of ^{105}Ag were studied. For the reasons discussed above, the data on the characteristics of the mass distributions in the second reaction were not included in Ref. 22. Regarding the energy distributions, according to Ref. 113, $\bar{E}_k$ and σ_E^2 are independent of both ℓ and, in contrast to the mass distributions, the detection angle θ_{CM}.

The study of Ref. 115 is quite interesting. Those authors studied the fission of ^{110}Sn in the reaction ^{45}Sc+^{65}Cu. Although this reaction is close to the one studied in Ref. 111 (^{52}Cr+^{56}Fe), the authors of Ref. 115, who measured the charge distributions of light fragments at $\theta_{CM}\sim 90°$, which are nearly Gaussian, and the multiplicity $\bar{M}_\gamma$ of γ rays from fragments as a function of the charge (mass) asymmetry, state that in this case a classical compound nucleus is formed, and that the charge distribution is well described by the statistical model based on the LDM including rotation. In comparing the charge distributions of fragments of ^{110}Sn obtained for large angular momentum ($\ell_c=70\hbar$) and of the similar nucleus ^{102}Rh from the reaction ^{93}Nd+^{9}Be (Ref. 19) at small angular momentum ($\ell_c=34\hbar$), the authors of Ref. 115 concluded that they had experimentally observed the narrowing of the mass distributions with increasing ℓ, as predicted by theoretical calculations for these nuclei (see Sec. 2.1).

In Table I we give the experimental data used in Ref. 22

TABLE I.

Reaction	A_{CN}	Data	Z^2/A x	E_i MeV	ℓ_c $\hbar$	E^* $E^*(\ell)$ MeV	θ_{sp}^0 (A·0.093) MeV	$\bar{\nu}_{pre}$	θ_{sp}^{eff} (A·0.093) MeV	$\bar{E}_k$ MeV	σ_E^2 MeV^2	σ_M^2 exp. σ_M^2 corr. u^2	$d\sigma_M^2/d\ell^2$ $\hbar^{-2}$ u^2	$d^2V/d\eta^2$ (A·0.093) MeV
1	2	3	4	5	6	7	8	9	10	11	12	13	14	15
^{84}Kr+^{27}Al	^{111}In	[22,151]	21.63	490	69	107.9	2.11	1.5	1.53			169±16	−0.100	1.8±1.8
			0.436			57.9	2.23		1.70			634	±0.020	2.1
^{16}O+^{89}Y	^{105}Ag	[22,113]	21.04	140	58	113.3	2.30	1.4	1.69	73±4	99±18	324±34		1.7±1.6
			0.422			69.5	2.45		1.90			667		1.9
^{93}Nb+^{12}C	^{105}Ag	[22,154]	21.04	1060	52	121.0	2.53	1.5	2.04	69±3		flat		
			0.422			85.2	2.68		2.20					
^{25}Mg+^{99}Ru	^{124}Ba	[22]	25.29	164	67	109.1	2.23	1.3	1.81	89±2	92±6	115±11	−0.038	5.6±0.8
			0.505			64.3	2.30		1.88			310	±0.012	5.8
^{12}C+^{112}Sn	^{124}Ba	[22]	25.29	137	56	114.7	2.40	1.5	1.91	87±3	90±8	167±14		6.0±0.8
			0.505			83.8	2.49		2.0			299		6.4
^{20}Ne+^{124}Sn	^{144}Nd	[22]	25.00	140	63	109.0	2.06	2.7	1.21	91±2	79±5	158±9		4.8±0.8
			0.517			74.9	2.15		1.36			325		5.6
^{20}Ne+^{118}Sn	^{138}Nd	[22]	26.09	124	56	89.3	1.82	1.8	1.20	92±6	80±6	133±8	−0.061	6.3±0.9
						61.0	1.92		1.34			227	±0.020	7.0
^{139}La+^{9}Be	^{148}Pm	[19,22]	25.14	1157	37	71.3	1.43	1.7	0.78			261±26		3.4±1.4
			0.523			60.0	1.57		1.03			318		4.3
^{132}Xe+^{30}Si	^{162}Er	[22,152]	28.54	713	67	84.6	1.74	2.3	1.05			113±17		11.5±1.4
			0.588			54.8	1.78		1.13			147		12.6
^{35}Cl+^{124}Sn	^{159}Ho	[22,165]	28.23	165	58	78.8	1.66	2.0	1.05	104±6		140±15	−0.011	10.1±1.5
			0.580			55.6	1.74		1.15			165	±0.010	11.5
^{3}He+^{162}Dy	^{165}Er	[22,26]	28.12	65	22	75.1	1.64	2.2	1.00	113±2	81±3	171±7		9.7
			0.584			71.6	1.71		1.10			176		10.6

Note. In columns 8 and 10 the temperatures θ_{sp}^0 and θ_{sp}^{ef1} were calculated with the barriers $E_f(\ell)$ from Ref. 36 (upper line) and Ref. 16 (lower line). The values of the stiffness in column 15 were obtained using these temperatures.

to determine the quantitative ℓ dependence of characteristics of the mass–energy distributions. Unfortunately, aside from the data studied in Ref. 22 in two reactions involving ^{124}Ba, for other nuclei it is not possible to choose such data satisfying the above requirements. For this reason, in Table I we give pairs or triplets of nuclei close in Z^2/A at identical or close temperatures θ_{sp}^{ef1} and obtained using various ion–target combinations with various critical angular momenta ℓ_c. It should be noted that in this region of nuclei the fission probability depends very strongly on ℓ (it increases sharply with increasing ℓ), and so it is usually assumed that, on the average, in fission angular momenta close to ℓ_c for fusion are realized, and in Ref. 22, following Refs. 113 and 115, it was assumed that $\ell_c=\ell$ for fission.

Comparing the nuclei in Table I in groups with identical or close temperatures θ_{sp}^{ef1}, we immediately see that at large ℓ_c the variance σ_M^2 is smaller. This is seen especially clearly for the lightest nuclei analyzed, ^{111}In (Ref. 151) and ^{105}Ag (Ref. 113) (the reaction ^{16}O+^{89}Y), where σ_M^2 differs by a factor of two. For the reaction ^{93}Nb+^{12}C (Ref. 154) the mass distribution is completely flat in a wide range about $A_{CN}/2$ even for $\ell_c\sim 50\hbar$ (see Fig. 20 below). This implies that the ℓ dependence of σ_M^2 is quite strong, the sensitivity coefficient is $d\sigma_M^2/d\bar{\ell}^2<0$, and, on the whole, the nature of the fragment mass distribution for ^{105}Ag corresponds to the region of nuclei below the BG point in Z^2/A for $\ell=0$. Comparison of the data in Table I reveals that the coefficient $d\sigma_M^2/d\bar{\ell}^2$ is different for different regions of Z^2/A. This experimental information was analyzed quantitatively in Ref. 22 to understand the ℓ dependence of σ_M^2 and σ_E^2 according to the linear approximation (24), because the data were clearly insufficient for using the more complete and accurate expression (27). As in Ref. 70, it was assumed that in (24) $X(0,0)=0$. The results of the analysis in the form of the sensitivity coefficient $d\sigma_M^2/d\bar{\ell}^2$ are shown in Fig. 18 (upper part) for the entire range of Z^2/A studied: for heavy nuclei at $\theta_i^j=1.5$ MeV, and for nuclei in the range $Z^2/A=20-30$ all at temperature θ_{sp}^{ef1} given in Table I, with the average value $\theta_{sp}^{ef1}=1.5-1.6$ MeV. For light nuclei the experimental points are satisfactorily described by a straight line:

$$d\sigma_M^2/d\bar{\ell}^2=0.0111Z^2/A-0.334 \quad \text{for } Z^2/A=20-31. \tag{28}$$

The solid line shows the θ_{sp}^{ef1} dependence over the entire scale of Z^2/A. Beginning at $Z^2/A=31$, the dashed and dot–dash lines show the values of $d\sigma_M^2/d\bar{\ell}^2$ for θ_{sp}^{ef2} and θ_{sp}^{ef3}, respectively.

The data in Fig. 18 present a curious picture: for nuclei with $Z^2/A>30$ we have $d\sigma_M^2/d\bar{\ell}^2>0$, while for lighter nuclei this coefficient is less than zero, and the lighter the nucleus (in this range), the more negative it is. The open symbols are the theoretical calculations of Adeev *et al.*[3,117] (see Fig. 10). Those calculations[3,117] underestimate the scale of the effect, but predict the passage of $d\sigma_M^2/d\bar{\ell}^2$ through zero at roughly the same values of Z^2/A. Here it should be

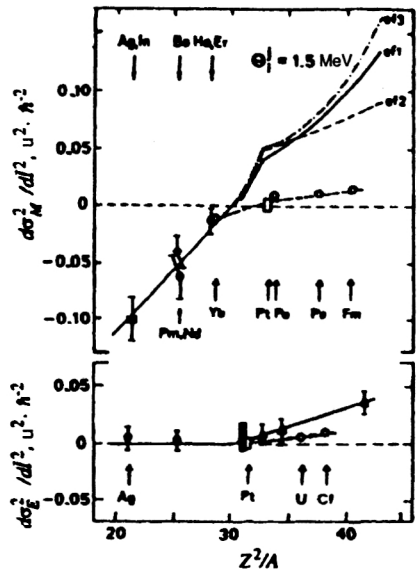

FIG. 18. Upper figure: Dependence of $d\sigma_M^2/d\ell^2$ on Z^2/A for $\theta_i^j = 1.5$ MeV, calculated for $Z^2/A \leqslant 31$ in Ref. 70. The points for $Z^2/A \leqslant 31$ are the data of Ref. 70, the solid lines for $Z^2/A \leqslant 31$ correspond to (28) and θ_{sp}^{ef1}, the dashed line is for θ_{sp}^{ef2}, and the dot–dash line is for θ_{sc}^{ef3}. Lower figure: Dependence of $d\sigma_E^2/d\ell^2$ on Z^2/A for $\theta_{sp}^{ef1} \cong 1.5$ MeV (Refs. 22 and 67). The open symbols are the theoretical calculation.[3,117]

remembered that descent from the top of the barrier appears for nuclei with $Z^2/A > 30-32$, and it becomes impossible to describe the fragment mass–energy distributions using the traditional statistical model neglecting the dynamical properties of nuclear matter.[2–5,21,70] The calculations in Refs. 3 and 117 were also made by taking these factors into account within the diffusion model, and, as seen from Fig. 18, they qualitatively reproduce the behavior of the experimental curve (solid line) as a function of Z^2/A. For nuclei with $Z^2/A < 30-32$ there is practically no descent from the saddle, the dynamics and viscosity become unimportant, and the standard statistical calculations on which the LDM is based begin to work well.

Let us discuss the physics of this process, but taking into account the changes introduced by the rotational degrees of freedom. It is known from the classical model of a rotating liquid drop[36] that the angular momentum and the associated rotational energy have an effect on the nucleus similar (but not identical) to that of the Coulomb repulsive forces, which tend to break up the nucleus. Accordingly, the ground equilibrium state becomes deformed, the saddle point in general is shifted to smaller deformations, approaching the ground state in this coordinate, and the fission barrier is lowered. However, the properties of the rotating nucleus are manifested differently in different ranges (different x). For light nuclei (small x) near the BG point the saddle point is hardly shifted at all to smaller deformations with increasing ℓ, and the nucleus remains a system with a thin, nearly unchanged, neck. In contrast, the equilibrium state becomes strongly deformed, approaching the saddle-point configuration. Numerous potential-energy calculations (see Sec. 1.1) show that in this case the stiffness of the fissioning system to a mass-asymmetric deformation at the saddle point $d^2V/d\eta^2$ grows with increasing ℓ, while the corresponding mass distribution naturally narrows.

The picture is reversed for heavy nuclei with $x > 0.7$: now as ℓ increases the saddle configuration approaches the equilibrium one, which itself is weakly changed, the neck disappears altogether at large ℓ, and, as shown by static calculations of the deformation potential energy by Faber[121] for ^{205}At and by Adeev *et al.*[3,117] for nuclei from ^{210}Po to ^{248}Fm, the stiffness at or near the saddle $d^2V/d\eta^2$ does not grow, as for light nuclei, but decreases with increasing ℓ. If the fissioning heavy nucleus "remembers" its prehistory in the descent to the scission point, as occurs in the diffusion model,[3,117] then σ_M^2 will grow with increasing ℓ, as is seen experimentally.

For intermediate nuclei falling between these two extremes, where there is almost no descent stage, σ_M^2 is determined by the saddle values of the viscosity.[117] As ℓ increases the equilibrium and saddle deformations shift toward each other by roughly equal amounts, and, as again follows from Refs. 3 and 117, $d^2V/d\eta^2$ is practically independent of ℓ, and so $d\sigma_M^2/d\ell^2 \sim 0$.

In the lower part of Fig. 18 we show the dependence of $d\sigma_E^2/d\ell^2$ on Z^2/A. There are few data for light nuclei, but it is clearly seen that σ_E^2 does not depend on ℓ within the errors. For heavier nuclei the data at $\theta_{sp}^{ef1} = 1.5$ MeV behave roughly like the mass variance: they grow with increasing Z^2/A.

Therefore, the experimental ℓ dependence of the characteristics of the fragment mass–energy distributions in a wide range of nuclei with $A \sim 100-260$ allows the determination of σ_M^2 and σ_E^2 for any values of ℓ and θ_i^j.

3. STATISTICAL PROPERTIES OF THE FRAGMENT DISTRIBUTIONS AND THE BUSINARO–GALLONE POINT

As already noted, in the fission of nuclei with $Z^2/A \leqslant 32$ the descent stage is absent (for small ℓ) and the dynamics of the passage of the nucleus from the saddle to the scission point is unimportant. The important factor in the theoretical study of the fission process in this case is the static properties of the deformation potential-energy surface. For highly excited nuclei they are described by the LDM, where one of the basic parameters is the stiffness of the nucleus to mass-asymmetric deformations (shape variations) $d^2V/d\eta^2$. We have already touched on some qualitative aspects of this subject in the preceding section for the example of ^{205}At. Let us now discuss this characteristic in more detail.

In his classic studies,[12] Strutinskiĭ defined the mass-asymmetric deformation η as

$$\eta = 2(V_L - V_R)/(V_L + V_R), \tag{29}$$

where V_L and V_R are the volumes of the parts of the asymmetric figure describing the fissioning nucleus located to the left and to the right of the middle of the neck. The deformation parameter η most naturally characterizes an asymmetric nuclear configuration and can be associated with the mass

asymmetry of the future fragments if it is assumed that breaking occurs at the "thinnest" part of the neck, i.e., in the middle. Then

$$\eta=(4/A)(M-A/2). \tag{30}$$

In the statistical approach[12] the probability for this fission mode or the fragment mass ratio $M/(A-M)$ is described as

$$Y(M)\sim\exp\{2(a[E^*-V(M)]^{1/2}\}, \tag{31}$$

where a is the level-density parameter and $V(M)$ is the potential energy of the system, which can be written as

$$V(\eta)=V(0)+\frac{1}{2}\left.\frac{d^2V}{d\eta^2}\right|_{\eta=0}\eta^2+\dots . \tag{32}$$

Restricting ourselves to the two terms in (32), assuming that the second term is small compared to the potential energy $V(0)$, and using (31), for $Y(M)$ we obtain the experimentally observed Gaussian distribution with variance

$$\sigma_M^2=\frac{A^2}{16}\left[\left.\left(\frac{d^2V}{d\eta^2}\right)\right|_{\eta=0}\right]^{-1}\theta, \tag{33}$$

where θ is the nuclear temperature.

Therefore, the shape of the distribution $Y(M)$ is determined by the dependence of the potential energy $V(\eta)$ on the mass-asymmetric deformation. In the simplest situation close to reality, this is the harmonic-oscillator potential, the stiffness of which to asymmetric oscillations of the nuclear shape $d^2V/d\eta^2$ determines the variance σ_M^2. Conversely, from the experimental data on σ_M^2 we can easily find this important static parameter of the LDM:

$$d^2V/d\eta^2=A^2\theta/16\sigma_M^2. \tag{34}$$

In principle, in any modification of the LDM, $d^2V/d\eta^2$ can be determined at each point of the nuclear deformation trajectory from the ground state to the scission point, as shown for the example of ^{205}At (Ref. 121) in Sec. 2. However, it is well known that the saddle point,[2,18,22,137,158] the descent stage,[3] and the scission point[6,132,159,160] play a special role.

The simplest assumptions are those of the statistical model, which originate from the idea that in a particular state of the nucleus, for example, at the saddle point or the scission point, the conditions for statistical equilibrium in all the nuclear degrees of freedom are satisfied. In this case, Eqs. (31)–(34) must involve quantities corresponding to the selected nuclear state, the saddle or the scission point $V_i(M)$, θ_i, $(d^2V/d\eta^2)_i$, where $i=$ sp or sc. On the other hand, the experimental determination of the stiffness $d^2V/d\eta^2$ using (34) requires only knowledge of the real temperature θ_i^{efl} and the experimentally measured dispersion σ_M^2. Comparison of the experimental stiffness with various versions of the theoretical LDM calculations shows whether or not a given model describes the experiment. However, practically all the existing calculations have been performed for the case of a nonrotating nucleus ($\ell=0$), and so the correct comparison with their results requires the use of variances σ_M^2 corrected for the effect of ℓ, as described above in Sec. 2.

The theoretical behavior of $d^2V/d\eta^2$ (Refs. 3 and 12) as a function of Z^2/A for nuclei in the β-stability valley is shown in Fig. 19. The solid line shows the stiffness calculated for the saddle point, and the dashed line shows it for the scission point. In this figure we clearly see that beginning at $Z^2/A\sim32$ the stiffness for the scission point begins to differ strongly from that for the saddle, i.e., this is when descent from the top of the barrier appears. The heavier the nucleus, the more extended this stage, and the stronger the effect of the dynamics and viscosity on the formation of the fragment mass–energy distributions.

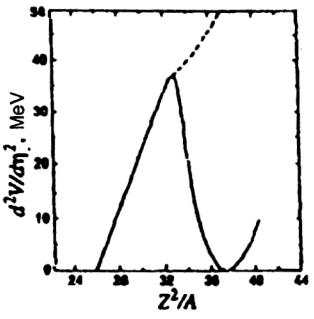

FIG. 19. Dependence of the nuclear stiffness to mass-asymmetric deformations $d^2V/d\eta^2$ on the fissility parameter Z^2/A. The solid line is for the saddle point, and the dashed line is for the scission point.[3,12]

It should be noted that the form of the Z^2/A dependence of $d^2V/d\eta^2$, while differing quantitatively by the location of the critical points on the two axes, is similar to that shown in Fig. 19 for any modification of the LDM.[12–16]

The first characteristic feature of the behavior of the theoretical curve $d^2V/d\eta^2$ for the saddle point as a function of Z^2/A is the presence of the maximum located in the range $Z^2/A=30$–33 with position depending on the specific modification of the LDM. This form of the stiffness curve with a maximum has been confirmed experimentally,[2,21,26,69,70] as will be discussed below. The second feature, which is the most important for us in this section, is the presence at small x of the BG point, at which the nuclear stiffness is $d^2V/d\eta^2=0$, i.e., at which the nucleus becomes absolutely unstable to mass-asymmetric deformations. The theoretical value of the BG point is also model-dependent and lies in the range $Z^2/A\sim19$–26. According to the theory, at this point, in the fission of a nucleus into approximately equal parts near $A/2$, there should be a flat, mass-independent fragment distribution corresponding to the limit of infinite variance.

Repeated attempts have been made to determine experimentally the BG point in reactions involving high-energy protons (0.6–1.0 GeV).[20,161–163] They have shown, more qualitatively than quantitatively, that in fact the fragment mass distribution becomes relatively broader as the mass number of the fissioning nucleus decreases. However, unfortunately, the quantitative interpretation of these data may not be reliable, owing to the large set of excitation energies and fissioning nuclei arising after the emission cascade, the number of particles in which can reach several dozen. These experimental studies are reviewed in Ref. 20, and we shall not dwell on them here.

Another class of experiments to study the fragment mass–energy distributions of light nuclei is based on heavy-ion reactions (Refs. 19, 22, 35, 55, 109–115, 122, 123, 126–

128, 151–156, and 164–168). They also have characteristic features, primarily owing to the significant angular momentum ℓ transferred to the nucleus by the incident ion, as shown in the preceding section. For ions (or targets, in reactions with inverse kinematics) which are not too heavy, such as ^{9}Be and ^{12}C with energy up to 10 MeV/nucleon, it is possible, to some degree, to neglect the effect of ℓ. Such experiments have been carried out by the Moretto group (see, for example, Ref. 19), and their results are summarized in Refs. 114 and 167. They showed that, as predicted by the LDM, a transition from Gaussian to U-shaped fragment charge (mass) distribution occurs as the mass of the fissioning nuclei decreases from 150 to 80 (see Fig. 1).

As already noted, the problem of separating true fission from deep-inelastic transfer and quasi-fission arises when ions heavier than Mg are used.[151]

Therefore, the shape of the mass distribution and the values of the experimental variances of light nuclei in heavy-ion reactions cannot be used directly to obtain a quantitative characteristic like the BG point, and so it is impossible to evaluate the validity of any particular version of the LDM. Until the studies carried out by the present authors in Refs. 22 and 35 were performed, this question remained open, although it was shown qualitatively in Ref. 168 that the experiments agree better with the rotating liquid-drop model of Sierk[16] than with the classical Cohen–Plasil–Swiatecki model.[36]

We recall that the same situation occurs for another characteristic that we do not study here: the fission barrier E_f. Let us give some examples.

The authors of Ref. 23 studied the strongly asymmetric fission modes of ^{111}In in the reaction ^{nat}Ag(^{3}He,f). The conditional fission barriers [the barriers at a given mass (charge) asymmetry] for the fragment Z studied were obtained by using the statistical description of the excitation functions of these modes. In Ref. 169 Sierk showed that these data are described well by the LDM taking into account the finite range of the nuclear forces,[15,16] the fission barriers in which are considerably lower (by 10–11 MeV for ^{111}In) than predicted.[13] This would appear to be a weighty argument in favor of the model of Refs. 15 and 16. However, in Ref. 170 the same data on the excitation functions of ^{111}In were analyzed, but taking into account the rotational enhancement of the level density. The barriers, obtained with the same good accuracy as in Ref. 169, corresponded to the LDM prediction, but according to Ref. 13.

The strongly asymmetric barriers of ^{149}Tb in the reaction ^{86}Kr+^{63}Cu were recently studied[171] as in Ref. 23. The barriers found experimentally lie between the predictions of Ref. 13 and those of Refs. 15 and 16.

Mention should also be made of Ref. 167. There, as in Ref. 23, the excitation functions were studied for individual Z of the fragments of the even lighter fissioning nucleus ^{75}Br in the inverse reaction ^{63}Cu+^{12}C. The fragment charge (mass) distribution has a U shape for all the excitation energies studied, which agrees with the predictions of any version of the LDM for such a light nucleus. The conditional barriers for each fragment Z were extracted by analyzing the cross sections σ_Z and accurately coincided with the Sierk

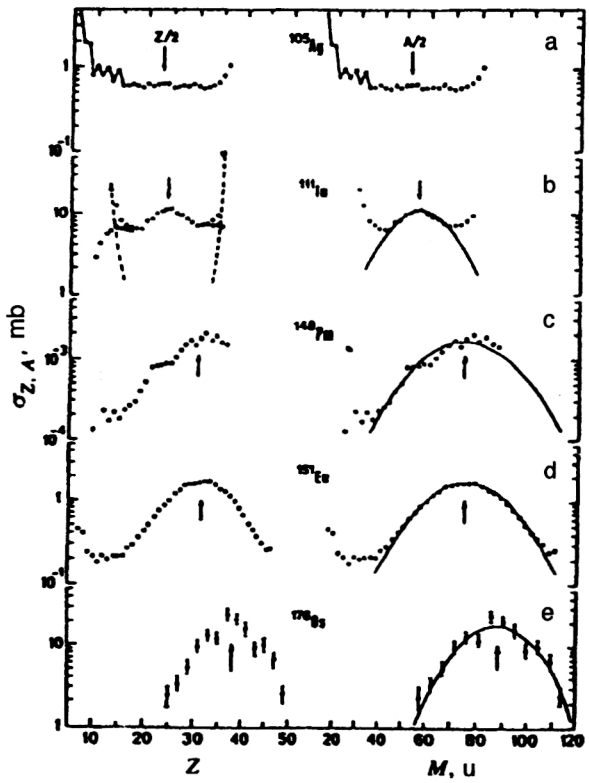

FIG. 20. Charge distributions (left) and mass distributions converted from them[22] of fragments or fragment-like particles (right) for the indicated nuclei and their Gaussian description (solid lines). (a) The reaction ^{93}Nb+^{12}C (Ref. 154); (b) ^{84}Kr+^{27}Al (Ref. 151); (c) ^{139}La+^{9}Be (Ref. 19); (d) ^{35}Cl+^{141}Pr (Ref. 165).

calculations.[16] This suggests that the results of analyzing such experiments are rather ambiguous, and that it is apparently premature to conclude that any particular model is correct, although the LDM of Refs. 15 and 16 is more realistic than the model of Ref. 13, and theoreticians themselves are convinced that it describes the physics of a real, heated, fissioning nucleus.[172]

Let us now discuss the experimental studies of Refs. 22, 35, and 70, where the questions of the BG point and the agreement between experiment and the theoretical ideas behind the LDM was studied in greatest detail. In addition to the fragment mass–energy distributions in the fission of light nuclei in reactions mainly involving ^{20}Ne ions, those studies analyzed a large number of results from other groups (Refs. 19, 26, 55, 62, 69, 107, 111–114, 127, 128, 151, 152, 154, 164–166, and 173). The fragment charge rather than mass distributions were measured in many of these studies (Refs. 19, 111, 114, 128, 151, 154, and 164–166). In Refs. 22, 35, and 70 these distributions were converted into mass distributions, using the proportionality of charge and mass, and then the resulting mass distributions were described by a Gaussian, using the least-squares method. As examples, in Fig. 20 we show typical charge distributions of fragments or fragment-like reaction products and the mass distributions obtained from them for several nuclei, together with their Gaussian description.

In Refs. 22, 35, and 70 only those results were analyzed for which, first, for fragment masses $M=A_{CN}/2$ ($Z_{CN}/2$) the

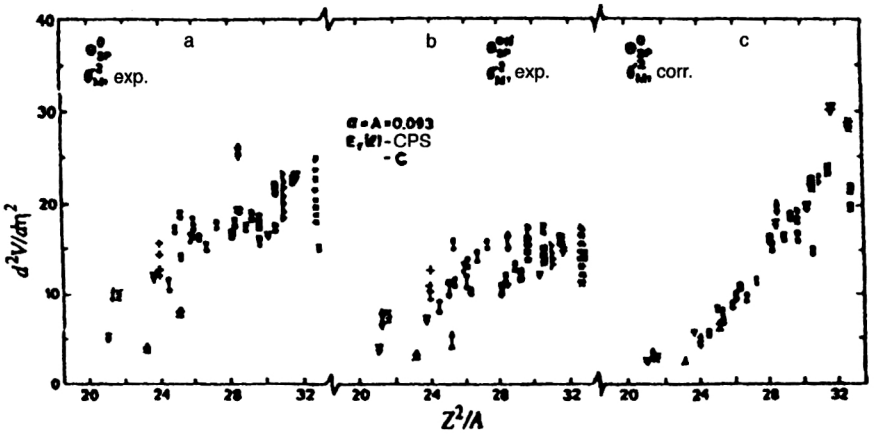

FIG. 21. Demonstration of the role of ℓ and evaporation ($\bar{\nu}_{\rm pre}$) corrections in the stiffness $d^2V/d\eta^2$ as a function of Z^2/A (Ref. 22). Each experimental point corresponds to two values of the stiffness. The upper ones were obtained with Sierk (S) barriers[16] and the lower ones with Cohen–Plasil–Swiatecki (CPS) barriers[36]. (a) No corrections at all; (b) the experimental σ_M^2 but for $\theta_{\rm sp}^{\rm efl}$; (c) σ_M^2 corrected for ℓ and with $\theta_{\rm sp}^0$ as the initial temperature. The notation for the points is given in Ref. 22.

clear peak corresponding to symmetric fission is observed and, second, the edges of this symmetric distribution are well separated from the peak corresponding to deep-inelastic transfer and quasi-fission reactions as, for example, in Ref. 151 for ^{111}In (see Fig. 20). Reactions like ^{37}Cl+^{68}Zn from Refs. 112 and 113, ^{32}S+^{76}Ge from Ref. 126, ^{28}Si+^{74}Ge from Ref. 127, and so on, were excluded from the analysis, because the charge (mass) distributions depend on the detection angle and it is not possible to separate true fission from the fission-like and quasi-fission components, which distort the mass distributions.[113,151,152]

The experimental variance σ_M^2 in the Gaussian description of the mass distribution (Figs. 17 and 20) was extracted from the data on the mass distributions used for the analysis in Refs. 22, 35, and 70. This was then corrected for the angular-momentum effect as described in Sec. 2. Then Eq. (34) was used to calculate the stiffness of the fissioning nucleus $d^2V/d\eta^2$. Equation (34) also involves the nuclear temperature $\theta_{\rm sp}$, the value of which depends on the barrier height $E_f(\ell)$ and the level-density parameter a. To make the analysis complete, $\theta_{\rm sp}^0$ and $\theta_{\rm sp}^{\rm ef}$ in these studies were calculated using the fission barriers from the Cohen–Plasil–Swiatecki (CPS) rotating liquid-drop model[36] and the Sierk (S) model.[16] In addition, $a=0.093A$ and $a=A/8$ were often used.

Figure 21 shows the role of the corrections for emission $\bar{\nu}_{\rm pre}$ in $\theta_{\rm sp}$ and for the angular-momentum effect in σ_M^2. Each experimental point corresponds to two values of the stiffness: the upper points were obtained with the Sierk barriers,[16] and the lower ones with the CPS barriers.[36] In Fig. 21a we show the values of $d^2V/d\eta^2$ without any of these corrections. The data show that the stiffness is approximately constant in the range $Z^2/A=24$–33, and, moreover, that the spread in the points is so large that reasonable extrapolation to the value $d^2V/d\eta^2=0$ is impossible. Therefore, the various models cannot be tested. It is also interesting to note one detail: the results of Refs. 62 and 107, where the fission of ^{186}Os and ^{186}Pt, respectively, was studied in reactions involving various ions, do not agree with the unified stiffness for each of these nuclei, as should follow from any LDM.

In Fig. 21b we show the same data, but with a correction introduced for $\bar{\nu}_{\rm pre}$, i.e., instead of $\theta_{\rm sp}^0$, as in Fig. 21a, we use the temperature $\theta_{\rm sp}^{\rm efl}$. The data basically have the same behavior as in Fig. 21a, although there is an overall decrease in the magnitude of the stiffness.

Figure 21c shows the influence of the ℓ effect on $d^2V/d\eta^2$ at $\theta_{\rm sp}^0$. This effect turns out to be stronger than the temperature effect. We see that in this case the experimental data already show a definite trend, i.e., $d^2V/d\eta^2$ decreases in going to light nuclei, although the point spread is still too large for an accurate determination of the BG point.

In Fig. 22 we show the experimental values of $d^2V/d\eta^2$ taking into account both corrections, i.e., with $\theta_{\rm sp}^{\rm efl}$ and σ_M^2 ($\ell=0$). It should first be noted that the point spread is much less than in Fig. 21c, and the values of $d^2V/d\eta^2$ for ^{186}Os and ^{186}Pt are transformed into single values of the stiffness for these nuclei, instead of an entire set of values, as in Figs. 21a and 21b.

These data are also compared with the theoretical calculations of the stiffness made for the β-stability valley for

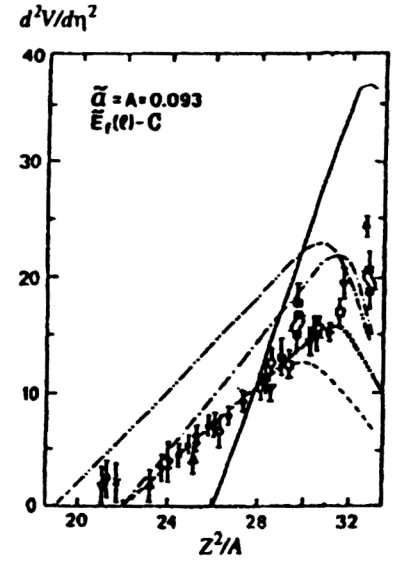

FIG. 22. The stiffness $d^2V/d\eta^2$ taking into account two corrections, i.e., σ_M^2 corrected for ℓ and $\theta_{\rm sp}^{\rm efl}$ (Ref. 22). The theoretical curves are the stiffness calculated for the saddle: the solid line is from Ref. 12, the dashed line with two dots is from Ref. 13, the dot–dash line is from Ref. 14, the dashed line is from Ref. 15 with parameters from Ref. 16, and the dotted line is from Ref. 22 with parameters from Ref. 16; $E_f(\ell)$ is from Ref. 16, and $a=0.093A$.

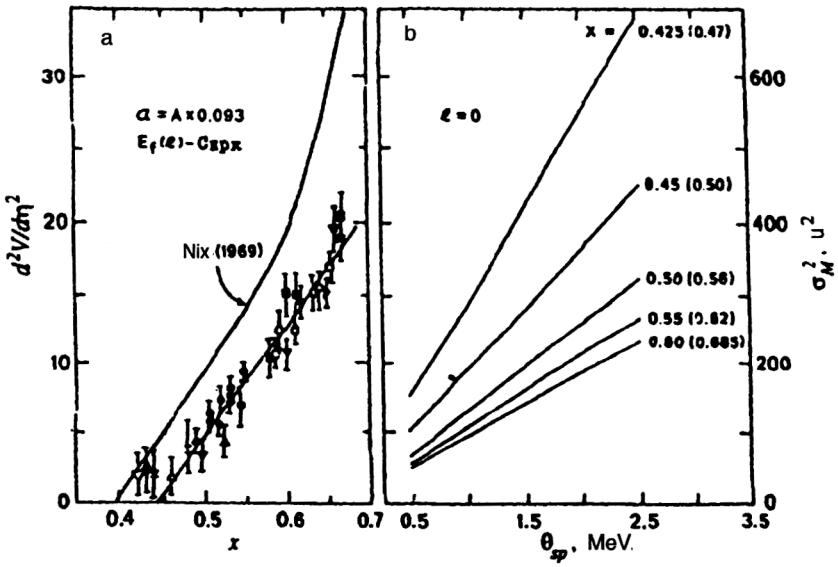

FIG. 23. (a) Dependence of $d^2V/d\eta^2$ obtained with $E_f(\ell)$ from Ref. 16 and $a=0.093A$ on the fissility parameter x. The straight line is the least-squares description of the data, and the curves are the theoretical calculations of Nix.[7] (b) Theoretical dependence of σ_M^2 on θ_{sp} for the indicated values of x from Ref. 7. The values of x corresponding to this growth of σ_M^2 with increasing θ_{sp}^{ef} (see the text) at $\ell=0$ actually found in experiment are given in parentheses.

various versions of the LDM: the simple Myers–Swiatecki (MS) LDM with sharp nuclear boundary;[13] the Strutinskiĭ (Str.) LDM taking into account the dependence of the surface tension on the surface curvature $\sigma=\sigma_0(1-\Gamma)$ for $\Gamma=-0.1$ and $(Z^2/A)_{crit}=45$ (Ref. 12); the Myers (M) droplet model;[14] and the Krappe–Nix–Sierk (KNS) LDM with finite nuclear-force range[15] with the Sierk drop parameters (S) of Ref. 16. The LDM including the finite range of the nuclear forces,[15] used for the calculations in Ref. 22, differs from the calculations of the Adeev group given in Ref. 21 in that the fission barrier is calculated for fixed fission asymmetry η taking into account the change of the elongation of the nucleus α (the basic fission deformation) for different η, i.e., along the ridge line mentioned earlier, which for nuclei with $Z^2/A>29$ tends to large α (large elongations of the nucleus) with increasing η. The resulting dependence $V(\eta)$ was approximated by a parabola for η in the range from 0 to $\eta \sim 0.2-0.3$, differentiation of which gives the effective value of $d^2V/d\eta^2$. Here the nuclear shape was described by the parametrization based on Cassini ovals.[174]

The experimental information shown in Fig. 22 reveals a clear alignment of the data, the totality of which is not described by any modification of the LDM. However, there is a surprising degree of agreement between experiment and the Sierk model[16] in the region $Z^2/A=22-30$ with $a=0.093A$ and barriers $E_f(\ell)$ from the same model.[16] Moreover, this model accurately predicts the location of the BG point, which is easily determined by linear extrapolation of the experimental data to zero: $(Z^2/A)_{BG}=22\pm0.6$. It has been shown[22] that the location of the BG point on the Z^2/A axis is not sensitive to variation of $E_f(\ell)$ and a.

To complete our discussion about the dependence of the nuclear stiffness $d^2V/d\eta^2$ on the nucleon content, temperature, and angular momentum for the experimental data on light nuclei, let us compare these data with the well known dynamical calculations of Nix,[7] performed in the statistical limit for a nonviscous, nonrotating nuclear liquid on the basis of the LDM with the parameters of Ref. 13.

This comparison is made in Fig. 23a. There we show the experimental and theoretical dependence of $d^2V/d\eta^2$ on the fissility parameter x (Ref. 7). Naturally, as in the LDM,[13] the theoretical calculations[7] give the BG point at $x_{BG}=0.396$. Extrapolation of the experimental data, from which several strongly diverging points in Fig. 23a have been excluded, to zero gives $x_{BG}=0.44\pm0.01$. A similar difference between the experimental and theoretical[7] BG points was discussed above; moreover, the Nix stiffness curve does not reproduce the general behavior of $d^2V/d\eta^2$ for $x>0.6$. This is completely understandable, because the calculations[7] neglected the nuclear viscosity and better reflect the behavior of the liquid as a function of x at the scission point, which in this case, according to Refs. 3, 7, and 11 and Fig. 19, grows monotonically with increasing nuclear mass.

Some of the calculated quantities,[7] in particular, the temperature dependence of σ_M^2, have been used in several experimental studies to extrapolate the data to a common temperature. It is now seen from comparison of theory and experiment that such an extrapolation is not completely correct. In Fig. 23b the straight lines show the theoretical dependences $\sigma_M^2(\theta_{sp})$ of Ref. 7 (naturally, for $\ell=0$) for the indicated x. In the parentheses we give the values of x for which this growth of $\sigma_M^2(\theta_{sp}^{ef})$ corresponds to the actual growth observed experimentally (also for $\ell=0$). These values of x were obtained from the solid line for the stiffness in Fig. 23a and Eq. (34).

In summary, we should again stress the surprising agreement between the static calculations of the stiffness in the model of Refs. 15 and 16, taking into account short-range nuclear forces and performed at the saddle point, and the "experimental" values of $d^2V/d\eta^2$ found in the statistical approach at the same point for nuclei in the range $Z^2/A=20-30$.

On the one hand, there would seem to be nothing surprising in this—for these nuclei the saddle point and the scission point really coincide, there is no descent dynamics, and the assumption of the Bohr–Wheeler transition-state model,[158] which has been tested many times, is valid. How-

ever, on the other hand, there is a dynamics of the passage of the nucleus from the ground state to the saddle configuration, and the above-mentioned experimental fact—the establishment of statistical equilibrium between the collective and internal degrees of freedom at the saddle point—requires that this passage be slow. This can occur if the viscosity of nuclear matter (its dissipation properties) is sufficiently large. In the opposite case of small viscosity ($\beta \leqslant 1$), according to Refs. 3 and 175 the nucleus will remember its prehistory—its state before reaching the saddle point, where the stiffness of the fissioning system is smaller than at the saddle. In this case there should be no agreement between theory and experiment in Fig. 22.

Dynamical calculations of the mass–energy distributions of fragments from the ground state taking into account viscosity and using the data on $\bar{\nu}_{\text{pre}}$, $\bar{p}_{\text{pre}}$, and so on, should shed light on this problem. Theory has taken only the first few steps in this direction.[2,8,175,176]

4. THE DYNAMICS OF THE FORMATION OF THE FRAGMENT MASS–ENERGY DISTRIBUTIONS OF NUCLEI WITH $Z^2/A>32$

There have been many studies devoted to the experimental investigation of the mass–energy distributions (MEDs) of fragments of excited heavy nuclei (Refs. 2, 4, 5, 9, 10, 20–22, 26, 35, 49, 50, 53, 55, 62, 67–70, 89–91, 93–97, 107, 108, 114, 129, 130, 133, 134, 138, 141, 155, 173, and 177–203). Various aspects of the fragmentation process as a function of the excitation energy (temperature) and nucleon content have been studied.

The theoretical description of the characteristics of the fragment MEDs for heated heavy nuclei encountered serious difficulties some time ago.[6,7,137,159,160,204] The comprehensive analysis of the experimental data performed in Ref. 202 in 1985 indicated that there is uncertainty in the description of the MED formation mechanism.

The first advances in this area were made in studies by Nix and Sierk and coauthors, who included friction forces (viscosity)—the dissipative properties of nuclear matter—in the dynamical fission model.[205–215] The model and its parameters and the conditions for breaking of the neck were modified.[206,208,211] It was assumed that the viscosity mechanism is a two-body one[205,206,208,210–213] similar to friction in an ordinary liquid, or a one-body one, owing to interaction of a nucleon with a "wall" [208–210] or with a wall and window[211] (inclusion of the presence of the neck), or with a surface and window.[214,215] However, all these calculations were performed only for the one-dimensional case. The total fragment kinetic energy E_k and other characteristics of the MEDs were not taken into account.

In the last ten years there has been considerable progress in explaining the features of the fragment MEDs in terms of the diffusion model (Refs. 3, 117, 119, 131, 157, 175, and 216–223). In it the evolution of the fissioning nucleus is described by the Fokker–Planck (FP) equations for the distribution functions of the collective variables, in which not only conservative forces and friction forces, as in ordinary dynamics, but also fluctuations of these variables are taken into account. This approach is fairly general, and it leads, as limiting cases, to the well known results of the statistical model (for large friction) and the dynamical model (for small or no friction).

The Adeev group,[3,18,131,156,220–223] whose work is summarized in Refs. 3 and 223, studied the entire spectrum of questions about the formation of the fragment mass–energy and charge distributions, and used the diffusion model systematically and successfully for describing their features quantitatively.

In the last few years studies have appeared where the fission process is described by the Langevin equation, a physical analog of the FP equations. In this approach it is assumed that fluctuations of the collective variables are taken into account "exactly," in contrast to the FP equations, where they are included "on the average." [8] These models are still in the developmental stage, but the first results on the description of pre-fission particles[59,71–75,224–226] and the energy distributions[8,78,176,224–227] are very promising.

Throughout this section, in analyzing the experimental data on $\bar{E}_k$, σ_M^2, and σ_E^2, we shall study the theoretical approaches describing the observed fragment MEDs in greater detail.

The authors of Refs. 67, 68, 89–91, 96, 111, 113, 126, 127, 134, 138, 139, 151, 178–180, 189, 192–194, 197–199, and 228, in studying (theoretically and experimentally) the fission of very light (near the BG point) nuclei and very heavy nuclei with $Z^2/A \geqslant 36$ in massive-ion ($A_i \geqslant 27$) reactions (or for very heavy targets in reactions with inverse kinematics), have shown that the fragment mass distributions and, for heavy nuclei, also the angular distributions, cannot be understood and described on the basis of the standard theoretical ideas which work well for lighter ions (targets). This process has become known as quasi-fission and is characterized by large angular anisotropy of the fragments and large width of the mass distribution compared to normal fission. It is often very difficult to determine experimentally the boundary between classical fission and quasi-fission. This question will also be discussed in this section.

4.1. The fragment energy distributions

The total fragment kinetic energy $\bar{E}_k$ and its variance σ_E^2 are the quantities usually measured in experiments. A typical example of the distributions $\bar{E}_k$ and σ_E^2 as functions of the fragment mass M for the fissile nuclei ^{206,204}Po and ^{260}Ku in several reactions is given in Fig. 12 in Sec. 2. These are liquid-drop distributions characteristic of excited nuclei:[3,7,107,137] $E_k(M)$ has a parabolic shape, and $\sigma_E^2(M)$ is nearly independent of the fragment mass. The distributions E_k and σ_E^2 for various nuclei averaged over all fragment masses have been investigated in very many studies. In our earlier review[2] we summarized the data on these characteristics, but there we assumed that $\bar{E}_k$ depends fairly strongly on the angular momentum ℓ transferred to the nucleus by the incident ion and, accordingly, we introduced corrections for this effect. After our measurements[22,67] and analysis of the work of other authors,[68,89,107,113,133,134] it became clear that $\bar{E}_k$ is practically independent of both ℓ and the excita-

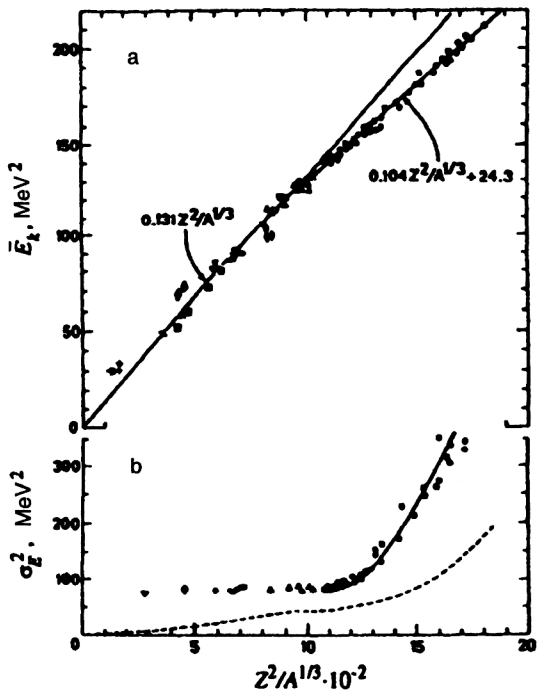

FIG. 24. (a) Dependence of the average total fragment kinetic energy $\bar{E}_k$ on the Coulomb parameter $Z^2/A^{1/3}$ (Ref. 35). The lines are the description of the data in the ranges $0<Z^2/A^{1/3}<900$ and $Z^2/A^{1/3}>900$ using the expressions given in the figure. (b) Dependence of the variance σ_E^2 on $Z^2/A^{1/3}$ for $\theta_{sp}^0=1.5$ MeV (Ref. 35). The solid line was calculated using the diffusion model,[3] and the dashed line is the Nix calculation.[7]

tion energy E^*, and that the corrections were not needed (see Sec. 2 above). Moveover, since the publication of our earlier review,[2] new, important information has been obtained about these fragment characteristics for various nuclei produced in reactions involving various ions (Refs. 9, 10, 21, 22, 35, 49, 50, 55, 67, 68, 70, 114, 127, 128, 134, 167, 177, 178, 183, 184, 197, 201, and 229–231).

It was shown in Refs. 2, 21, and 35 that if we use only the data on sufficiently heated nuclei, discarding low-energy and spontaneous fission (which are strongly influenced by shell effects) and also quasi-fission reactions involving massive ions, the dependence of $\bar{E}_k$ on the Coulomb parameter $Z^2/A^{1/3}$ is not a linear function, as follows from the systematics of Refs. 93 and 94, but has a kink at $Z^2/A^{1/3}\sim1000$.

This is illustrated in Fig. 24a, where the various symbols show the experimental results from different authors, and the two straight lines show the least-squares description of these data in the ranges $Z^2/A^{1/3}=0-900$ and 900–1800 given by Eqs. (19) and (20), respectively.

Figure 24b shows σ_E^2 at $\theta_{sp}^0\sim1.5$ MeV as a function of $Z^2/A^{1/3}$. Of course, it would be more correct to use the temperature at the scission point θ_{sc}^{ef3}, since it is this which is mainly responsible for the width of the E_k distribution. However the theoretical calculations[3] with which the experimental data in Fig. 24b are compared were performed for the temperature at the saddle point $\theta_{sp}=1.5$ MeV. Then the real temperature θ_{sp}^{ef1} or θ_{sp}^{ef2} is desirable, but our analysis showed that, on the one hand, the inclusion of $\bar{\nu}_{pre}$ makes the dependence $\sigma_E^2(\theta_{sp})$ steeper while, on the other, the ℓ correction of the data in Fig. 24b, obtained mainly in reactions involving ^{12}C, ^{16}O, and ^{20}Ne ions,[21] is such that it smooths out this dependence. The two effects cancel out and, on the average, the dependence remains unchanged. We have therefore not introduced any corrections into the data of Fig. 24b.

In this figure we clearly see the sharp increase of σ_E^2 beginning at $Z^2/A^{1/3}\sim1000$, while σ_E^2 is almost constant for $0\leq Z^2/A^{1/3}\leq1000$. The kink in $\bar{E}_k$ and the start of the growth of σ_E^2 at the same value of $Z^2/A^{1/3}$ are naturally interpreted as the starting point of the descent stage.

The dashed line in Fig. 24b shows the results of the Nix calculations[7] using the LDM for a nonviscous liquid. The solid line shows the calculations of the Adeev group[3] using the diffusion model with two-body viscosity with coefficient $\nu_0=1.5\times10^{-23}$ MeV·sec·F^{-3}, which corresponds to the hydrodynamical viscosity $\mu\sim0.024$ tP (1 terapoise $=6.24\times10^{-22}$ MeV·sec·F^{-3}), and in the language of damping of the collective motion corresponds to $\beta\sim2-3$, low viscosity. We shall see that the diffusion model[3] is capable of describing the data well, beginning at $Z^2/A^{1/3}\sim1100$, i.e., where the descent dynamics must be taken into account. However, a drawback of this model is the fact that it cannot be used to calculate the fragment MEDs for nuclei which do not have the descent stage, since in it the evolution of the fissioning system starts at the top of the barrier.

Another important detail concerning the determination of the conditions for the nucleus to break up into fragments should be mentioned. This is the scission criterion, for which there are two fundamental theoretical points of view: the scission criterion is either taken to be the vanishing of the neck thickness $r_n=0$ (this criterion has been used in many studies by Nix *et al.*[7,137,205–207,211,214,215]), or the condition that the Coulomb and nuclear forces are equal: $F_C=F_N$.

When the criterion $r_n=0$ is used, the scission configurations lie outside the range of possible continuous nuclear shapes in the liquid-drop model.[11,12,208,232] Moreover, the LDM completely loses meaning when r_n becomes comparable to the internucleon separation. The scission criterion $F_C=F_N$ is physically more justified. After the fissioning nucleus passes through this point it becomes extremely unstable to breakup—the system passes from the fission valley into the valley of separated fragments.[3,11,232] Rapid breaking of the fairly thick neck occurs almost without any change in the elongation of the nucleus, and there certainly is no gradual thinning of the neck with increasing deformation. It is this scission criterion which has been used in all the diffusion-model calculations of Adeev *et al.*,[3] shown by the solid line in Fig. 24b.

In Fig. 25 we show the neck radii r_n in fermis calculated in Ref. 208 with the condition $F_C=F_N$ for two types of nuclear viscosity, two-body (left) and one-body (right), as a function of $Z^2/A^{1/3}$. The neck radius r_n grows with the nuclear mass, becoming about 2–2.5 F for $Z^2/A^{1/3}\sim2000$.

Whereas in the studies of the Adeev group[3,117,175,220–222] the main emphasis was on the theoretical description of the variances σ_E^2 and σ_M^2, in the studies of Nix and Sierk *et al.* a large number of variants were used to calculate the total fragment kinetic energy for symmetric fission as a function

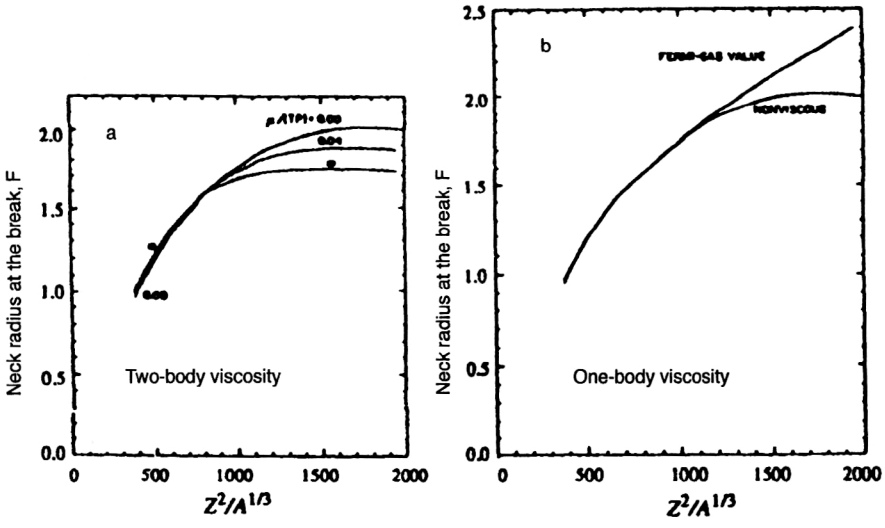

FIG. 25. Calculations of the neck radius r_n (in F) from Ref. 208 at which the nucleus breaks up into fragments with the condition $F_C=F_N$ for two-body (left) and one-body (right) viscosity as a function of $Z^2/A^{1/3}$.

of the type of viscosity and the neck radius r_n.

In Fig. 26 we compare all the experimental information on $\bar{E}_k$ (the same as in Fig. 24a), for clarity represented as a deviation $\Delta\bar{E}_k=\bar{E}_k-0.131\,Z^2/A^{1/3}$ from the linear dependence describing experiment for $Z^2/A^{1/3}\leqslant 1000$ (Fig. 24a), with various modifications of the theoretical calculations (solid lines).[208,211,215] Figures 26a and 26b are for two-body viscosity, and Figs. 26c and 26d are for one-body viscosity.

In Fig. 26a we show the results of Ref. 211, where the LDM including short-range nuclear forces[15] was used to calculate E_k for fission into equal parts at $r_n=0$. The experimental data for heavy nuclei are described fairly well for $\mu=0.015$ tP, but for lighter nuclei in the range $Z^2/A^{1/3}\sim 900-1200$ the coefficient $\mu=0.010$ tP is preferable.

Figure 26b shows the results of Ref. 208 obtained using a liquid-drop model close to that in Ref. 211 (Fig. 26a), but with the scission criterion $F_C=F_N$, when scission occurs at finite neck thickness, as shown on the left in Fig. 25. In this case a satisfactory description of experiment is obtained for $\mu=0.03$ tP, i.e., for viscosity coefficient twice as large as in the case of zero neck. This is associated with the extent (in deformation) of the descent stage: for the criterion $r_n=0$ the descent is, of course, longer. This, on the one hand, tends to decrease the Coulomb repulsion energy of the fragments E^c_{sc} owing to the elongation of the fissioning nucleus compared to the shape with the neck. On the other hand, it tends to raise the pre-scission kinetic energy E_{ps} accumulated by the nucleus during the descent, because the two-body viscosity hinders the formation of the neck.[205] That is, the larger μ is, the more elongated is the scission configuration of the nucleus. According to Ref. 208, the interplay of the terms in the kinetic energy $E_k=E^c_{sc}+E_{ps}$ causes E_k to be larger for the criterion $F_C=F_N$ for a given μ, and to obtain agreement with experiment it is necessary to increase the viscosity coefficient, thereby decreasing the calculated E_k. In the end, the theoretical description of E_k using the two-body friction mechanism is insensitive to the scission criterion.

The authors of Ref. 8 arrived at the same conclusion. They calculated E_k with the scission criteria $F_C=F_N$ and $r_n=0$, but using Langevin dynamics. The "exact" inclusion of the fluctuations of the collective variables in the two cases had practically no effect on the average values of these variables.

As mentioned above, the two-body friction mechanism is similar to friction in an ordinary liquid, when energy is

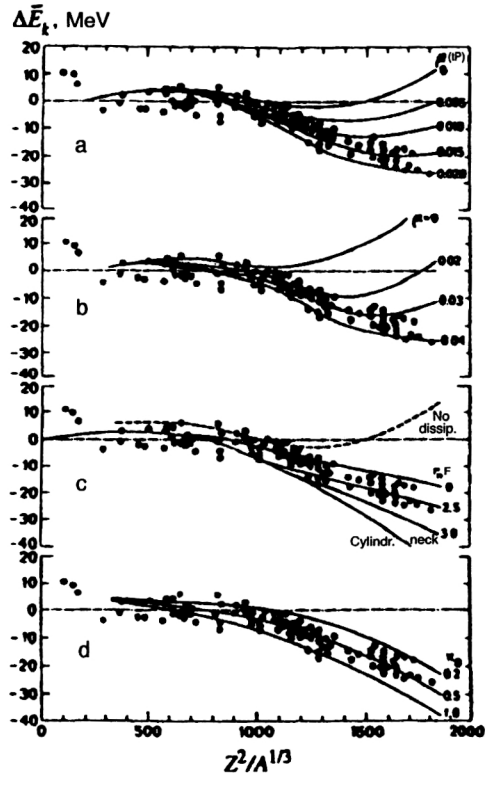

FIG. 26. Comparison of various versions of the theoretical calculation of E_k with the experimental data in the form of the deviation $\Delta\bar{E}_k$ from the line $\bar{E}_k=0.131Z^2/A^{1/3}$ as a function of $Z^2/A^{1/3}$. (a) Calculations of Ref. 213 using the dynamical model with $r_n=0$ and two-body viscosity; μ is the viscosity in tP. (b) The same as in (a) but with the scission condition $F_C=F_N$ (Ref. 208). (c) The calculations of Ref. 211 using the wall-and-window one-body dissipation mechanism for variable neck thickness r_n. (d) The calculations of Ref. 215 using the surface-and-window one-body dissipation mechanism; k_s is the reduction coefficient.

dissipated in collisions of nucleons with each other. However, owing to the Pauli principle, the nucleon mean free path in the nucleus exceeds the nuclear diameter, and so the validity of models based on this mechanism is doubtful. Nevertheless, as we shall see in examples of the theoretical description of σ_E^2 and E_k (Figs. 24b, 26a, and 26b) and, later, σ_M^2 (see Sec. 4.2), they give good results. This can be treated phenomenologically as the case of small friction.

A physically more justified assumption is that the nuclear viscosity mechanism is one-body in nature, as proposed and developed by Swiatecki *et al.*[233] This mechanism is based on nucleon interactions (collisions) with a stationary "wall" rather than with each other. The wall is a simplified image of the nuclear surface. If the presence of the neck is taken into account in the interaction with the wall at large deformations, when the nucleus is dumbbell-shaped, this viscosity (dissipation) mechanism is referred to as wall-and-window one-body dissipation.

In Ref. 211 Sierk and Nix used this mechanism to describe E_k while varying the neck radius (the window) r_n. In Fig. 26c we show the results of their calculations for $r_n=0$, 2.5, and 3.0 F and a cylindrical neck. The experimental data for $Z^2/A^{1/3}\leqslant 1100$ are described best for $r_n=0$, while for the heaviest nuclei $r_n=2.5$ F. Since for the condition $F_C=F_N$ (right-hand side in Fig. 25) r_n for light nuclei decreases to 1–1.5 F and the real scission point as a function of $Z^2/A^{1/3}$ corresponds not to a strictly defined radius but to one varying from a minimum to a maximum value, the description of the entire set of data will be very good. For heavy nuclei the condition $r_n=0$ does not satisfy the experimental requirements.

Griffin and Dworzecka[234] have studied a quantum version of one-body dissipation and have shown that viscosity in a real nucleus amounts to only about 10% of the value calculated using the wall expression. Accordingly, Nix and Sierk proposed a modified version of the one-body dissipation mechanism,[214,215] called surface-plus-window dissipation. In it the contribution to the dissipation from nucleon interactions with the nuclear surface is decreased by almost a factor of 4. The reduction coefficient (window) k_s was found by analyzing the experimental widths of isoscalar and octupole resonances and was $k_s=0.27$, with $k_s=1$ corresponding to complete one-body viscosity.

In calculations of E_k with the scission criterion $r_n=0$ in Ref. 215, the authors varied k_s from 0.1 to 1.0. The results of those calculations[215] are compared with experiment in Fig. 26d. A practically ideal description is obtained for $k_s=0.5$, but it should be stressed that all the theoretical calculations of E_k in Fig. 26 were obtained for strictly symmetric fission, i.e. for fragment mass equal to $A/2$. The experimental data correspond to average values $\bar{E}_k$ which on the average are usually 2–4 MeV smaller than $E_k(A/2)$. This means that to correctly compare theory and experiment, all the data in Fig. 26 should be raised by ~3 MeV on the average (or the theoretical values should be lowered). Then in Fig. 26d the best description will be for $k_s\sim 0.3$, which practically coincides with $k_s=0.27$, found independently of fission.

Therefore, the surface-plus-window and wall-and-window versions apparently agree best with the experiment. However, the two-body viscosity mechanism should not be excluded. As seen in Figs. 26a and 26b, it may be essential for describing E_k in the region of very heavy nuclei with $Z^2/Z^{1/3}\geqslant 1600$, where the theoretical values of E_k are too high, and those for the one-body mechanism are too low. Accurate experimental values of the fragment $\bar{E}_k$ become extremely important in this range of nuclei. The available data on $\bar{E}_k$ for $Z^2/A^{1/3}\sim 2000$ pertain to quasi-fission reactions and, as will be shown below, apparently are not suitable for testing the viscosity mechanism in the case of classical fission.

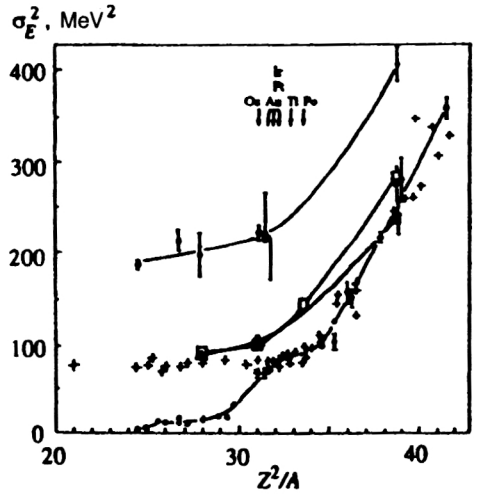

FIG. 27. Comparison of the calculated[8,227] values of σ_E^2 with the experimental data (crosses) for $\theta_{sp}^0=1.5$ MeV (Refs. 8, 10, and 227). The dark points are the calculation with the condition $F_C=F_N$, and the light circles and circles with the crosses are the calculation with $r_n=0$, both for two-body viscosity. The open squares and triangles are the calculation of Ref. 227 with two- and one-body viscosity, respectively, for random breaking of the neck. The theoretical points are joined by hand.

Now let us turn to the more detailed discussion and theoretical analysis of the variance of the total kinetic energy σ_E^2. As shown in Fig. 24b, the experimental dependence of σ_E^2 on $Z^2/A^{1/3}$ for heavy nuclei is reproduced well by the diffusion model[3] with two-body viscosity, and the scission condition is close to $F_C=F_N$.

Recently, in Ref. 8 the fragment energy distributions were described by a two-dimensional model based on the Langevin equation, which the authors refer to as Langevin fluctuation–dissipation dynamics (LFDD). Here the fission process is modeled numerically as the behavior of Brownian particles—fissioning nuclei, whose motion is studied.[8]

The dependences of E_k and σ_E^2 on $Z^2/A^{1/3}$ were calculated for the same two-body viscosity coefficient and temperature as in Ref. 3, but with different scission conditions: $F_C=F_N$ and $r_n=0$. It turned out that in this model E_k is not sensitive to the scission criterion, which corresponds to the theoretical calculations of Nix and Sierk shown in Figs. 26a and 26b.

The situation regarding the variance σ_E^2 is different. The experimental data on σ_E^2 (crosses; Refs. 10, 21, and 35) are compared with the calculations[8,227] in Fig. 27. The darkened points are for the condition $F_C=F_N$, and the open circles

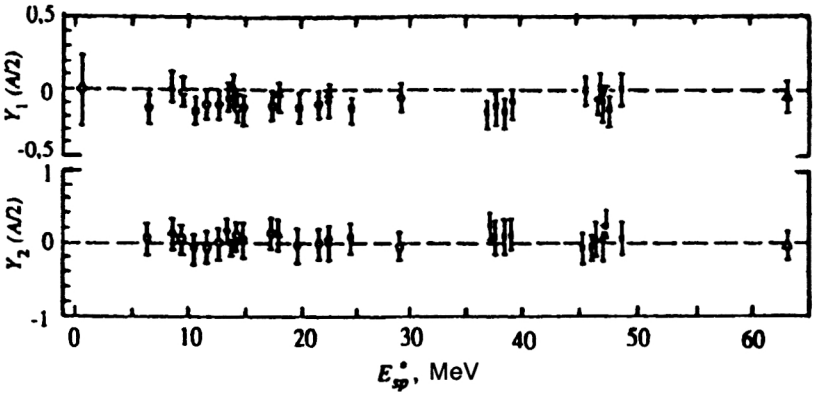

FIG. 28. Experimental dependence of the asymmetry coefficient $\gamma_1(A/2)$ and the excess $\gamma_2(A/2)$ of the energy distributions for nuclei in the range from ^{186}Os to ^{235}U on the initial excitation energy at the saddle point E^*_{sp} (Ref. 10).

and circles with a cross are for the condition $r_n=0$. As in Ref. 3, agreement with experiment is obtained for the scission condition $F_C=F_N$ at $Z^2/A\geqslant 31$. For lighter nuclei the calculation gives values of σ_E^2 which are much too low. This is the region of nuclei where the saddle-point configuration practically coincides with the scission configuration, and so in Ref. 8 the dynamical calculations were started at the top of the barrier. Both the evolution of the nucleus to the saddle point and the effect of the post-scission motion (oscillations) of the fragments were neglected. This is apparently the reason why the calculated values of σ_E^2 for light nuclei are much too low in this case.

An alternative point of view on the formation of σ_E^2, suggested in Ref. 8, is the following. For nuclei with $Z^2/A^{1/3}\leqslant 31$ the saddle-point configuration coincides with the scission configuration only for the condition $F_C=F_N$. If the criterion $r_n=0$ is used, descent occurs for these nuclei, and fluctuations of the collective variables during the descent succeed in pushing the variance to values considerably higher than the experimental ones, as shown by the open circles in Fig. 27. In principle, by decreasing the two-body viscosity coefficient and thereby lowering σ_E^2, it is possible to reproduce the experimental data with the criterion $r_n=0$, but then E_k apparently is not described (see Fig. 26a).

Change of the viscosity mechanism does not correct the situation. In Ref. 227 Kosenko carried out LFDD calculations similar to those of Ref. 8, but for the one-body surface viscosity mechanism with $k_s=0.27$. The results for the two scission criteria were practically the same as in Ref. 8. In Ref. 8 it was suggested that for a real nucleus the situation regarding the scission point might be intermediate between the two extreme cases considered. In Ref. 227 it was assumed that the neck is broken randomly after passing through the nuclear configuration with $F_C=F_N$, and σ_E^2 was calculated for both types of viscosity. This showed that the intermediate version of the scission conditions is much closer to experiment for nuclei with $Z^2/A^{1/3}\leqslant 31$. These results are shown in Fig. 27 by the squares (two-body viscosity) and triangles (one-body). However, we see that the situation is worse for heavier nuclei. We think that at present, when there are no LFDD calculations describing the dynamics for light nuclei from the ground state, and the effect of the post-scission motion of the fragments has not been taken into account, it is too early to maintain that the intermediate version of the scission conditions is realized in fission. Even though it is a beautiful and plausible scission mechanism, it is unlikely that a real nucleus breaks up at a strictly defined point with $F_C=F_N$; rather, there is probably a small region of nuclear deformations involved.

In addition to E_k and σ_E^2, the first and second moments of the energy distribution, for symmetric fission the authors of Ref. 8 also calculated the third and fourth moments, respectively referred to as the asymmetry coefficient γ_1 and the excess coefficient γ_2, defined as

$$\gamma_1=\overline{(E_k-\bar{E}_k)^3}/(\sigma_E^2)^{3/2}, \tag{35}$$

$$\gamma_2=\overline{(E_k-\bar{E}_k)^4}/(\sigma_E^2)^2-3. \tag{36}$$

These characterize the difference of the distributions from Gaussians, for which $\gamma_1=0$ and $\gamma_2=0$. The calculations[8] of γ_1 and γ_2 were again performed for the two scission criteria and for the two-body viscosity mechanism, and, in Ref. 227, for the one-body surface viscosity mechanism. It turned out that the values of γ_1 and γ_2 calculated for the two criteria $F_C=F_N$ and $r_n=0$ differ greatly not only in magnitude, but also in their Z^2/A dependence: γ_1 and γ_2 have a maximum in the vicinity of Pt ($Z^2/A\sim 32$) in the first case ($r_n=0$), and are close to zero in the second.

These results[8] stimulated Zhdanov *et al.* to perform special experiments[9,10] to carefully measure and analyze the four moments of the energy distributions for compound nuclei from Os to U, produced in reactions involving light charged particles (p, ^{3}He, and α) at various excitation energies.

In Fig. 28 we give the data on γ_1 and γ_2 for all the nuclei studied as a function of the initial excitation energy at the saddle point E^*_{sp} for fragment masses near $A/2$ (Refs. 9 and 10). The set of all experimental data shows that the energy distributions of the symmetric mode are characterized by a small, constant coefficient $\gamma_1=-0.1$ (slightly extending the low-energy tail of the distributions) and $\gamma_2=0$. These results hold for nuclei from ^{186}Os to ^{235}U and for excitation energies E^*_{sp} practically from zero to several tens of MeV. The smallness of γ_1 and γ_2 implies that it is a satisfactory approximation to take the energy distribution to be a Gaussian for fixed fragment masses.

In Fig. 29 we compare the values of γ_1 and γ_2 calculated in Ref. 8 for the two scission criteria with the experi-

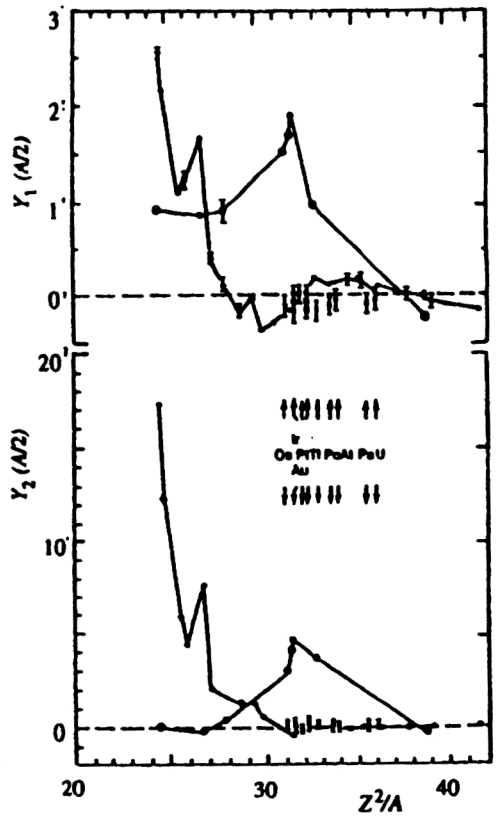

FIG. 29. Comparison of $\gamma_1(A/2)$ and $\gamma_2(A/2)$ calculated[8] for two-body viscosity with the experimental data (Ref. 10) (crosses) as a function of Z^2/A. The dark points are the calculation with the condition $F_C=F_N$, and the open circles and circles with crosses are for the condition $r_n=0$. The theoretical points are connected by lines.

mental data[9,10] represented as a function of Z^2/A. Experiment obviously rejects the criterion $r_n=0$, as the difference between the compared quantities is so large for it. The situation regarding the other criterion $F_C=F_N$ is not so clear. The experimental and the calculated values are of the same order of magnitude and quite small. However, one cannot speak of quantitative agreement in the case of the asymmetry γ_1, because for one half of the nuclei studied the signs are the same, while for the other half they are the opposite. The calculated excess γ_2 is in better agreement with experiment for the criterion $F_C=F_N$. Use of the one-body dissipation mechanism hardly changes the situation shown in Fig. 29 (Ref. 227).

It should be emphasized that the experiments[9,10] were performed for the range of nuclei where the data on σ_E^2 agree with theory, i.e., for $Z^2/A\geqslant 31$. For lighter nuclei it is apparently not worth calculating γ_1 and γ_2, which for $F_C=F_N$ tend to large values with decreasing Z^2/A. The theory in this case does not describe the second moment σ_E^2, and so it is not likely that the higher-order moments correspond to reality.

Unfortunately, so far there are no statistically significant calculations for the intermediate version of the scission criterion.

Therefore, experimental and theoretical study of the fragment energy distributions shows that their description is practically insensitive to the viscosity mechanism of nuclear matter. It depends much more strongly on the conditions for the nucleus to break up into fragments. This is particularly true of the higher moments of the energy distribution, the experimental characteristics of which reject the scission criterion $r_n=0$.

There are a few other studies in which two-dimensional models based on Langevin dynamics were used to calculate the fragment energy distributions for the nuclei ^{200}Pb (Ref. 78), ^{213}At (Ref. 176), and ^{215}Fr (Refs. 224 and 225). All these calculations differ from that in Ref. 8 in that they treat the evolution of the fissioning system starting not from the barrier, but from the ground state. We discussed Ref. 78 in Sec. 1. Its main conclusions, and also those of an earlier study by the same authors,[176] amount to the statement that the best description of the fusion–fission process, including the fusion cross sections, the evaporation residues, the multiplicities of pre-fission neutrons, and also E_k, is obtained by using the one-body wall-and-window dissipation mechanism.[211]

In Refs. 224 and 225 the calculated values of $\bar{E}_k$, σ_E^2, and the n, p, and α multiplicities for ^{215}Fr were compared with the experimental data from Ref. 55. The use of two-body viscosity with the coefficient μ varying in the range from 0.015 to 0.060 tP did not lead to agreement between the calculated values and experiment: $\bar{E}_k$, σ_E^2, and $\bar{\nu}_{pre}$ turned out to be smaller than the experimental values.

4.2. The fragment mass distributions

One of the most important problems in fission physics is to understand the mechanism for the formation of the fragment mass distributions. This was the case ten years ago,[202] and it is still the case now. Of course, during these years a great deal has been done experimentally, and theory has gone a long way in making sense of all the data. The most important area is the spontaneous and low-energy fission of nuclei with $A\geqslant 200$. Here the new idea of multimode (heteromode) fission, associated with discovery of valleys in the potential-energy surface in the multidimensional deformation space, has, in a fairly simple and physically clear way, led to a unified explanation of the main features and regularities of the asymmetric fission of these nuclei. There have been many original studies devoted to this problem. Their results are summarized in Refs. 2, 235, and 236.

The situation regarding highly excited nuclei is somewhat different. As shown in the preceding section, the theoretical description of the energy distributions is a prominent topic in the literature. Unfortunately, this cannot be said of the mass distributions. In fact, the only series of studies devoted to the theoretical aspects of the formation of the mass distributions of excited nuclei (for the modern concept of them) which has produced results that can be compared with experiment was that performed by Adeev *et al.* using the diffusion mode.[3,117,131,157,220–223] We shall base our analysis of the experimental data on these results.

It was shown in the experimental studies of Refs. 2, 4, 5, 21, 26, 68–70, and 181 that the fragment mass distributions for heavy nuclei excited above $E^*\geqslant 40$–50 MeV are nearly Gaussian, and their widths (variances) at equal (or similar)

E^* increase with increasing mass of the fissioning nucleus. In practice, the only characteristic of the mass distributions requiring analysis is the variance σ_M^2.

The authors of Ref. 70 collected and analyzed practically all the experimental information on σ_M^2 for fission fragments of heavy nuclei obtained in reactions involving electrons,[182] light charged particles (Ref. 2, 26, 62, 69, 173, and 177), and heavy ions (Ref. 21, 49, 55, 68, 89, 91, 152, 165, 180, 184, and 185) up to ^{40}Ar (Refs. 50, 55, 178, 179, 181, and 183). To systemize the data on the mass distributions, the results of the analysis[70] were represented as the dependence of the nuclear stiffness to mass-asymmetric deformations $d^2V/d\eta^2$ (34) on Z^2/A. Of course, it might be objected that $d^2V/d\eta^2$ is a static parameter, which theoretically should be determined only at specific points of the nuclear deformation trajectory, and that it does not reflect the dynamical picture of fragment mass formation in the case of an extended descent. However, owing to the amount and diversity of the experimental data in this case, this is simply a convenient method for representing the data which is independent of the reaction and excitation energy (temperature) at which a particular result was obtained.

The only parameter in the expression for the stiffness (34) is the temperature θ_i^j, where $i=$ sp or sc, $j=$ ef1, ef2, or ef3 (see Sec. 1), and σ_M^2 is the experimental variance corrected for the ℓ effect (i.e., for $\ell=0$) according to the procedure described in Sec. 2.

The data for nuclei with $Z^2/A \geqslant 33$ should be split into two parts: those obtained in reactions involving ions with $A_i \leqslant 26$ and those for which $A_i = 27-40$. This is because for ions of the first group the fission process occurs, as a rule, via the formation of a classical compound nucleus, and the fragment characteristics, in particular, σ_M^2, always correspond to true fission. For heavier ions quasi-fission processes may occur together with the associated broadening of the mass distributions (Refs. 21, 55, 68, 89, 96, 136, and 138). Let us therefore first consider the first group of data.

In Fig. 30 we show the dependences of $d^2V/d\eta^2$ on Z^2/A obtained in reactions involving ions with $A_i \leqslant 26$ for a reasonable definition of the temperature: for θ_{sp}^{ef1} in Fig. 30a, for θ_{sp}^{ef2} in Fig. 30b, and for θ_{sc}^{ef3} in Fig. 30c. The temperature was calculated for the level-density parameter $a=0.093A$ and fission barriers $E_f(\ell)$ from the study by Sierk.[16] The open circles are the results of Ref. 22 (the same as given in Sec. 3). The other points are from the analysis of the data of various authors in Ref. 70. Since in Ref. 22 and in Fig. 22 the analysis was performed only for the temperature θ_{sp}^{ef1} (all the neutrons $\bar{\nu}_{pre}$ emitted before the saddle), in Figs. 30b and 30c these data were redefined, beginning at $Z^2/A=28.5$ in accordance with the systematics for $\bar{\nu}_{pre}^{gs}$ [Eq. (17) and Fig. 7] and the value of the temperature at the scission point (18). In Fig. 30 we also show the theoretical calculations of the stiffness for $\ell=0$. The solid line shows the calculations of Ref. 3 using the simple LDM with sharp nuclear boundary[13] for the saddle point, and the dotted line shows the calculations of Ref. 22 using the LDM with finite-range nuclear forces[16] also for the saddle. In Fig. 30c, where the stiffness was calculated using the temperature or the scission point, the dot–dash line shows $d^2V/d\eta^2$ calculated using the model of Ref. 13 also for the scission configuration. The dashed line in Fig. 30 shows the calculations of Adeev *et al.*[3] using the diffusion model with the two-body dissipation mechanism.

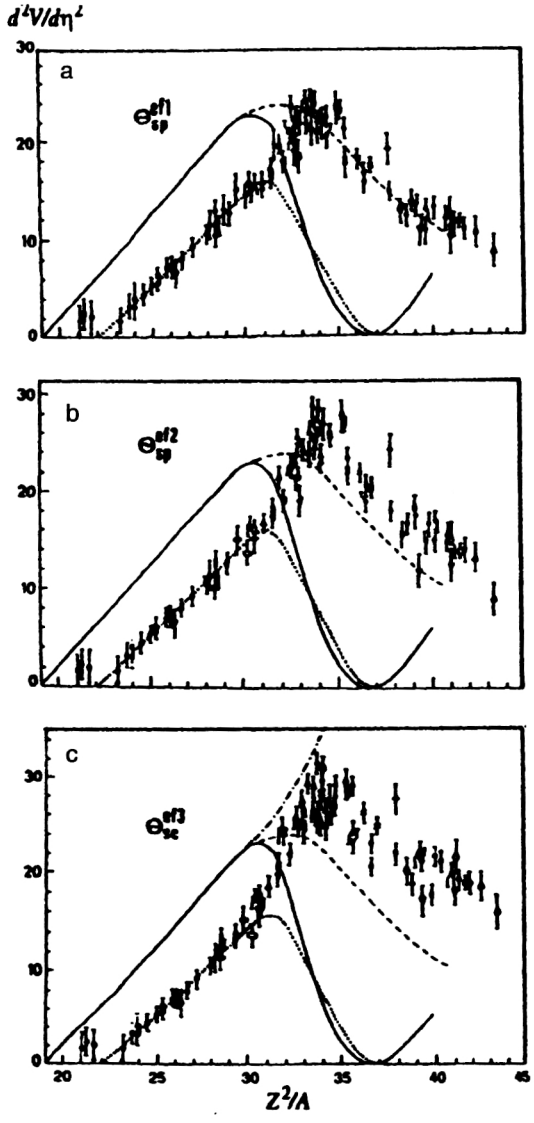

FIG. 30. Dependence of the experimental stiffness $d^2V/d\eta^2$ in the entire range of Z^2/A for $\ell=0$ for various definitions of the temperature θ_i^j (Ref. 70). The light circles are the same data as in Fig. 22 (leaving out some individual points not following the overall behavior). Theoretical curves: solid line—the calculation of Ref. 3 with the LDM parameters of Ref. 13 for the saddle point; dotted line—the calculation of Ref. 22 using the LDM including short-range nuclear forces,[16] also for the saddle; dot–dash line—the calculation of Ref. 3 with the parameters of Ref. 13 for the scission point; dashed line—the calculation of Ref. 3 using the diffusion model with the parameters of Ref. 13 and two-body viscosity.

The physical results which follow from the data on $d^2V/d\eta^2$ are:

1. The existence of a maximum in the experimental stiffness curve allows a qualitative understanding, from simple arguments, of why the angular momentum ℓ affects the variance σ_M^2 of the mass distributions differently, decreasing it for light nuclei and increasing it for heavy nuclei (see Fig. 18).

As is known from Ref. 36, the effect of ℓ on a fissioning

nucleus is like making the nucleus heavier, i.e., it corresponds to an effective increase of Z^2/A (or x).[29] As ℓ increases for a light nucleus, i.e., as $(Z^2/A)_{ef}$ becomes large, the nucleus becomes stiffer, i.e., $d^2V/d\eta^2$ grows, which in turn corresponds to decrease of σ_M^2 with increasing ℓ.

The situation is the reverse for heavy nuclei: as ℓ grows the parameter $(Z^2/A)_{ef}$ also tends to large values, and so these nuclei have smaller $d^2V/d\eta^2$ (downward slope), i.e., the stiffness decreases, σ_M^2 increases, and this corresponds to positive values of the total derivative $d\sigma_M^2/d\ell^2$. Therefore, the relation between the experimental characteristics in Figs. 18 and 30 is obvious, and this allows understanding of the entire set of data on σ_M^2, $d^2V/d\eta^2$, and $d\sigma_M^2/d\ell^2$.

2. Different definitions of the temperature θ_i^j do not lead to qualitatively new results. For heavy nuclei the absolute values of $d^2V/d\eta^2$ are somewhat changed.

3. The values of the stiffness calculated using $\theta_{sp}^{ef2}(\bar{\nu}_{pre}^{gs})$ depend strongly on model representations of the emission $\bar{\nu}_{pre}^{gs}$. In particular, if the number of neutrons emitted during the descent $\bar{\nu}_{pre}^{ss}$ is not very large, as in Refs. 59 and 72–75, the stiffness curves for θ_{sp}^{ef1} and θ_{sp}^{ef2} must approach each other, particularly in the region $Z^2/A=31-37$.

4. The experimental stiffness determined at the scission point was, we recall, obtained by using the maximum value θ_{sp}^{ef3}. If the deformation energy E_{def} is somehow included in (18), the stiffness at this temperature will approach that at the other two.

5. The stiffnesses obtained from reactions involving electrons and light charged particles, and from heavy-ion reactions, do not stand out in Fig. 30, but fit in with the complete set of points. This indicates that the corrections to σ_M^2 for the influence of ℓ have been introduced correctly.

6. The experimentally determined stiffness for nuclei with $Z^2/A\leqslant 30$ is well described by the LDM[16] independently of the definition of θ_i^j. This conclusion is trivial, because for these nuclei the saddle and scission points practically coincide in deformation and energy.

7. For nuclei with $Z^2/A\geqslant 34$ the experimental stiffness does not correspond to the theoretical calculations either for the saddle point, where the prediction is $d^2V/d\eta^2=0$ for $Z^2/A\sim 37$, or for the scission point, where the stiffness should grow continuously with increasing Z^2/A. The values of the experimental stiffness lie between these two extremes, although the effect of the saddle is significant. This conclusion is far from new, but it acquired a rigorous quantitative foundation in Ref. 70, where a large amount of experimental data was analyzed and the effect of ℓ on σ_M^2 and of $\bar{\nu}_{pre}$ on θ_i^j was correctly taken into account.

The diffusion-model calculations of Adeev *et al.*[3] (dashed line in Fig. 30) give a good reproduction of the experimental stiffness in Fig. 30a for nuclei with $Z^2/A\geqslant 34$, while for other cases (Figs. 30b and 30c) they qualitatively describe the behavior of these dependences. However, they were obtained by using the parameters of the LDM[13] (solid line), which itself for light nuclei, where there is no descent stage and the dynamics is not important, does not correspond to experiment. Unfortunately, there are still no calculations using the diffusion model based on the LDM including the finite range of the nuclear forces.[15,16]

This problem has yet another interesting theoretical aspect. The dashed line in Fig. 30 was calculated by assuming a two-body dissipation mechanism of nuclear matter. However, experiments performed in the last decade to determine the multiplicity of pre-fission neutrons[37,38] (see Sec. 1), the features of pre-fission γ rays emitted from a giant dipole resonance,[237] the properties of quasi-fission,[89] and also our analysis of the energy distributions in the preceding section, all favor a one-body diffusion mechanism in the nucleus,[233] or, according to the studies of Frobrich and Gontchar,[59,72–75] some combination of such mechanisms (an intermediate version).

Calculations using a surface one-body dissipation mechanism with $k_s=0.27$ were performed in Refs. 3 and 222. It turned out that σ_M^2 is weakly (within 10–20%) sensitive to the dissipation mechanism, but the reasons why large values of σ_M^2 occur for heavy nuclei are different. For two-body dissipation the descent from the saddle occurs over a finite, relatively short time ($4-8\times 10^{-21}$ sec; Ref. 3). In this case the fissioning system at the scission point "remembers" its prehistory, and the faster the descent, the closer to the saddle are the remembered stiffnesses. Since the stiffness grows monotonically in going from the top of the barrier to the scission point, fewer of its values are remembered than at the scission point, and the corresponding variance σ_M^2 grows.

For the one-body mechanism the descent proceeds nearly an order of magnitude more slowly ($20-50\times 10^{-21}$ sec; Ref. 3), and this causes the prehistory to be forgotten. However, the large magnitude of the viscosity (friction) leads to strong dissipation of the energy concentrated in the collective degrees of freedom into the internal degrees of freedom. The nucleus is more strongly heated by the time scission occurs, and this is naturally accompanied by a significant increase of the fluctuations of the collective variables, including the mass asymmetry. In the end, this causes the stiffnesses determining the values of σ_M^2 to be averaged over a large part of the descent and, accordingly, over the time progression of the process.[3,5] It thus becomes clear why the experimental variances σ_M^2 and the corresponding stiffnesses in Fig. 30 lie between the two extremes, saddle and scission. The data in Fig. 30 can therefore be averaged for a given temperature at the barrier and in scission:

$$[(d^2V/d\eta^2)_{1\text{ or }2}+(d^2V/d\eta^2)_3]/2. \tag{37}$$

In this case

$$(\theta_{sp}^{ef1\text{ or }2}+\theta_{sc}^{ef3})/2, \tag{38}$$

which will correspond to the experimental stiffness and temperature roughly in the middle of the descent (not shown in Fig. 30).

We see that the mass distributions, like the energy characteristics, cannot give any direct answer to the question of which friction mechanism, two- or one-body, is realized in the nucleus.

The basic feature distinguishing one friction mechanism from the other in calculations is the time for the descent from

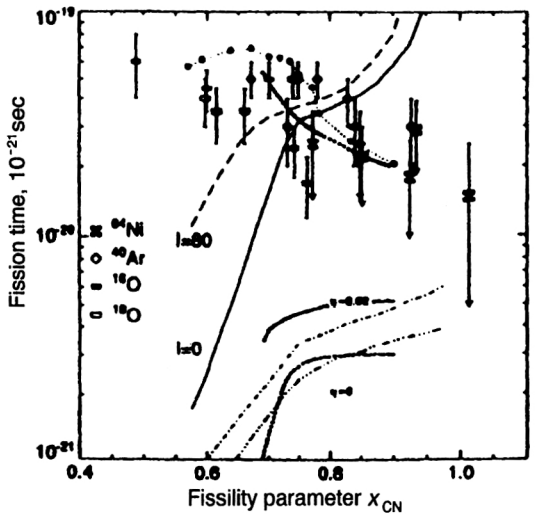

FIG. 31. The total fission time (the symbols with errors), extracted from the data on $\bar{\nu}_{pre}$ for the indicated reactions for various nuclei, as a function of x (Refs. 37, 55, and 75). Theoretical curves: dot–dash lines—the calculation[213] of the descent time using the dynamical model with two-body viscosity for $\mu=\eta=0$ and $\mu=\eta=0.02$ tP; lower dotted lines—the calculation[3] using the diffusion model also with two-body viscosity for $\mu=0$ and $\mu=0.02$ tP; solid line—the calculation[213] with one-body viscosity for $\ell=0$; the dashed line is the same as the solid line but adapted to $\ell=80\hbar$ (Refs. 37 and 75); dark circles—the calculation[75] of the most probable fission time; upper dotted line—the average descent time in the diffusion model[3] with the one-body surface viscosity mechanism for $k_s=0.27$.

the saddle to the scission point. As mentioned above, the difference between the times in the two cases can reach an order of magnitude. If it were possible to measure the time experimentally, the friction mechanism could be determined.

A special sort of clock for measuring the average fission time (the time for the nucleus to reach the barrier, plus the descent time) is, according to Refs. 37, 47, 49, 50, and 55–58, the average multiplicity of pre-fission neutrons $\bar{\nu}_{pre}$. To emit an observable number $\bar{\nu}_{pre}$ in going from the ground state to the scission point, the nucleus needs to survive for some finite time. Conversely, the desired fission time can be extracted from the data on $\bar{\nu}_{pre}$ by using model representations of the neutron evaporation. A procedure of this type, based on a modified statistical model with the introduction of a time-delay parameter to allow the model to describe experiment, was suggested in Ref. 50 and used in Ref. 55 to analyze the experimental data on $\bar{\nu}_{pre}$ as a function of the excitation energy and nucleon content of fissioning nuclei.

In Fig. 31 (Refs. 37, 55, and 75) we show the "experimental" average total fission times (the symbols with errors) obtained in the indicated reactions as a function of the fissility parameter x. The results for ^{64}Ni ions should have been excluded from these data, because they characterize quasifission (more on this in the following section). The various curves are the theoretical average descent times and not the total fission times. Although this comparison is not completely correct, for heavy nuclei ($x\geqslant 0.75$), for which the saddle-point configuration is close to the ground-state one and the fission process essentially consists of a single descent, it is to some extent justified.

In the lower part of Fig. 31 the dot–dash and dotted lines show the calculations of Refs. 213 and 3, respectively, for a nonviscous nucleus ($\eta=\mu=0$) and using two-body viscosity with $\eta=\mu=0.02$ tP. The solid line shows the calculations of the dynamical model[213] for $\ell=0$, and the dashed line is the same but adapted to $\ell=80\hbar$ (Refs. 37 and 75) for the one-body wall-and-window mechanism. The upper dotted line is the calculation of Adeev *et al.*[3] for the diffusion model using the one-body surface-and-window mechanism with $k_s=0.27$. The large darkened circles are the calculations of Gontchar[59,75] with the intermediate dissipation mechanism (see Sec. 1 above).

What do we learn from Fig. 31? The calculations[3,213] using two-body friction are not capable, in contrast to the mass–energy distributions, of reproducing the "experimental" fission times. The dynamical model[213] with one-body viscosity gives a behavior as a function of x which is opposite to that observed experimentally: the descent time grows with increasing nuclear mass along with the extent of the descent.[213] A picture close to the experimental one is obtained in the diffusion model.[3] Here the fissioning system spends a long time near the saddle, and then it leaves it and reaches the scission point.[3] For a relatively light nucleus ($x\sim 0.7$) there is almost no energy difference between the saddle and the scission point, and the nucleus "fluctuates" for a long time on the nearly flat potential surface. In this case the descent time is large. For heavy nuclei ($x=0.8–0.9$) the saddle–scission-point energy difference becomes large, and the fissioning nucleus begins the descent right away, which leads to smaller times than those seen in Fig. 31.

We stress the fact that the diffusion model[3] was not used to describe $\bar{\nu}_{pre}$. In it the descent times for one-body viscosity were calculated for the fragment mass–energy distributions, and the agreement between the "experimental" and calculated values in Fig. 31 undoubtedly favors the one-body dissipation mechanism.

For the "intermediate" version of viscosity proposed by Frobrich and Gontchar,[59,72–75] the behavior of the most probable fission time is also close to the experimental behavior.

However, we should not be seduced by the quantitative agreement between the "experimental" times and the theoretical ones, because the experimental times are themselves model-dependent. These times, extracted from the $\bar{\nu}_{pre}$ data of the same study,[55] have recently been reanalyzed in Ref. 238, using a new time-dependent combined statistical model taking into account the fusion dynamics.[139] The new values of the experimental fusion–fission times turned out to be an order of magnitude larger than those in Fig. 31. On the average they are $(2–5)\times 10^{-19}$ sec. However, the tendency for the time to decrease with increasing x remains.

Another, in our opinion, convincing (although indirect) argument for the nature of dissipation in the nucleus is the case of low-energy fission, which is rather far from our situation. It is well known that in the thermal-neutron induced fission of actinide nuclei, the proton even–odd effect in the fragment yields decreases with increasing nuclear mass,[236,239,240] which is interpreted in those studies as a

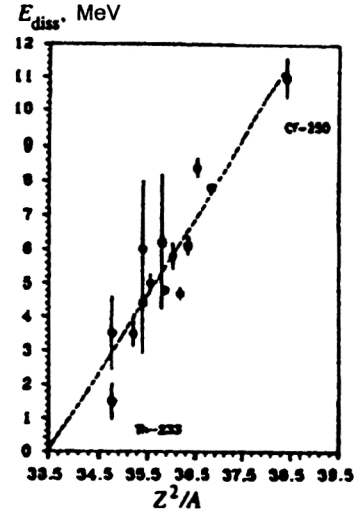

FIG. 32. Dependence of the dissipated energy E_{diss} on Z^2/A extracted from the data on the even–odd effect in low-energy actinide fission.[240] The dashed line is the least-squares description of the data.

manifestation of the viscosity properties of nuclear matter during the descent stage. The heaver the nucleus, the longer the descent (in the deformation, but possibly not in the time), and it is natural to expect that the energy dissipated from the collective degrees of freedom to the single-particle ones is larger. The proton pairs are split, owing to heating of the nucleus. The energy going into the breaking of these pairs, i.e., the dissipation energy E_{diss}, can be found from the experimental data on even–odd effects and the fragment yields, using theoretical representations of the energetics of this breaking.[236,239,240] In Fig. 32, taken from Ref. 240, we show the dependence of E_{diss} on the parameter Z^2/A. The dashed line is the least-squares description of the data. Here $E_{diss}=0$ for $Z^2/A=33.5$. Let us now return to the stiffness $d^2V/d\eta^2$ in Fig. 30. As already mentioned, the maximum of the stiffness curve is located at $Z^2/A\approx34$, and the changeover from the monotonic growth characteristic of light nuclei occurs at $Z^2/A\approx33.5$. It is this point which can be interpreted as the beginning of the manifestation of the descent from the top of the barrier, because the stiffness grows continuously for the scission point.

Therefore, the relation between these apparently heterogeneous data on the properties of low-energy fission and excited nuclei is obvious. It would appear to indicate that the same dissipation mechanism, one-body friction, is realized in both cases, because in fission induced by thermal neutrons, and especially the shell process, the Pauli principle imposes even more rigorous conditions on two-body nucleon collisions than at high excitations.

There is a viewpoint regarding the formation of the mass distributions differing from that of Adeev *et al.*[3] Brosa *et al.*[235,241] have constructed a model of fission which attributes the large variance of the mass distributions to breaking of the neck by random fluctuations (a similar possibility was also considered in Ref. 5), completely neglecting the viscosity of nuclear matter. However, the parametrization of the fissioning nucleus with a thick, elongated, cylindrical neck chosen in Refs. 235 and 241 seems rather artificial. For a physically more realistic neck, as, for example, in Refs. 3, 11–16, 205–215, and 232, the contribution to the observed variance from fluctuations of the scission location is no more than 5–10% (Ref. 3).

Now let us consider the variances of the mass distributions as functions of the temperature θ_i^j, the angular momentum ℓ, and the nucleon content.

Figure 33 shows the behavior of σ_M^2 for $\theta_i^j=1.5$ MeV as a function of the fissility parameter x for $\ell=0$ and $\ell=50\hbar$. The values of σ_M^2 for $l=0$ were obtained from the experimental averaged stiffness curves in Fig. 30a and Eq. (33). The variance for $\ell=50\hbar$ was found by using the coefficients $d\sigma_M^2/d\overline{\ell}^2$ (Figs. 16 and 18) for the corresponding temperatures θ_i^j. In Fig. 33 the circles show the data for light nuclei,[22] and the squares show the data for heavy nuclei.[70] In Figs. 33b and 33c the data begin at $x=0.6$, because for lighter nuclei the dependence $\sigma_M^2(\theta_i^j,\overline{\ell}^2)$ is the same as in Fig. 33a. We hope that Fig. 33 needs no further commentary.

4.3. The properties of quasi-fission

In studying the properties of the mass distributions in the preceding subsection we limited ourselves to reactions involving ions (or targets in inverse kinematics) with $A_i<27$.

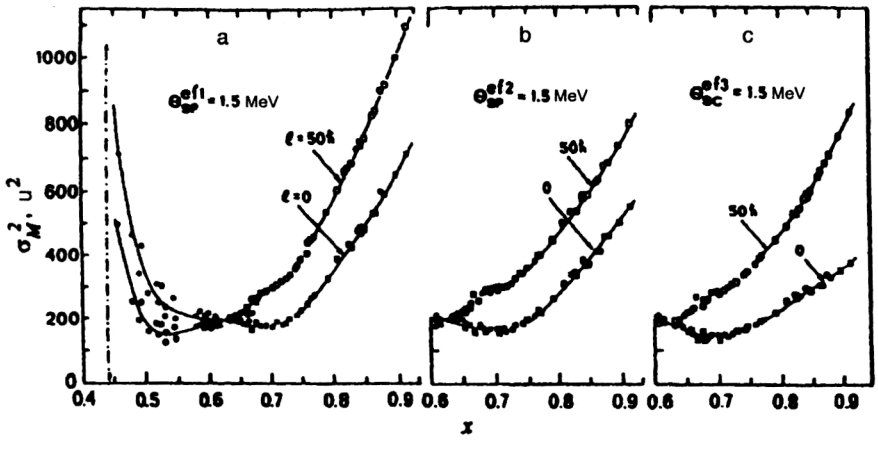

FIG. 33. Dependence of σ_M^2 on x for $\theta_i^j=1.5$ MeV for $\ell=0$ and $\ell=50\hbar$. The circles (light and dark) are the data for light nuclei,[22] and the squares are the results of Ref. 70 for heavy nuclei.

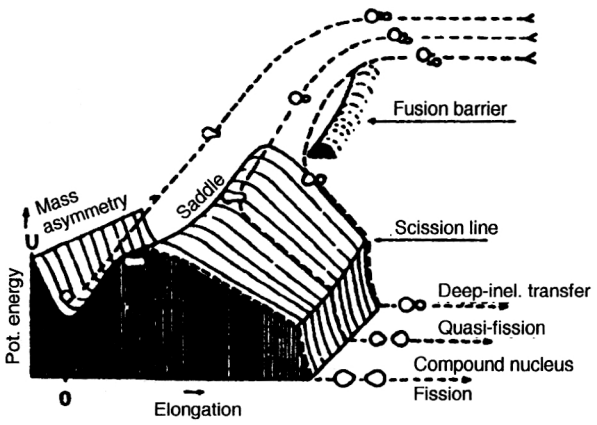

FIG. 34. Schematic depiction of the trajectories in the interaction of a massive ion with a target nucleus leading to true fission, quasi-fission, and deep-inelastic scattering.[242]

In interactions with such ions, nuclei undergo complete fusion followed by true fission, which is what we have studied up to now.

Now let us consider the features of reactions involving ions with $A_i \geqslant 27$, which often lead to a process referred to as quasi-fission.

Theoretical approaches to the description of fusion and quasi-fission in reactions involving massive ions have been worked out in greatest detail by Swiatecki *et al.*[233] and Feldmeier[139] using dynamical models with a one-body dissipation mechanism.

The interaction of a massive ion with a nucleus is shown schematically in Fig. 34 (Ref. 242). The following can occur in such a collision, depending on the impact parameter: complete fusion with the formation of a classical compound nucleus which can then undergo fission in the usual manner; deep-inelastic scattering; or the intermediate case, quasi-fission. In the latter the colliding nuclei at some time form a double system with a neck. Then nucleon exchange and mass redistribution begin, after which the neck can disappear altogether without the system reaching the deformations characteristic of a fission barrier or, even more so, of the ground state. Complete relaxation of the mass-asymmetric coordinate does not occur. The last stage of the fission process, descent, does occur, apparently often without a complete trajectory.

We thus see that the quasi-fission process occurs over a time shorter than that for true fission. The "nuclear clock"—the multiplicity $\bar{\nu}_{\text{pre}}$—for such reactions clearly indicates this[55] (see Fig. 31, for reactions involving ^{64}Ni ions).

Experimentally, one naturally observes a superposition of all possible nuclear decay channels. The contribution of each component depends on the particular reaction studied: the mass, the ion and target charges, the incident ion energy, the excitation energy of the system, the detection angle of the products, etc., and it is often quite difficult to separate one reaction channel from the others, for example, to separate true fission and quasi-fission.

The properties of quasi-fission reactions have been studied in greatest detail in Refs. 89, 96, and 138, where the fusion–fission–quasi-fission cross sections, the fragment angular distributions, the fragment mass–energy distributions, and the mass–energy and mass–angle correlations were studied in the inverse kinematics using beams of ^{208}Pb (Ref. 138) and ^{238}U (Refs. 89 and 96) ions and targets from ^{16}O to ^{89}Y.

As an example, in Fig. 35 we show the results from Ref. 96, which reflect the main properties of fission and quasi-fission in the reactions ^{238}U+^{16}O, ^{27}Al, ^{48}Ca for uranium-ion beam energy equal to 6 MeV/nucleon.

On the left in Fig. 35 are the two-dimensional fragment distribution matrices in the total kinetic energy and mass (E_k, M), in the middle are the two-dimensional mass–angle matrices in the c.m. of the system, and on the right are the mass distributions (yields) of the reaction products summed over angles.

The reaction ^{238}U+^{16}O is an example of true fission: the fragment matrix (E_k, M) has the classical triangular form,[3,137] and the mass distribution itself is independent of the angle; accordingly, the yields for forward and backward angles are the same (dot–dash lines on the right-hand figure).

The reaction ^{238}U+^{27}Al has similar properties, but the mass–angle correlation clearly displays a rotation of the matrix for the lightest and heaviest fragments, reflecting the nonequilibrium nature of the process for these fragments. This is also manifested in the width of the mass yields (right-hand figure). It is increased, because the distributions for forward and backward angles no longer coincide (dot–dash lines). However, it should be noted that the mass yields measured in such reactions for $\theta_{\text{c.m.}} \sim 90°$ and nearby angles in many experiments are obtained by using fragment detectors, and the width will in practice not be distinguished from that in ordinary fission. In this case the quasi-fission process can be identified only from the fragment angular distributions,[228] the anisotropy of which turns out to be larger than in true fission.[89]

The reaction ^{238}U+^{48}Ca shows that the contribution of quasi-fission dominates with a clearly expressed forward–backward asymmetry of fragment-like products. While the shape of the distribution is reminiscent of a Gaussian with large variance, it is formed, as seen in the right-hand figure of Fig. 35 (dot–dash line) from nonequilibrium fission-like products.

The signs of quasi-fission were clearly formulated in Ref. 89:

(a) a large width of the mass distributions incompatible with the fission of a compound nucleus;

(b) asymmetry in the fragment mass–angle correlations;

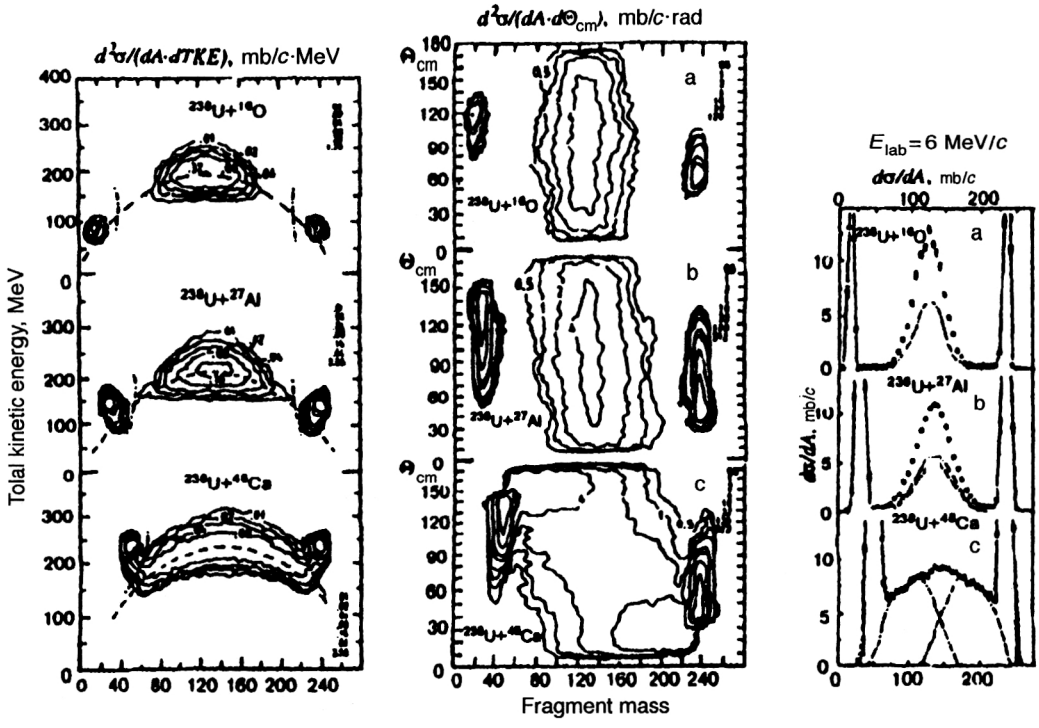

FIG. 35. The main features of fission fragments or fission-like products in the reactions $^{238}U+^{16}O$, ^{27}Al, and ^{48}Ca at the uranium ion energy 6 MeV/nucleon (Ref. 96). Left—the two-dimensional mass–energy matrices of the reaction products; middle—the two-dimensional mass–angle correlation matrices in the c.m. frame; right—yields of reaction products. The dot–dash line is the forward–backward product distribution according to the average pictures.

(c) large angular anisotropy of the fragments, which cannot be attributed to the fission of a compound nucleus.

Characteristics of the fission and quasi-fission processes as detailed as those obtained in Refs. 89, 96, and 138 have not been obtained in most of the experimental studies (Refs. 5, 55, 67, 68, 107, 108, 178–181, 183, 186, and 198). Often only the variance σ_M^2 or the full width at half the maximum of the mass distribution are obtained, and from these alone it is difficult and often impossible to understand the formation mechanism in a particular reaction. For example, the large width of the mass distribution for heavy nuclei can be associated both with the effect of the angular momentum ℓ in the standard mechanism of true fission and with, as we shall see, quasi-fission.

In Fig. 36 from Ref. 68 we show the experimental data directly as the variances σ_M^2 and σ_E^2 measured in Refs. 2, 21, 89, 138, 181, 186–189, 195, and 203 and the values calculated using the diffusion model[3] (solid lines) for nuclei with $x>0.6$. No corrections for ℓ and θ_i^j have been introduced. Here the reactions differ noticeably in the excitation energy in the entrance channel, but the differences in the effective temperature θ_i^j are small, within 20%. In Fig. 36 we introduce differentiation with respect to the incident-ion mass. The dark symbols show the data for reactions involving "light" heavy ions for strongly asymmetric ion–target systems, $A_t/A_i \geq 10$, the light symbols are for reactions involving massive ions, $A_t/A_i < 10$, and the stars are for reactions involving light charged particles ($A_i \leq 4$).

The x dependence of σ_M^2 (Fig. 36a) has two branches. Up to $x=0.85$ the data are, on the average, located at the same mass and correspond to true fission, practically independently of the entrance channel, the temperature, and the angular momentum. Beginning at $x=0.85$ ($Z^2/A\sim 40$) they abruptly split. For "light" ions σ_M^2 in general is less than 800 u^2, and for massive ions quasi-fission comes into play, strongly broadening the mass distributions, and σ_M^2 grows by nearly an order of magnitude.

A different situation occurs for the variance σ_E^2 shown in Fig. 36b. If there are differences between the cases of light and heavy ions, in general they are small.

An interesting picture is observed for the total fragment kinetic energy. In Fig. 37 we compare the experimental values of $\bar{E}_k$ for true fission and quasi-fission. This figure has been constructed like Fig. 26. The data are shown in the form of deviations $\Delta\bar{E}_k$ for two types of reaction. The dark points are the same as in Fig. 26 beginning at $Z^2/A^{1/3}=800$, and the light points are the results of Refs. 55, 89, 96, and 196, where quasi-fission was studied in reactions involving ions (targets) from ^{27}Al to ^{nat}Zn. For comparison, in this figure we show the same theoretical calculations of $\bar{E}_k$ by Nix and Sierk as in Figs. 26a and 26d with two- and one-body viscosity.

The measurement results displayed in this form show that in quasi-fission there is probably no complete relaxation of $\bar{E}_k$; on the average, it is clearly higher than for normal fission. Moreover, the actual value for a particular nucleus apparently depends on the conditions in the entrance channel, in contrast to true fission, where there is no such dependence[67,107] (see Sec. 2).

Let us confirm this by some typical examples. The authors of Ref. 55 studied the fragment mass–energy distribu-

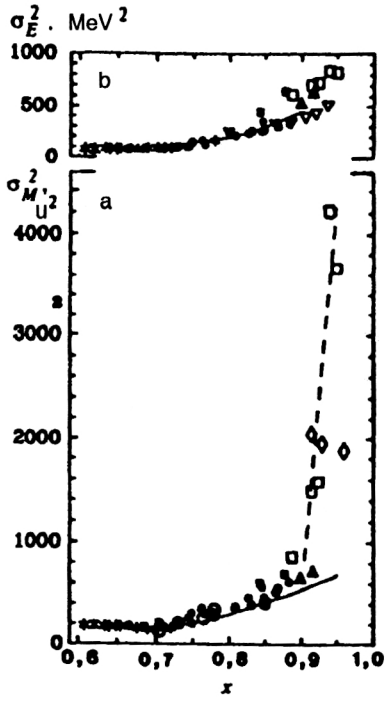

FIG. 36. Experimental data on σ_M^2 and σ_E^2 for $x>0.6$ (Ref. 68). No corrections have been introduced. The dark symbols, including the stars, are for reactions involving light charged particles and heavy ions for strongly asymmetric ion–target combinations with the ratio $A_t/A_i<10$. The solid lines were calculated using the diffusion model.[3] The dashed line shows the quasi-fission branch.

tions in the reactions $^{16}O+^{208}Pb\rightarrow^{224}Th$ and $^{64}Ni+^{154}Sm\rightarrow^{218}Th$, leading to fission and quasi-fission of thorium. In the second case $\bar{E}_k$ and σ_E^2 are, respectively, 8 MeV and $\sim$200 MeV^2 higher than in the first reaction, although for reactions involving ^{16}O ions the initial excitation energy is higher (by $\sim$50 MeV). One might get the impression that different thorium isotopes are studied in these reactions. However, the data of Glagola *et al.*[107] for true fission show that in the reactions $^{32}S+^{144-154}Sm\rightarrow^{176-186}Pt$, where the platinum isotopes undergo fission and the isotope chain reaches 10, $\bar{E}_k$ is the same for all isotopes to within 1 MeV.

Furthermore, in Ref. 89 in the reactions $^{238}U+^{40,48}Ca$ it was found that $\bar{E}_k$ for the ^{48}Ca ion is again higher by 6 MeV on the average than for ^{40}Ca ions. The variance σ_E^2 is also

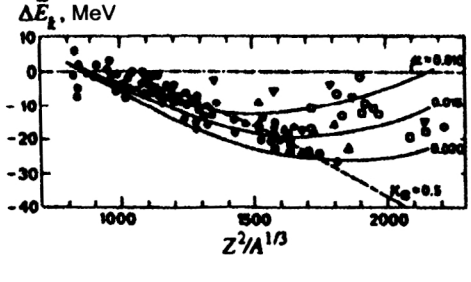

FIG. 37. Comparison of the experimental values of $\bar{E}_k$ for true fission and quasi-fission, represented as $\Delta\bar{E}_k$ (as in Fig. 26). The dark symbols are the same as in Fig. 26 beginning at $Z^2/A^{1/3}=800$. The light symbols are the results of Refs. 55, 89, 96, and 195 for reactions involving ions with $A_i>27$. The solid and dashed lines are the same as in Figs. 26a and 26d.

somewhat larger for the heavier ion. These examples show that it is very likely that the quasi-fission trajectories in the configuration space of a composite (but not compound) ion–target system differ, even in the final (descent) stage, from the trajectories characteristic of true fission. Apparently, in quasi-fission the nucleus is broken up in more compact configurations. The authors of Ref. 89 arrived at the same conclusion.

Unfortunately, at present there are no direct experimental data on the comparison of the energy characteristics of the fragments of "classical" fission and the fragment-like products of quasi-fission for the same nucleus. Such experiments could shed light on the fusion–fission–quasi-fission dynamics of massive ions and nuclei.

The problem of the fragment kinetic energy was studied theoretically in Ref. 243 for the reactions $^{32}S+^{238}U$ and $^{40}Ar+^{232}Th$ leading to the quasi-fission of $^{270,272}108$ nuclei. There it was noted, first, that the Swiatecki parametrization[233] of the nucleus with a neck is quite suitable for such reactions, because the calculated mass dependence of the distance between the fragment centers of mass $D(M)$ characterizing the Coulomb repulsion energy are quite close to experiment.[189] Second, breaking of the neck occurs not at zero neck radius, but at finite r_n. The best agreement with experiment was obtained for $r_n=2/9$ of its length, as suggested in Refs. 235 and 241. Third, it turned out that $D(M)$ is actually the same for these two reactions, both in absolute value and in behavior. However, the authors of Ref. 243 considered only central ion–target collisions, and it is not known how the system will behave for other possible impact parameters which are characteristic also of quasi-fission (Fig. 34) and for which it is important to include the angular momentum of the system. In addition, it is not clear in that study[243] which pre-scission energy is realized for these reactions: is it the same one? Therefore, the theoretical understanding of the properties of the energy distributions for quasi-fission essentially remains incomplete.

CONCLUSION

In this review we have analyzed the characteristics of the fragment mass–energy distributions in the fission of excited nuclei covering the range of Z^2/A from 20 to 43.

We have considered a wide range of questions related to the static properties of the liquid-drop model and the ability of various modifications of it to describe experiment. Comparison of the theoretical and experimental information about the stability of heated nuclei to mass-asymmetric shape variations leads to the conclusion that the LDM including short-range nuclear forces, at least for light nuclei with $Z^2/A=20-30$, gives a sufficiently good reproduction of the experimentally observed dependence of $d^2V/d\eta^2$ on the nucleon content and correctly predicts the location of the BG point.

Dynamical processes play an enormous role for heavy nuclei with $Z^2/A>32$. They lead to dissipation of the energy stored in the collective degrees of freedom to the internal degrees of freedom. Therefore, in the theoretical study of the formation of the fragment mass–energy distributions it is

impossible not to introduce the concept of the viscosity of nuclear matter, though neither the energy nor the mass distributions are sensitive to the viscosity mechanism. Only a combined analysis of the experimentally observed characteristics for both the fissioning nucleus ($\bar{\nu}_{\text{pre}}, \sigma_{\text{fus}}, \sigma_{\text{f}}$) and the fragments (the mass–energy distributions) can confirm that the one-body dissipation mechanism dominates in the nucleus.

The fragment kinetic energy and its variance depend weakly on the conditions under which the nucleus breaks up into fragments, but the higher moments of the energy distribution rule out the scission criterion $r_{\text{n}}=0$.

The solution of the complete set of problems associated with the formation of the fragment mass–energy distributions has been made possible by the experimental determination of the angular-momentum dependence in a wide range of fissioning nuclei with $A_{\text{CN}}=100-260$. This dependence has turned out not to be so simple, as it changes sign with increasing nuclear mass.

A large but secondary role is played by the systematics of the average neutron multiplicity $\bar{\nu}_{\text{pre}}$, $\bar{\nu}^{\text{gs}}_{\text{pre}}$, and $\bar{\nu}_{\text{pe}}$, which allow the fairly accurate determination of the temperature of a fissioning nucleus with any nucleon content.

On the whole, the recent experimental and theoretical studies of the various aspects of the fission of heated nuclei give a fairly complete picture of this complicated phenomenon.

The study of the properties of quasi-fission reactions shows that in this case there is no complete relaxation in either the mass coordinate or, apparently, in the energy characteristics.

The authors of the present study hope that it will stimulate both experimental groups and theoreticians to solve the remaining important problems, such as the energy characteristics of superheavy compound systems, the properties of quasifission as a function of A_{t}, Z_{t}, A_{i}, Z_{i}, E_{i}, and so on, the fragment mass–energy distributions near the BG point in reactions involving light particles at $\ell\sim 0$, the dynamical aspects of the description of the mass–energy distributions in the model with short-range nuclear forces, the more accurate theoretical analysis of the dependences of σ^2_M and σ^2_E on ℓ and on the nucleon content, and, finally, the complete theoretical analysis of all experimentally observed properties of the fusion–fission process from a unified point of view.

It seems to us that the most promising technique for further progress will be based on 3-or perhaps n-dimensional Langevin dynamics.

The authors are grateful to G. D. Adeev, V. V. Pashkevich, I. I. Gonchar, G. I. Kosenko, Yu. Ts. Oganesyan, and V. N. Okolovich for many fruitful discussions and their enduring interest in this topic.

[1)]We do not take into account the studies of this problem in the low-energy asymmetric fission of actinide nuclei.

[1] V. M. Strutinskiĭ and V. M. Kolomiets, in *Proceedings of the Eighth Winter School of the LIYaF on Nuclear Physics* (Nauka, Leningrad, 1973), Vol. 2, p. 483 [in Russian].
[2] M. G. Itkis, V. N. Okolovich, A. Ya. Rusanov, and G. N. Smirenkin, Fiz. Élem. Chastits At. Yadra **19**, 701 (1988) [Sov. J. Part. Nucl. **19**, 301 (1988)].
[3] G. D. Adeev, I. I. Gonchar, V. V. Pashkevich *et al.*, Fiz. Élem. Chastits At. Yadra **19**, 1229 (1988) [Sov. J. Part. Nucl. **19**, 529 (1988)]; G. D. Adeev and V. V. Pashkevich, Nucl. Phys. A **502**, 405c (1989).
[4] S. A. Karamyan *et al.*, Yad. Fiz. **8**, 690 (1968) [Sov. J. Nucl. Phys. **8**, 401 (1969)]; **9**, 715 (1969) [Sov. J. Nucl. Phys. **9**, 414 (1969)]; *Physics and Chemistry of Fission* (IAEA, Vienna, 1969), p. 759.
[5] S. A. Karamyan, Yu. Ts. Oganesyan, and B. I. Pustyl'nik, Yad. Fiz. **11**, 982 (1970) [Sov. J. Nucl. Phys. **11**, 546 (1970)].
[6] G. A. Pik-Pichak and V. M. Strutinskiĭ, *The Physics of Nuclear Fission* [in Russian] (Gosatomizdat, Moscow, 1962), p. 12.
[7] J. R. Nix, Nucl. Phys. A **130**, 241 (1969).
[8] G. I. Kosenko, I. I. Gonchar, O. I. Serdyuk, and N. I. Pischasov, Yad. Fiz. **55**, 920 (1992) [Sov. J. Nucl. Phys. **55**, 514 (1992)].
[9] S. V. Zhdanov, M. G. Itkis, S. I. Mul'gin *et al.*, Yad. Fiz. **55**, 3169 (1992) [Sov. J. Nucl. Phys. **55**, 1766 (1992)].
[10] S. V. Zhdanov, M. G. Itkis, S. I. Mul'gin *et al.*, Yad. Fiz. **56**, No. 2, 55 (1993) [Phys. At. Nucl. **56**, 175 (1993)].
[11] V. M. Strutinskiĭ, N. Ya. Lyashchenko, and N. A. Popov, Zh. Éksp. Teor. Fiz. **43**, 584 (1962) [Sov. Phys. JETP **16**, 418 (1963)]; Nucl. Phys. **46**, 639 (1963).
[12] V. M. Strutinskiĭ, Zh. Éksp. Teor. Fiz. **45**, 1891 (1963) [Sov. Phys. JETP **18**, 1298 (1964)]; Yad. Fiz. **1**, 821 (1965) [Sov. J. Nucl. Phys. **1**, 588 (1965)].
[13] W. D. Myers and W. J. Swiatecki, Ark. Fys. **36**, 343 (1967).
[14] W. D. Myers, *Droplet Model of Atomic Nuclei* (IFI, Plenum, New York, 1977).
[15] H. J. Krappe, J. R. Nix, and A. J. Sierk, Phys. Rev. C **20**, 992 (1979).
[16] A. J. Sierk, Phys. Rev. C **33**, 2039 (1986).
[17] U. L. Businaro and S. Gallone, Nuovo Cimento **1**, 629, 1277 (1955).
[18] L. G. Moretto, Nucl. Phys. A **247**, 211 (1975).
[19] L. G. Sobotka, M. A. McMahan, R. J. McDonald *et al.*, Phys. Rev. Lett. **53**, 2004 (1984).
[20] L. N. Andronenko, L. A. Vaĭshnene, A. A. Kotov *et al.*, Fiz. Élem. Chastits At. Yadra **18**, 685 (1987) [Sov. J. Part. Nucl. **18**, 289 (1987)].
[21] M. G. Itkis, S. M. Luk'yanov, V. N. Okolovich *et al.*, Yad. Fiz. **52**, 23 (1990) [Sov. J. Nucl. Phys. **52**, 15 (1990)].
[22] I. G. Itkis, Yu. A. Muzychka, Yu. Ts. Oganesyan *et al.*, Yad. Fiz. **58**, 2140 (1995) [Phys. At. Nucl. **58**, 2026 (1995)].
[23] M. A. McMahan, L. G. Moretto, M. L. Padgett *et al.*, Phys. Rev. Lett. **54**, 1995 (1985).
[24] L. G. Sobotka, M. L. Padgett, G. J. Wozniak *et al.*, Phys. Rev. Lett. **51**, 2187 (1983).
[25] F. D. Becchetti, K. H. Hicks, C. A. Fields *et al.*, Phys. Rev. C **28**, 1217 (1983).
[26] E. N. Gruzintsev, M. G. Itkis, S. I. Mul'gin *et al.*, Yad. Fiz. **43**, 1101 (1986) [Sov. J. Nucl. Phys. **43**, 703 (1986)]; Z. Phys. A **323**, 307 (1986).
[27] T. Sikkeland, Phys. Rev. **135**, 669 (1964); T. Sikkeland, J. E. Clarkson, N. H. Steiger-Shafrir, and V. E. Viola, Phys. Rev. C **3**, 329 (1971).
[28] M. Beckerman and M. Blann, Phys. Rev. C **17**, 1615 (1978).
[29] M. Blann and T. A. Komoto, Phys. Rev. C **26**, 472 (1982).
[30] S. E. Vigdor and H. J. Karwowski, Phys. Rev. C **26**, 1068 (1982).
[31] D. J. Hinde, J. R. Leigh, J. O. Newton *et al.*, Nucl. Phys. A **385**, 109 (1982); **398**, 308 (1983).
[32] S. D. Beĭzin, M. G. Itkis, Yu. A. Muzychka *et al.*, Yad. Fiz. **37**, 809 (1983) [Sov. J. Nucl. Phys. **37**, 482 (1983)].
[33] J. Van der Plicht, H. C. Britt, M. M. Fowler *et al.*, Phys. Rev. C **28**, 2022 (1983).
[34] R. J. Charity, J. R. Leigh, J. J. M. Bokhorst *et al.*, Nucl. Phys. A **457**, 441 (1986).
[35] M. G. Itkis, V. N. Okolovich, A. Ya. Rusanov *et al.*, in *Proceedings of the Intern. School–Seminar on Heavy Ion Physics*, Dubna, Russia, 1993 (JINR, Dubna, 1993), Vol. 1, p. 213.
[36] S. Cohen, F. Plasil, and W. J. Swiatecki, Ann. Phys. (N.Y.) **82**, 557 (1974).
[37] D. Hilsher and H. Rossner, Ann. Phys. (Paris) **17**, 471 (1992).
[38] É. M. Kozulin, A. Ya. Rusanov, and G. N. Smirenkin, Yad. Fiz. **56**, No. 2, 37 (1993) [Phys. At. Nucl. **56**, 166 (1993)].
[39] A. V. Ignatyuk, G. N. Smirenkin, M. G. Itkis *et al.*, Fiz. Élem. Chastits At. Yadra **16**, 709 (1985) [Sov. J. Part. Nucl. **16**, 307 (1985)].
[40] A. Gavron, J. R. Beene, B. Cheynis *et al.*, Phys. Rev. Lett. **47**, 1255 (1981); **48**, 83(E) (1982).
[41] A. Gavron, A. Gayer, J. Boissenain *et al.*, Phys. Rev. C **35**, 579 (1987).

[42] E. Holub, D. Hilscher, G. Ingold *et al.*, Phys. Rev. C **28**, 252 (1983).
[43] W. P. Zang, D. Hilscher, G. Ingold *et al.*, Phys. Rev. C **33**, 519 (1986).
[44] D. Ward, R. J. Charity, D. J. Hinde *et al.*, Nucl. Phys. A **403**, 189 (1983).
[45] D. J. Hinde, R. J. Charity, G. S. Foote *et al.*, Nucl. Phys. A **452**, 550 (1986).
[46] D. J. Hinde, J. R. Leigh, J. J. Bokhorst *et al.*, Nucl. Phys. A **472**, 318 (1987).
[47] J. O. Newton, D. J. Hinde, R. J. Charity *et al.*, Nucl. Phys. A **483**, 126 (1988).
[48] D. J. Hinde, H. Agata, M. Tanaka *et al.*, Phys. Rev. C **37**, 2923 (1988).
[49] D. J. Hinde, H. Agata, M. Tanaka *et al.*, Phys. Rev. C **39**, 2268 (1989).
[50] H. Rossner, D. Hilscher, D. J. Hinde *et al.*, Phys. Rev. C **40**, 2629 (1989).
[51] H. Rossner, D. J. Hinde, J. R. Leigh *et al.*, Phys. Rev. C **45**, 719 (1992).
[52] M. V. Blinov, V. M. Bordyug, É. M. Kozulin *et al.*, Yad. Fiz. **51**, 42 (1990) [Sov. J. Nucl. Phys. **51**, 27 (1990)].
[53] Z. Fraenkel, I. Mayk, J. P. Unik *et al.*, Phys. Rev. C **12**, 1809 (1975).
[54] M. Strecker, R. Wien, P. Plischke, and W. Scolbel, Phys. Rev. C **41**, 2172 (1990).
[55] D. J. Hinde, D. Hilscher, H. Rossner *et al.*, Phys. Rev. C **45**, 1229 (1992).
[56] A. Saxena, A. Chatterjee, R. K. Choudhury *et al.*, Phys. Rev. C **49**, 932 (1994).
[57] D. J. Hinde, D. Hilscher, and H. Rossner, Nucl. Phys. A **502**, 497c (1989).
[58] J. O. Newton, Fiz. Élem. Chastits At. Yadra **21**, 821 (1990) [Sov. J. Part. Nucl. **21**, 349 (1990)].
[59] I. I. Gonchar, Fiz. Élem. Chastits At. Yadra **26**, 932 (1995) [Phys. Part. Nuclei **26**, 394 (1995)].
[60] H. W. Schmitt, W. E. Kiker, and C. W. Williams, Phys. Rev. **137**, 837 (1965).
[61] H. W. Schmitt, J. H. Neiler, and F. G. Walter, Phys. Rev. **141**, 1146 (1966).
[62] F. Plasil, D. S. Burnett, H. C. Britt, and S. G. Thompson, Phys. Rev. **142**, 696 (1966).
[63] L. Fiore, G. Viesti, P. F. Bortignon *et al.*, Phys. Rev. C **47**, 1835 (1993).
[64] L. Fiore, G. Viesti, P. F. Bortignon *et al.*, Phys. Lett. B **298**, 283 (1993).
[65] A. N. Wapstra, G. Audi, R. Hoekstra, At. Data Nucl. Data Tables **39**, 281 (1988).
[66] P. Moller and J. R. Nix, Preprint LA-UR-86-3983, Los Alamos National Laboratory, Los Alamos, NM (1986); At. Data Nucl. Data Tables **39**, 213 (1988).
[67] G. G. Chubaryan, M. G. Itkis, S. M. Luk'yanov *et al.*, Yad. Fiz. **56**, No. 3, 3 (1993) [Phys. At. Nucl. **56**, 286 (1993)].
[68] G. G. Chubaryan, S. M. Luk'yanov, B. É. Penionzhkevich *et al.*, Yad. Fiz. **53**, 1195 (1991) [Sov. J. of Nucl. Physics **53**, 738 (1991)].
[69] E. N. Gruzintsev, M. G. Itkis, V. N. Okolovich, and G. N. Smirenkin, Yad. Fiz. **39**, 1336 (1984) [Sov. J. Nucl. Phys. **39**, 844 (1984)]; Preprint 10-83, Institute of Nuclear Physics, Acad. Sci. Kazakh SSR, Alma-Ata (1983) [in Russian].
[70] A. Ya. Rusanov, M. G. Itkis, and V. N. Okolovich, Yad. Fiz. **60**, 773 (1997) [Phys. At. Nucl. **60**, 683 (1997)].
[71] N. D. Mavlitov, P. Frobrich, and I. I. Gontchar, Z. Phys. A **342**, 195 (1992).
[72] P. Frobrich, I. I. Gontchar, and N. D. Mavlitov, Nucl. Phys. A **556**, 281 (1993).
[73] P. Frobrich and I. I. Gontchar, Nucl. Phys. A **563**, 329 (1993).
[74] I. I. Gontchar and P. Frobrich, Yad. Fiz. **57**, 1249 (1994) [Phys. At. Nucl. **57**, 1181 (1994)].
[75] D. Hilcher, I. I. Gontchar, and H. Rossner, Yad. Fiz. **57**, 1255 (1994) [Phys. At. Nucl. **57**, 1187 (1994)].
[76] B. B. Back, in *Proceedings of the Intern. School–Seminar on Heavy Ion Physics*, Dubna, Russia, 1993 (JINR, Dubna, 1993), Vol. 1, p. 317.
[77] D. J. Hofman, B. B. Back, and P. Paul, Phys. Rev. C **51**, 2597 (1995).
[78] N. Wada, Y. Abe, and N. Carjan, Phys. Rev. Lett. **70**, 3538 (1993).
[79] J. P. Lestone, Phys. Rev. Lett. **70**, 2245 (1993).
[80] R. J. Charity, Phys. Rev. C **51**, 217 (1995).
[81] H. A. Kramers, Physica **7**, 284 (1940).
[82] P. Grange, Li Jun-Qing, and H. A. Weidenmuller, Phys. Rev. C **27**, 2063 (1983).
[83] P. Frobrich and J. Marten, Z. Phys. A **339**, 171 (1991); Nucl. Phys. A **545**, 854 (1992).
[84] E. Shrumberger, K. Dietrich, and K. Pomorski, Nucl. Phys. A **529**, 522 (1991).
[85] D. J. Hinde, Nucl. Phys. A **553**, 255c (1993).
[86] N. V. Eremin, G. Giardina, and I. I. Gontchar, Phys. Lett. B **353**, 432 (1995).
[87] P. Frobrich and H. Rossner, Z. Phys. A **349**, 99 (1994).
[88] V. Ogihara, H. Fujiwara, S. C. Jeong *et al.*, Z. Phys. A **335**, 203 (1990).
[89] W. Q. Shen, J. Albinski, A. Gobbi *et al.*, Phys. Rev. C **36**, 115 (1987).
[90] J. G. Keller, B. B. Back, B. G. Glagola *et al.*, Phys. Rev. C **36**, 1364 (1987).
[91] M. B. Tsang, D. Ardouin, C. K. Gelbke *et al.*, Phys. Rev. C **28**, 747 (1983).
[92] H. Rossner, J. R. Huizenga, and W. U. Schroder, Phys. Rev. C **33**, 560 (1986).
[93] V. E. Viola, Nucl. Data Tables **1**, 391 (1966).
[94] V. E. Viola, K. Kwiatkowski, and M. Wolker, Phys. Rev. C **31**, 1550 (1985).
[95] E. N. Gruzintsev, M. G. Itkis, S. I. Mul'gin *et al.*, Yad. Fiz. **48**, 312 (1988) [Sov. J. Nucl. Phys. **48**, 197 (1988)].
[96] J. Toke, R. Bock, G. X. Dai *et al.*, Nucl. Phys. A **440**, 327 (1985).
[97] E. N. Gruzintsev, M. G. Itkis, V. N. Okolovich *et al.*, Yad. Fiz. **40**, 616 (1984) [Sov. J. Nucl. Phys. **40**, 394 (1984)]; M. G. Itkis, R. G. Kalpakchieva, V. N. Okolovich *et al.*, Yad. Fiz. **36**, 824 (1982) [Sov. J. Nucl. Phys. **36**, 483 (1982)].
[98] J. P. Lestone *et al.*, Phys. Rev. Lett. **67**, 1078 (1991); Nucl. Phys. A **559**, 277 (1993).
[99] H. Ikezoe *et al.*, Phys. Rev. C **42**, R1187 (1990); **46**, 1922 (1992); **49**, 968 (1994).
[100] J. Bartel and P. Quentin, Phys. Lett. B **152**, 29 (1985).
[101] C. Guet, E. Strumderger, and M. Brack, Phys. Lett. B **205**, 427 (1988).
[102] M. G. Mustafa, Vopr. At. Nauki Tekh. Ser. Yad. Konst. No. 1, 75 (1988) [in Russian].
[103] F. Garcias *et al.*, Nucl. Phys. A **495**, 169c (1989); Phys. Rev. C **40**, 1522 (1989); Z. Phys. A **336**, 31 (1990).
[104] G. Royer and J. Mignen, J. Phys. G **18**, 1781 (1992).
[105] F. Haddad and G. Royer, J. Phys. G **21**, 1357 (1995).
[106] J. O. Newton, D. G. Popescu, and J. R. Leigh, Phys. Rev. C **42**, 1772 (1990).
[107] B. G. Glagola, B. B. Back, and R. R. Betts, Phys. Rev. C **29**, 486 (1984).
[108] C. Lebrun, F. Hanappe, J. F. Lecolley *et al.*, Nucl. Phys. A **321**, 207 (1979); B. Borderie, M. Berlanger, D. Gardes *et al.*, Z. Phys. A **299**, 263 (1981).
[109] L. G. Moretto *et al.*, Phys. Lett. B **58**, 31 (1975); R. P. Babinet *et al.*, Nucl. Phys. A **258**, 172 (1976).
[110] J. B. Natowitz, M. N. Namboodiry, and E. T. Chulick, Phys. Rev. C **13**, 171 (1976).
[111] S. Agarwal, J. Galin, B. Gatty *et al.*, Z. Phys. A **296**, 287 (1980).
[112] Y. Nagame, Y. Ikezoe, S. Baba *et al.*, Nucl. Phys. A **510**, 518 (1990).
[113] Y. Nagame, Y. Ikezoe, and T. Ohtsuki, Phys. Rev. C **47**, 1586 (1993).
[114] L. G. Moretto and G. J. Wozniak, Pramana, J. Phys. **33**, 209; Prog. Part. Nucl. Phys. **21**, 401 (1988).
[115] L. G. Sobotka, D. G. Sarantites, Ze Li *et al.*, Nucl. Phys. A **471**, 131c (1987).
[116] N. Carjan and M. Kaplan, Phys. Rev. C **45**, 2185 (1992).
[117] G. D. Adeev *et al.*, Report R4-86-247, JINR, Dubna (1986) [in Russian]; Yad. Fiz. **43**, 1137 (1986) [Sov. J. Nucl. Phys. **43**, 727 (1986)].
[118] L. G. Moretto and R. P. Schmitt, Phys. Rev. C **21**, 204 (1980).
[119] C. Gregoire and F. Scheuter, Z. Phys. A **303**, 337 (1981).
[120] M. E. Faber, Z. Phys. A **297**, 277 (1980).
[121] M. E. Faber, Phys. Rev. C **24**, 1047 (1981).
[122] G. V. Mathews, J. B. Moulton, G. J. Wozniak *et al.*, Phys. Rev. C **25**, 300 (1982).
[123] S. J. Sanders, Phys. Rev. C **44**, 2676 (1991).
[124] G. V. Ravi Prasad, V. S. Ramamurthy, and R. T. Yadav, Phys. Rev. C **51**, 2833 (1995).
[125] C. Gregoire *et al.*, Nucl. Phys. A **361**, 443 (1981); **383**, 392 (1982); **387**, 37c (1982).
[126] G. Guillaume, J. P. Coffin, F. Rami *et al.*, Phys. Rev. C **26**, 2458 (1982).
[127] P. Boccaccio, L. Vannucci, M. Bettiolo *et al.*, Phys. Rev. C **38**, 2108 (1988).
[128] R. J. Charity, K. X. Jing, D. R. Dowvan *et al.*, Nucl. Phys. A **511**, 59 (1990).
[129] J. P. Unik, J. G. Cuninghame, and I. F. Groall, in *Proceedings of the Conf. on the Physics and Chemistry of Fission*, Vienna, 1969 (IAEA, Vienna, 1969), p. 717.
[130] J. G. Cuninghame, J. A. Goodall, J. E. Freeman *et al.*, in *Proceedings of the Conference on the Physics and Chemistry of Fission*, Jülich, 1979 (IAEA, Vienna, 1980), Vol. 1, p. 551.

[131] G. Saupe, O. I. Serdyuk, G. D. Adeev, and V. V. Pashkevich, Yad. Fiz. **48**, 42 (1988) [Sov. J. Nucl. Phys. **48**, 26 (1988)].
[132] B. D. Wilkins, E. P. Steinberg, and R. R. Chasman, Phys. Rev. C **14**, 1832 (1976).
[133] C. Ngo, J. Peter, and B. Tamain, in *Proceedings of the Intern. Conference on Reactions of Complex Nuclei*, Nashville, Tennessee, 1974 (North-Holland, Amsterdam, 1974), Vol. 1, p. 114.
[134] Y. El Masri, F. Hanappe, J. C. Steckmeyer, *et al.*, Nucl. Phys. A **517**, 340 (1990).
[135] R. M. Williams, R. D. Kieburtz, and E. F. Neuzil, J. Inorg. Nucl. Chem. **35**, 3651 (1973).
[136] D. R. Huizenga, M. A. Batler, H. Rosner et al., Vopr. At. Nauki Tekh. Ser. Yad. Konst. No. 1, 65 (1988) [in Russian].
[137] J. R. Nix and W. J. Swiatecki, Nucl. Phys. **71**, 1 (1965).
[138] R. Bock, Y. T. Chu, M. Dakovski *et al.*, Nucl. Phys. A **388**, 334 (1982).
[139] H. T. Feldmeier, Rep. Prog. Phys. **50**, 915 (1987).
[140] L. Nowicki, M. Berlanger, B. Borderie *et al.*, Phys. Rev. C **26**, 1114 (1982).
[141] R. P. Schmitt, G. Mouchaty, and D. R. Haenni, Nucl. Phys. A **427**, 614 (1984).
[142] R. P. Schmitt, G. Mouchaty, D. R. Haenni, and M. Tition, Z. Phys. A **321**, 411 (1985).
[143] R. P. Schmitt, D. R. Haenni, L. Cooke *et al.*, Nucl. Phys. A **487**, 370 (1988).
[144] J. R. Leigh, W. R. Phillips, J. O. Newton *et al.*, Phys. Lett. B **159**, 9 (1985).
[145] L. G. Moretto, G. F. Peaslee, and G. J. Wozniak, Nucl. Phys. A **502**, 453c (1989).
[146] B. B. Back, S. Bjornholm, T. Dossing *et al.*, Phys. Rev. C **41**, 1495 (1990).
[147] A. Gavron, Phys. Rev. C **21**, 230 (1980).
[148] L. D. Landau and E. M. Lifshitz, *Statistical Physics*, Parts 1 and 2, 3rd ed. (Pergamon Press, Oxford, 1980) [Russ. original, Nauka, Moscow, 1964].
[149] I. I. Gonchar and G. I. Kosenko, Yad. Fiz. **53**, 133 (1991) [Sov. J. Nucl. Phys. **53**, 86 (1991)].
[150] E. Mordhorst, M. Strecker, H. Frobcen *et al.*, Phys. Rev. C **43**, 716 (1991).
[151] B. Heusch, H. Freisleben, W. F. Schneider *et al.*, Z. Phys. A **322**, 309 (1985).
[152] H. Oeschler *et al.*, Phys. Rev. C **22**, 546 (1980); Phys. Lett. B **87**, 193 (1979).
[153] Y. Nagame, H. Nakahara, K. Sueki *et al.*, Z. Phys. A **317**, 31 (1984).
[154] R. J. Charity, M. A. McMahan, G. J. Wozniak *et al.*, Nucl. Phys. A **483**, 371 (1988).
[155] C. Cabot, C. Ngo, H. Peter, and B. Tamain, Nucl. Phys. A **244**, 134 (1975).
[156] L. G. Moretto *et al.*, Phys. Rev. Lett. **74**, 3557 (1995).
[157] G. D. Adeev, I. I. Gonchar, V. V. Pashkevich, and O. I. Serdyuk, Yad. Fiz. **50**, 1242 (1989) [Sov. J. Nucl. Phys. **50**, 774 (1989)].
[158] N. Bohr and J. Wheeler, Phys. Rev. **56**, 426 (1939).
[159] P. Fong, Phys. Rev. **102**, 434 (1956).
[160] A. V. Ignatyuk, Yad. Fiz. **7**, 1043 (1968) [Sov. J. Nucl. Phys. **7**, 626 (1968)]; **9**, 357 (1969) [Sov. J. Nucl. Phys. **9**, 208 (1969)].
[161] G. Andersson, M. Areskoug, H.-A. Gusstafsson *et al.*, Z. Phys. A **293**, 241 (1979).
[162] H.-A. Gusstafsson, G. Hylten, B. Schoder, and E. Hagebo, Phys. Rev. C **24**, 769 (1981).
[163] L. N. Andronenko, A. A. Kotov, M. M. Nesterov *et al.*, Z. Phys. A **318**, 97 (1984).
[164] B. Heusch, J. P. Coffin, P. Engelstein *et al.*, Z. Phys. A **312**, 109 (1983).
[165] J. Bisplinghoff, P. David, M. Blann *et al.*, Phys. Rev. C **17**, 177 (1978).
[166] G. J. Mathews, G. J. Wozniak, R. P. Schmitt, and L. G. Moretto, Z. Phys. A **238**, 247 (1977).
[167] D. N. Delis, Y. Blumenfeld, D. R. Bowman *et al.*, Z. Phys. A **339**, 279 (1991); Nucl. Phys. A **534**, 403 (1991).
[168] P. M. Evans, A. E. Smith, C. N. Pass *et al.*, Nucl. Phys. A **526**, 365 (1991).
[169] A. J. Sierk, Phys. Rev. Lett. **55**, 582 (1985).
[170] E. M. Rastopchin, S. I. Mul'gin, Yu. B. Ostapenko *et al.*, Yad. Fiz. **53**, 120 (1991) [Sov. J. Nucl. Phys. **53**, 78 (1991)].
[171] J. Boger and J. M. Alexander, Phys. Rev. C **50**, 1006 (1994).
[172] P. Moller, J. R. Nix, W. D. Myers, and W. J. Swiatecki, At. Data Nucl. Data Tables **59**, 185 (1995).
[173] F. Plasil and H. W. Schmitt, Phys. Rev. C **5**, 528 (1972).
[174] V. V. Pashkevich, Nucl. Phys. A **169**, 275 (1971).
[175] G. D. Adeev and N. I. Pischasov, Yad. Fiz. **44**, 897 (1986) [Sov. J. Nucl. Phys. **44**, 579 (1986)].
[176] T. Wada, N. Carjan, and Y. Abe, Nucl. Phys. A **538**, 283c (1992).
[177] M. G. Itkis, N. A. Kondrat'ev, S. I. Mul'gin *et al.*, Yad. Fiz. **53**, 1225 (1991) [Sov. J. Nucl. Phys. **53**, 757 (1991)].
[178] M. F. Rivet, R. Alami, B. Borderie *et al.*, Z. Phys. A **330**, 295 (1988).
[179] Z. Zheng, B. Borderie, D. Gardes *et al.*, Nucl. Phys. A **422**, 447 (1984).
[180] V. Bernard, C. Gregoire, C. Mazur *et al.*, Nucl. Phys. A **385**, 319 (1982).
[181] C.-C. Sahm, H. Schulte, D. Vermeulen *et al.*, Z. Phys. A **297**, 241 (1980).
[182] J. C. McGeorge, A. C. Shotter, D. Brenford, and J. M. Reid, Nucl. Phys. A **326**, 108 (1979).
[183] A. V. Kuznetsov, V. A. Rubchenya, D. N. Vakhtin *et al.*, in *Proceedings of the Fifteenth Nuclear Physics European Division Conf. on Low Energy Nuclear Dynamics*, St. Petersburg, Russia, 1995, edited by Yu. Ts. Oganessian and R. Kalpakchieva (World Scientific, Singapore, 1995), p. 252.
[184] M. G. Itkis, Yu. Ts. Oganessian, G. G. Chubarian *et al.*, in *Proceedings of the Fifteenth Nuclear Physics European Division Conf. on Low Energy Nuclear Dynamics*, St. Petersburg, Russia, 1995, edited by Yu. Ts. Oganessian and R. Kalpakchieva (World Scientific, Singapore, 1995), p. 177.
[185] R. L. Ferguson, F. Plasil, H. Freisleben *et al.*, Phys. Rev. C **8**, 1104 (1973).
[186] R. Kalpakchieva, Yu. Ts. Oganessian, Yu. E. Penionzhkevich *et al.*, Phys. Lett. B **69**, 287 (1977).
[187] R. Kalpakchieva, Yu. Ts. Oganessian, Yu. E. Penionzhkevich, and H. Sodan, Z. Phys. A **283**, 253 (1977).
[188] R. G. Kalpakchieva, Candidate's Dissertation, JINR, Dubna (1980) [in Russian].
[189] P. Gippner, K. D. Schilling, W. Seidel *et al.*, Z. Phys. A **325**, 335 (1986); H. Sodan, S. M. Luk'yanov, Yu. E. Penionzhkevich *et al.*, in *Proceedings of the Intern. School–Seminar on Heavy Ion Physics*, Dubna, Russia, 1986 (Report D7-87-68, JINR, Dubna, 1987), p. 479.
[190] C. Ngo, J. Peter, B. Tamain *et al.*, Z. Phys. A **283**, 161 (1977).
[191] J. Galin, B. Gatty, D. Guerreau *et al.*, Z. Phys. A **283**, 173 (1977).
[192] M. A. Butler, S. S. Datta, R. T. de Souza *et al.*, Phys. Rev. C **34**, 2016 (1986).
[193] G. Guarino, A. Gobbi, K. D. Hildenbrand *et al.*, Nucl. Phys. A **424**, 157 (1984).
[194] S. Lerey, X. S. Chen, G. Y. Fan *et al.*, Nucl. Phys. A **423**, 175 (1984).
[195] F. Hanappe, C. Ngo, J. Peter, and B. Tamain, in *Proceedings of the Conference on the Physics and Chemistry of Fission*, Rochester, NY, 1973 (IAEA, Vienna, 1974), Vol. 2, p. 289.
[196] B. Borderie, F. Hanappe, C. Ngo *et al.*, Nucl. Phys. A **220**, 93 (1974).
[197] H. Schulte, B. Jäckel, R. A. Esterlund *et al.*, Phys. Lett. B **232**, 37 (1989).
[198] H. Keller, K. Lützenkirchen, and J. V. Kratz, Z. Phys. A **326**, 313 (1987).
[199] K. Lützenkirchen, J. V. Kratz, G. Wirch *et al.*, Nucl. Phys. A **452**, 351 (1986).
[200] T. Sikkeland, Phys. Lett. B **31**, 451 (1970).
[201] O. A. P. Tavares and M. L. Terranova, Nuovo Cimento C **105**, 723 (1992).
[202] Yu. Ts. Oganessian and Yu. A. Lazarev, in *Treatise on Heavy Ion Science*, edited by D. A. Bromley (Plenum, New York, 1985), Vol. 4, p. 3.
[203] Yu. P. Gangrskiĭ, B. Dalkhsuren, and B. N. Markov, *Nuclear Fission Fragments* [in Russian] (Énergoatomizdat, Moscow, 1986).
[204] R. W. Hasse, Nucl. Phys. A **128**, 609 (1969); Phys. Rev. C **4**, 572 (1971).
[205] K. T. R. Davies, A. J. Sierk, and J. R. Nix, Phys. Rev. C **13**, 2385 (1976).
[206] S. E. Koonin and J. R. Nix, Phys. Rev. C **13**, 209 (1976).
[207] A. J. Sierk and J. R. Nix, Phys. Rev. C **16**, 1048 (1977).
[208] K. T. R. Davies, R. A. Managan, J. R. Nix, and A. J. Sierk, Phys. Rev. C **16**, 1890 (1977).
[209] A. J. Sierk, S. E. Koonin, and J. R. Nix, Phys. Rev. C **17**, 646 (1978).
[210] J. W. Negele, S. E. Koonin, P. Moller *et al.*, Phys. Rev. C **17**, 1098 (1978).
[211] A. J. Sierk and J. R. Nix, Phys. Rev. C **21**, 982 (1980).
[212] J. R. Nix and A. J. Sierk, Nucl. Phys. A **428**, 161c (1984).
[213] N. Carjan, A. J. Sierk, and J. R. Nix, Nucl. Phys. A **452**, 381 (1986).
[214] J. R. Nix and A. J. Sierk, in *Proceedings of the Intern. School–Seminar on Heavy Ion Physics*, Dubna, Russia, 1986 (Report D7-87-68, JINR, Dubna, 1987), p. 453.
[215] J. R. Nix and A. J. Sierk, in *Proceedings of the Intern. Symp. on Perspectives in Nuclear Physics*, Madras, India, 1987 (Preprint LA-UR-87-

133, Los Alamos National Laboratory, Los Alamos, 1987).
[216] H. Hofmann, A. S. Jensen, and F. Scheuter, in *Proceedings of the Twelfth Intern. Symp. on Nuclear Physics*, Gaussig, GDR, 1982 (ZfK-491, Rossendorf, 1982), p. 96; F. Scheuter and C. Gregoire, *ibid.*, p. 102.
[217] H. Hofmann and J. R. Nix, Phys. Lett. B **122**, 117 (1983).
[218] J. R. Nix, A. J. Sierk, H. Hofmann *et al.*, Nucl. Phys. A **424**, 239 (1984).
[219] F. Scheuter, C. Gregoire, H. Hofmann, and J. R. Nix, Phys. Lett. B **149**, 303 (1984).
[220] G. D. Adeev and I. I. Gonchar, Yad. Fiz. **37**, 1113 (1983) [Sov. J. Nucl. Phys. **37**, 661 (1983)]; Z. Phys. A **320**, 451 (1985); **322**, 479 (1985).
[221] O. I. Serdyuk, G. D. Adeev, I. I. Gonchar *et al.*, Yad. Fiz. **46**, 710 (1987) [Sov. J. Nucl. Phys. **46**, 399 (1987)].
[222] G. D. Adeev, V. V. Pashkevich, and O. I. Serdyuk, JINR Brief Commun. E4(24)-87, JINR, Dubna (1987) [in Russian].
[223] G. I. Adeev, Fiz. Élem. Chastits At. Yadra **23**, 1572 (1992) [Sov. J. Part. Nucl. **23**, 684 (1992)].
[224] G.-R. Tillack, Phys. Lett. B **278**, 403 (1992).
[225] G.-R. Tillack, R. Reif, A. Schülke *et al.*, Phys. Lett. B **296**, 296 (1992).
[226] G. I. Kosenko, I. G. Kolyari, and G. D. Adeev, Yad. Fiz. **60**, 404 (1997) [Phys. At. Nucl. **60**, 404 (1997)].
[227] G. I. Kosenko, Candidate's Dissertation, Tomsk (1992) [in Russian].
[228] B. B. Back *et al.*, Phys. Rev. Lett. **46**, 1068 (1981); **50**, 818 (1983); Phys. Rev. C **31**, 2104 (1985); **32**, 195, 1786 (1985); **33**, 385 (1985).
[229] H. Y. Han, K. X. Jing, E. Plagnol *et al.*, Nucl. Phys. A **492**, 138 (1989).
[230] F. D. Becchetti, P. M. Letter, J. Jänecke *et al.*, in *Proceedings of the Conference "Fifty Years with Nuclear Fission,"* Gaithersburg, Tennessee, 1989, p. 688.
[231] K. Grotowski, Z. Majka, R. Planeta *et al.*, Phys. Rev. C **30**, 1214 (1984).
[232] M. Brack, J. Damgaard, A. S. Jensen *et al.*, Rev. Mod. Phys. **44**, 320 (1972).
[233] J. Blocki, Y. Boneh, J. R. Nix *et al.*, Ann. Phys. (N.Y.) **113**, 330 (1978); J. Bandrup and W. J. Swiatecki, Ann. Phys. (N.Y.) **125**, 193 (1980); W. J. Swiatecki, Prog. Part. Nucl. Phys. **4**, 383 (1980); W. J. Swiatecki, Phys. Scr. **24**, 113 (1981); S. Bjornholm and W. J. Swiatecki, Nucl. Phys. A **391**, 471 (1982); J. Randrup and W. J. Swiatecki, Nucl. Phys. A **429**, 105 (1984); J. Blocki, H. Feldmeier, and W. J. Swiatecki, Nucl. Phys. A **459**, 145 (1986).
[234] J. J. Griffin and M. Dworzecka, Nucl. Phys. A **455**, 61 (1986).
[235] U. Brosa, S. Grossmann, and A. Müller, Phys. Rep. **194**, 167 (1990).
[236] F. Gonnenwein, in *The Nuclear Fission Process*, edited by C. Wagemans (CRC Press, Boca Raton, Florida, 1991), p. 287.
[237] M. Thoennessen *et al.*, Phys. Rev. Lett. **59**, 2860 (1987); R. Butsch *et al.*, Phys. Rev. C **44**, 1515 (1991); D. J. Hofmann *et al.*, Phys. Rev. Lett. **72**, 470 (1994); P. Paul, Nucl. Phys. A **569**, 73c (1994).
[238] K. Siwek–Wilczynska, J. Wilczynski, R. H. Siemssen, and H. W. Wilschut, Phys. Rev. C **51**, 2954 (1995).
[239] J. P. Bocquet and R. Brissot, Nucl. Phys. A **502**, 213c (1989).
[240] A. A. Goverdovskiĭ, Preprint FÉI-2430, Obninsk (1995) [in Russian].
[241] U. Brosa *et al.*, Z. Phys. A **310**, 177 (1983); J. Phys. G **10**, 933 (1984).
[242] S. Bjornholm, in *Proceedings of the Symp. "Ten Years of the Uranium Beam at the UNILAC,"* Darmstadt, FRG, 1986 (GSI-86-19, Darmstadt, 1986), p. 119.
[243] R. V. Dzholos, A. K. Nasirov, and V. P. Permyakov, Yad. Fiz. **48**, 1304 (1988) [Sov. J. Nucl. Phys. **48**, 829 (1988)].

Translated by Patricia A. Millard